University of Exeter

Department of Mathematics

Quasi-geostrophic influence of the polar stratosphere on the troposphere

Simon James Clark

November 2017

Supervised by Prof Mark Baldwin and Prof David Stephenson

Submitted by Simon James Clark, to the University of Exeter as a thesis for the degree of Doctor of Philosophy in Mathematics , November 2017.

I certify that all material in this thesis which is not my own work has been identified and that no material has previously been submitted and approved for the award of a degree by this or any other University.

(signature) .....

Declaration

No work in this thesis has previously been published in any journal. This thesis is original work, inspired by the concept of an averaged polar cap pressure index, discussed in the forthcoming paper *Polar Amplification of Stratospheric Variability* (Baldwin et al., 2018), but developing dynamics of this index and performing analysis which is wholly original. The concept, mathematics, and analysis of vertical and horizontal mass flux forcing this pressure index, as well as the separation of stratospheric influence on these fluxes by piecewise inversion, is wholly original to this thesis.

Simon James Clark

Abstract

This thesis considers the tropospheric response to extreme events in the stratosphere known as sudden stratospheric warmings (SSWs). These events have been shown to influence the troposphere through persistent, descending circulation anomalies. The thesis quantifies and tests the hypothesis that changes in stratospheric potential vorticity remotely influence mass flux into the polar troposphere, and so influence tropospheric pressure, in the aftermath of SSWs. Firstly, the thesis introduces a new metric of stratosphere-troposphere coupling, defining a pressure index on height surfaces over the polar region which is demonstrated to capture the same behaviour as the traditionally used Arctic Oscillation (AO) index. Secondly, quasi-geostrophic (QG) theory is used to derive expressions for horizontal and vertical mass flux into the polar region, which force the polar pressure index. The QG horizontal mass flux is found to be non-linear in the streamfunction associated with a QG potential vorticity (QGPV) distribution, with the interaction of mass flux associated with stratospheric QGPV and with tropospheric QGPV being substantial in the troposphere. Pressure index tendencies are approximated using these mass flux expressions, and found to generally compare with reanalysis moderately well in the stratosphere but poorly in the troposphere. Two algorithms used to define and categorise SSWs as splits and displacements are compared in this mass flux framework, with the approximation of the influence of vortex displacements by QG theory being more accurate than the approximation of the influence of vortex splits. There is little difference seen in the tropospheric pressure response to vortex split and vortex displacement SSWs. Lastly, the stratosphere is not demonstrated to substantially influence the polar troposphere via QG mass fluxes in the aftermath of SSWs given streamfunctions calculated in this thesis.

"My friends have always been the best of me"

- *(Doctor, T)*

To my parents, Bob and Gill, to whom I owe everything.

To the teachers who inspired me to believe in myself: Jeff Harris, Duncan Bird, Sue Skyrme, Harry Backhouse, Sally Cartwright, Karen Frost, Naomi Greenough, Damian Knowles, and Garret Cotter.

To Liv, without whom I wouldn't have made it to the end.

To Michael Graham and my fellow scholars of the University of Exeter Chapel Choir. To Hannah, for the radio and the cards.

Huge thanks to Drs Mike Kelleher and Stephen Thomson for all their help with the PV inversion code. And to all those at Exeter who helped me along the way: Drs Penny Maher, Hugo Lambert, Blanca Ayarzaguena, and Phil Sansom.

Contents

List of Figures

List of Tables

Nomenclature and Glossary

Acronyms

AO	Arctic Oscillation
EOF	Empirical Orthogonal Function
ERA	European Reanalysis
ERA-Interim	European Reanalysis Interim
NAM	Northern Annular Mode
NAO	North Atlantic Oscillation
PDF	Probability Density Function
PPVI	Piecewise Potential Vorticity Inversion
PV	Potential Vorticity
QBO	Quasi-biennial Oscillation
QG	Quasigeostrophic
QGPV	Quasigeostrophic Potential Vorticity
RMS	Root Mean Square
SSW	Sudden Stratospheric Warming

Key papers

AH02	Ambaum and Hoskins (2002)
BD01	Baldwin and Dunkerton (2001)
BD99	Baldwin and Dunkerton (1999)
CP07	Charlton and Polvani (2007)
DM13	Mitchell et al. (2013)

Greek letters

β	$\partial f/\partial\varphi$	
λ	Longitude	$^\circ$
ω	Vertical velocity	$Pa\ s^{-1}$
ϕ	Geopotential	$m^2\ s^{-2}$
ψ	Streamfunction	$m^2\ s^{-1}$
ρ	Density	$kg\ m^{-3}$
θ	Potential temperature	K
φ	Latitude	$^\circ$

Roman letters

a	Earth mean radius	$6371km$
f	Coriolis parameter	s^{-1}
g	Gravitational acceleration	$9.81\ m\ s^{-2}$
H	Horizontal mass flux	$kg\ s^{-1}$
N^2	Brunt–Väisälä frequency	s^{-1}
p	Pressure	$N\ m^{-2}$
Q	Potential Vorticity	$m^{-2}\ s^{-1}\ K\ kg^{-1}$
q	Quasigeostrophic Potential Vorticity	s^{-1}
R	Specific gas constant for dry air	$287\ J\ kg^{-1}\ K^{-1}$
T	Temperature	K
t	Time	s
T_v	Virtual temperature	K
u	Zonal wind	$m\ s^{-1}$
V	Vertical mass flux	$kg\ s^{-1}$
v	Meridional wind	$m\ s^{-1}$
x, y	Horizontal distances	m
z	Vertical distance	m

1. Introduction

"I've got a bad feeling about this"
- *(Solo, H)*

On December 25th of 1984, something peculiar happened in the Arctic night. Despite having not seen sunlight for weeks, the air in the middle atmosphere, 40km above the surface, started to heat up. Within days temperatures had increased by nearly 40 degrees Celsius. While this was happening, the rotating mass of air centred over the pole split into two huge, distinct vortices, each the size of Australia. This is shown in fig. 1.1. The effect of these violent changes to the atmospheric circulation worked their way downwards, creeping towards the surface. Storms tracking eastward across the Atlantic were deflected south, cold Arctic air masses spilled out over northern Europe, and in the two months following December 25th cities all over the northern parts of Europe and America recorded extremely low temperatures.

This violent event is not unique - something similar occurs approximately six times every decade. The heating and splitting (or displacement) of the polar vortex is known as a *sudden stratospheric warming*, or SSW. This thesis is about understanding the process linking such SSWs in the middle atmosphere to changes in the lower atmosphere and the surface.

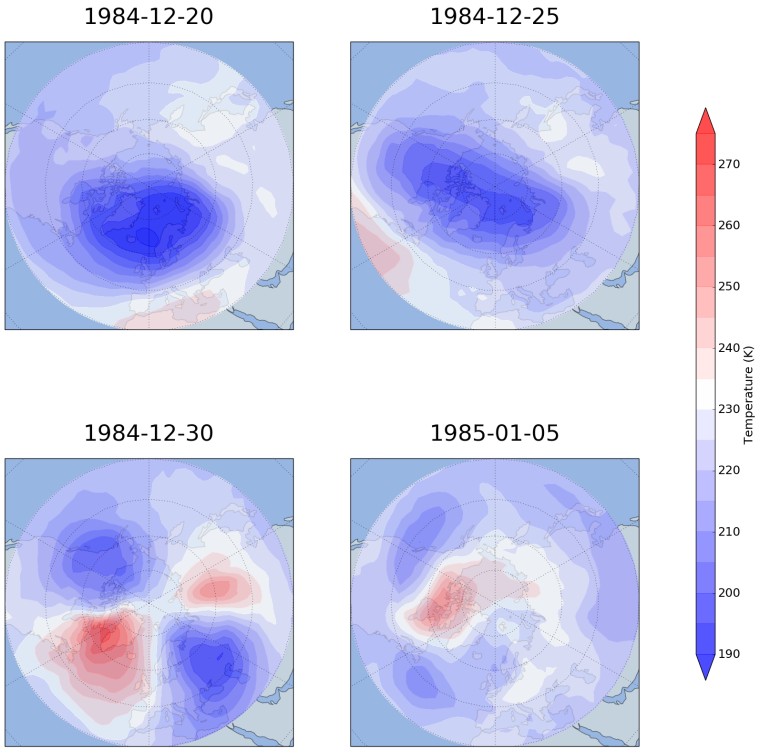

Figure 1.1.: Temperature on the 10hPa surface in the northern hemisphere on four dates. Data from ERA-Interim. Note the extremely rapid increase in temperature and the splitting of the polar vortex in two.

1.1. Thesis aims

Linking changes in the middle atmosphere, in the region known as the *stratosphere*, to those in the lower atmosphere, known as the *troposphere*, can be described as part of *stratosphere-troposphere coupling*. This thesis will be examining the downward component of this coupling, and in particular will be suggesting a new theory with extreme events like SSWs in mind. This theory will attempt to answer the following questions:

1. How can the effect of variations in stratospheric dynamics on the polar troposphere be described?

2. Does the troposphere exhibit different responses in the aftermath of different kinds of SSW?

3. Does the stratosphere influence the troposphere in a substantial way in the aftermath of SSWs?

4. Is it possible to theoretically approximate the tropospheric response to a SSW, and are there different mechanics associated with vortex splits and vortex displacements?

1.2. Thesis plan

The rest of this thesis is structured into chapters as follows:

2. The background chapter. Existing literature is reviewed, providing all the necessary information to understand the original work included in the thesis, and to put its conclusions into perspective.

3. The theory chapter. A new metric of stratospheric influence on the troposphere is introduced, along with a first order dynamical theory of how it varies with changes in the stratosphere.

4. The gross results chapter. The theory from the previous chapter is tested by comparing its approximations to reanalysis, and its performance in different parts of the atmosphere and at different times examined.

5. The SSW chapter. Similar to the previous chapter but specifically looking at SSWs, the calculations of the theory proposed in chapter 3 are compared to SSWs in reanalysis. The performance of two algorithms which categorise SSWs are also examined within this theoretical framework, attempting to see if there is a dynamical difference between split and displaced polar vortices.

6. The conclusion. Bringing together the work of the previous chapters, discussing the significance and limitations of the results, and suggesting further work.

The events of December 1984 will continue to appear throughout the following chapters. However before a new theory of stratospheric influence on the troposphere to explain such events can be introduced, the atmospheric system and the relevant physics must be reviewed. This is done in the next chapter.

2. Background

"Well, something sure the hell ain't right."
- *(Reynolds, M)*

2.1. Aims

This chapter covers relevant background information referred to in the rest of the thesis. The gross structure of the atmosphere will be introduced, an overview of the dynamics of the stratosphere given, and finally existing literature on stratosphere-troposphere coupling reviewed. Further technical details are supplied when necessary in later chapters.

2.2. Structure of the atmosphere

The atmosphere is a continuous stratified fluid stretching from the surface of the Earth to space, with a density that decreases approximately exponentially with altitude. There is no universally agreed altitude at which the atmosphere stops, but one common convention is 100km, the Kármán line. The atmosphere is formed largely of nitrogen and oxygen, with traces of other compounds, behaving to a decent approximation as an ideal gas.

The bottom-most layer of the atmosphere, containing approximately 80% of its total mass, is the *troposphere* (Wallace and Hobbs, 2006). The layer above this, extending from approximately 10km to 50km above the surface, containing the vast majority of the remaining atmospheric mass, is the *stratosphere*. Above the stratosphere the mesosphere extends from approximately 50km to 80km in altitude, and above the mesosphere the

thermosphere from 80km to approximately 600km in altitude (shown in fig. 2.1). This thesis will be concerned with the lowest two layers only - the stratosphere and the troposphere. The boundary between these regions - the *tropopause* - is typically determined by the vertical temperature profile, but there are several alternative definitions.

In the troposphere the air temperature normally decreases with altitude (Schlatter, 2009). This is not the case in the stratosphere, as due to absorption of short wavelength solar radiation by high local concentrations of ozone (Cornu, 1881) the temperature increases with altitude from a minimum of approximately -50°C at the tropopause, to a maximum of approximately 0°C at the boundary with the mesosphere above (Teisserenc de Bort, 1902; Assmann, 1907). This positive vertical temperature gradient results in the stratosphere having dynamics which are very different dynamics to those of the troposphere, outlined in sections 2.3 and 2.4 respectively.

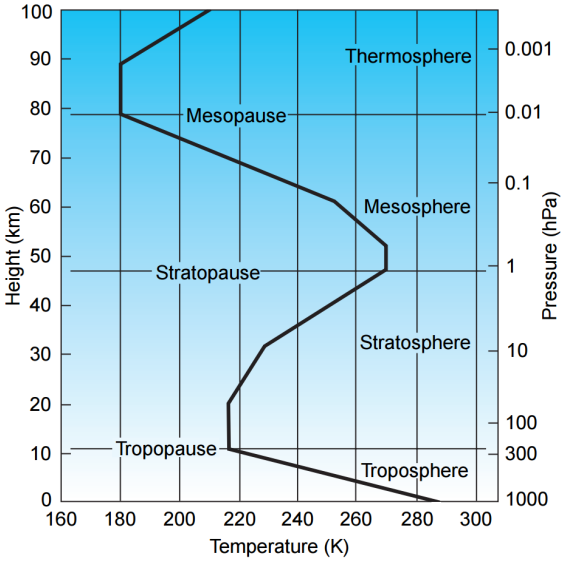

Figure 2.1.: A vertical temperature profile of the atmosphere in the midlatitudes with the key layers noted. From Wallace and Hobbs (2006), using data from the U.S. Standard Atmosphere.

As it is convectively unstable and has the majority of mass in the atmosphere, the troposphere exerts a significant influence on higher layers through, e.g., the generation of gravity waves (Hines, 1960). Less certain however is the impact of the higher layers in the atmosphere on the troposphere, through a downward influence of one form or another (Kidston et al., 2015). In the past few decades this influence has been observed and identified, and many theories presented to explain it, as detailed in section 2.5.

Before proceeding it is worth briefly reviewing the concept of a vertical coordinate in the atmosphere. In the above, the word 'altitude' was used to refer to a point above the Earth's surface, horizontally specified through latitude and longitude coordinates. Specifically this refers to geometric height z, the distance to the point - in metres - above mean sea level. However one could also refer to a point above the surface using its pressure, or potential temperature θ, or some scaled version of either. As many equations describing the atmosphere are rendered in a clearer form when pressure is used as a vertical coordinate,

pressure is typically used. This is referred to as using isobaric coordinates. For much of this thesis however z will be used as a vertical coordinate. How data in isobaric coordinates can be interpolated to z-coordinates is described in chapter 3.

With the atmosphere now broadly introduced, much of this thesis will be concerned with events in the polar stratosphere specifically. The dynamics of this layer of the atmosphere are now covered in more detail.

2.3. Stratospheric dynamics

The defining characteristic of the stratosphere is that it is dynamically stable. This is due to its vertical temperature profile, with temperature increasing with altitude. An air parcel vertically displaced from its equilibrium position by some forcing will re-equilibrate (Murray, 1960). This is in contrast to the troposphere, where temperature decreases with altitude. Displaced tropospheric air parcels may not return to their equilibrium position and instead continue in vertical motion until they reach a domain boundary, depending on the local stability and moisture content. This convective instability drives extensive vertical convection and transport in the troposphere, and its absence in the stratosphere results in a highly stratified system which is almost entirely dry, as water vapour from the troposphere cannot propagate vertically into it, though it can enter the lower stratosphere through advection along isentropes and the Brewer-Dobson circulation (Holton et al., 1995).

As a result of stratospheric air being almost completely dry, and its constituent gases behaving as ideal gases (being point particles only interacting with each other by perfectly elastic collisions) it can be well described by the ideal gas equation,

$$p = \rho RT \tag{2.1}$$

where p is the pressure, ρ is the density, and T is the air temperature. Constant R is the specific gas constant for dry air, equal to 287.058 $J\ kg^{-1}K^{-1}$.

The dynamics of the the stratosphere vary strongly in time, altitude, longitude, and latitude, but most strongly in latitude and height. There is a significant difference between the dynamics of the summer and winter hemispheres. The summer hemisphere is char-

acterised by easterly winds while the winter hemisphere has a strong *stratospheric polar vortex*, a large system of strong westerly winds. This is shown in fig. 2.2. The wind reversal in the stratosphere that occurs with the changing of the seasons was first discovered by Whipple (1935) through an acoustic study of artillery used in the First World War. At the equator, the stratosphere oscillates between descending easterly and westerly winds with a period of between two and three years. This circulation is known as the Quasi Biennial Oscillation (QBO), and has wide-reaching teleconnections, see e.g. Baldwin et al. (2001). These longitudinally averaged or zonal mean circulations are typically referred to as the mean state, and in order to understand them it is necessary to understand the interaction between deviations from the mean - termed *waves* or *eddies* - and the mean itself.

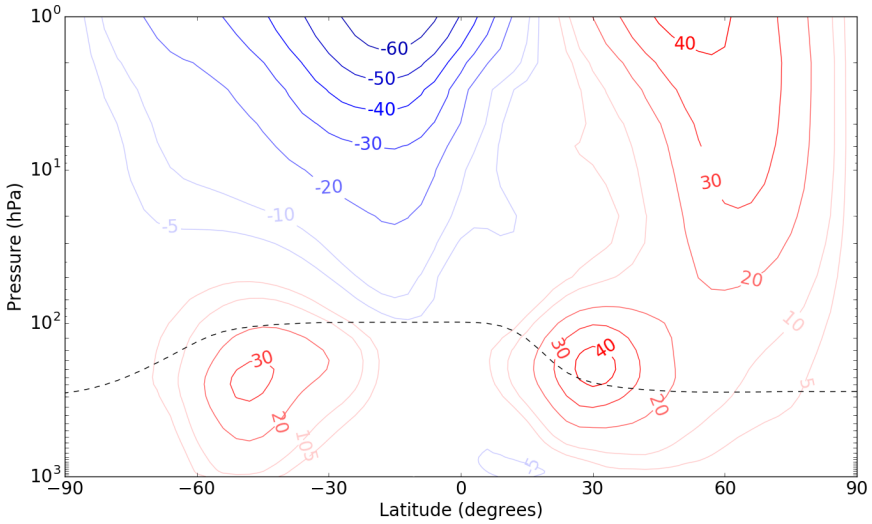

(a) January

(b) July

Figure 2.2.: Time-averaged zonal mean zonal wind for the months of January and July. The dashed line gives the location of the thermally-defined tropopause. Isobaric zonal wind data from 1979-2016 from ERA-Interim was used. Tropopause data also from ERA-Interim.

The large-scale dynamics - meaning large in physical extent - of the stratosphere are well described by the time evolution of a single scalar variable, the Ertel *potential vorticity* (hereafter PV) Q, and its associated 'balanced' flow. This is flow where the three-dimensional velocity field is functionally related to the mass field, presumed to be hydrostatically related to the pressure field (McIntyre, 2003, 2015). PV is materially conserved in adiabatic, frictionless motion; in other words,

$$\frac{DQ}{Dt} = 0 \tag{2.2}$$

where $D/Dt = \partial/\partial t + \underline{u} \cdot \nabla$ is the material or Lagrangian derivative. For such flow there is also the material conservation of potential temperature θ,

$$\frac{D\theta}{Dt} = 0. \tag{2.3}$$

The PV at a given location is proportional to the absolute Kelvin circulation, C_Γ,

$$C_\Gamma = \lim_{\Gamma \to 0} \oint_\Gamma u^a \cdot dx$$

where Γ is a closed contour bounding infinitesimal area δA and u^a is the three-dimensional velocity field in the inertial (i.e. non-rotating) frame with spatial integral component dx. Kelvin's circulation theorem states that this circulation is conserved following motion in a dissipationless fluid. This is what makes C_Γ, and so PV, useful. The constant of proportionality between PV and C_Γ is $\delta\theta$, the potential temperature increment between a part of neighbouring isentropic surfaces, divided by the mass of the small material fluid element between those surfaces and bound by Γ. As $Dw/Dt << g$ in the atmosphere, the equation for vertical motion

$$\rho \frac{Dw}{Dt} = \frac{\partial p}{\partial z} + \rho g$$

can be simplified to *hydrostatic balance*,

$$\frac{\partial p}{\partial z} = -\rho g. \tag{2.4}$$

As such PV is given by

$$Q = -g \frac{C_\Gamma}{\delta A} \frac{\partial \theta}{\partial p},$$

where the assumption has also been made that the slopes of isentropic surfaces are small compared to unity (Rossby, 1940). These assumptions of hydrostatic balance and small

isentropic slope usually hold extremely well (Andrews et al., 1987). Exactly equivalent to this statement via application of Stokes' theorem (Riley et al., 2006) is the Ertel or Rossby-Ertel formula (see Schubert et al. (2004) for English translations of Ertel's original papers)

$$Q = -g\xi_z \frac{\partial \theta}{\partial p},$$

where ξ_z is the vertical component of the absolute vorticity vector. Example distributions of this Q are shown in fig. 2.3. The Ertel PV can be split into a local contribution - the local vorticity - and a global contribution from the rotation vector of the Earth, vertical component f, giving the final formula for the Ertel PV under the assumptions of hydrostatic balance and small θ slopes:

$$Q = -g\left(\nabla \times u + f\right)\frac{\partial \theta}{\partial p}. \tag{2.5}$$

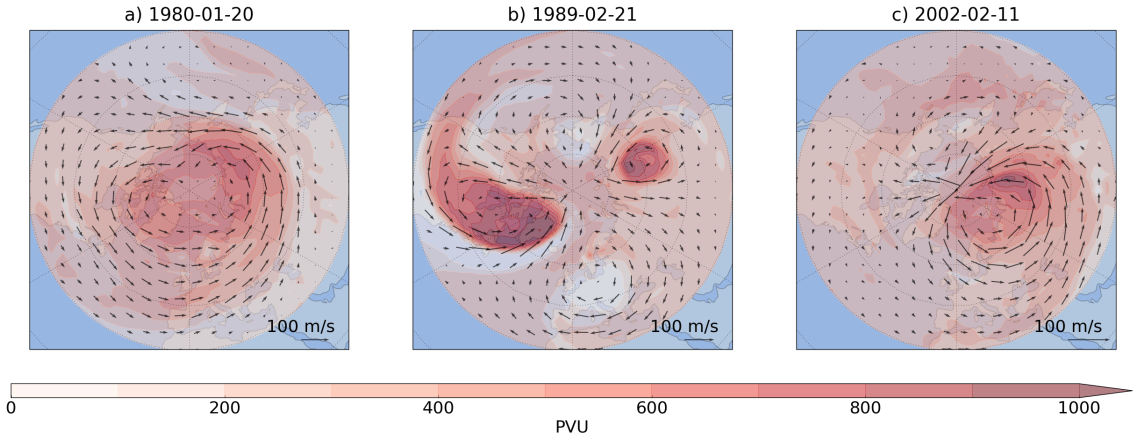

Figure 2.3.: The stratospheric Ertel PV and velocity fields on the 10hPa surface on three separate dates. Data is from ERA-Interim. PV is given in potential vorticity units (PVU), defined as $1\ PVU \equiv \frac{10^{-6} K \cdot m^2}{kg \cdot s}$. a) shows a coherent high PV core over the pole - corresponding to a well-organised stratospheric polar vortex. b) shows a vortex split, with two clear maxima in the PV field and multiple distinct circulations in the wind field. c) shows a vortex displacement, with the high PV core of the polar vortex displaced - and the associated large circulation - to approximately 70N. Note that the PV field during most SSWs resembles a combination of these two subfigures, with the high PV core of the vortex displaced equatorwards and often a smaller daughter vortex forming. It is rare for events to be as clearly distinguishable as either split or displacement as they are presented here.

Consideration of the time evolution of this PV field shows that winter stratospheric dynamics can be split into two distinct processes:

1. Linear upward propagation of Rossby waves from the troposphere, causing reversible displacements and distortions of the high PV region corresponding to the polar vortex shown in fig. 2.3a. This process accounts for most deviations from the mean stratospheric circulation (Schubert et al., 2004; Vallis, 2006).

2. Non-linear breaking of these Rossby waves in the region outside the polar vortex - the 'stratospheric surf zone' - causing irreversible deformation of material contours, and mixing of the PV associated with the polar vortex into lower latitudes. This behaviour was first identified by McIntyre and Palmer (1983). Variations in the degree of wave forcing force the polar vortex (see below, section 2.3.2) and the stratospheric system as a whole - by breaking in the surf zone, waves strip PV from the polar regions and redistribute it at lower latitudes (Juckes and McIntyre, 1987). This acts to reduce the size of the polar vortex and intensify latitudinal PV gradients.

If Q is known everywhere, then, with appropriate boundary and balance conditions, it can be inverted to give a 'balanced flow'; velocity, pressure, and temperature fields. The usefulness of casting stratospheric dynamics as the dynamics of PV - rather than of individual temperature and velocity fields - is its material conservation and invertibility. If the PV field is known at a given time then advection of this field and subsequent inversion allows for the time-evolved atmospheric state to be predicted. Eqn. 2.5 can be expressed abstractly as $Q = \mathcal{L}\psi$, such that Q is given by some operator $\mathcal{L}$ acting on the stream-function of the balanced flow, ψ. Inverting Q to get ψ then consists of inverting $\mathcal{L}$, and acting it on Q. Fields u, v and T can then be calculated from the spatial derivatives of ψ, as detailed below. It is desirable for mathematical ease that an approximation to the Rossby-Ertel PV be derived which can be inverted in a linear fashion.

2.3.1. Quasi-geostrophic potential vorticity theory

Away from the equator and under other assumptions[1] the Rossby-Ertel PV can be approximated by *quasi-geostrophic potential vorticity* (hereafter QGPV) q, first derived by Charney (1948). QGPV is by construction a linear function of a streamfunction ψ, and so can be relatively simply inverted. As a consequence of this simplification, instead of being advected in both vertical and horizontal directions - as Rossby-Ertel PV is - QGPV is only advected by horizontal velocities. QGPV represents a useful simplification of the full Rossby-Ertel PV while still retaining most of the same large-scale dynamics.

In QGPV theory variables are split into background terms that only vary in the vertical coordinate, which for reasons which will become clear is chosen to be geometric height z, and anomaly terms which can vary in both vertical coordinate and time, denoted by subscript $_0$ and prime $'$ respectively:

$$p(z,t) = p_0(z) + p'(z,t)$$
$$\rho(z,t) = \rho_0(z) + \rho'(z,t),$$

and using these terms the buoyancy frequency N can be defined in terms of a background and anomaly,

$$N(z,t) = N_0(z) + N'(z,t), \qquad N^2 = \frac{g}{\theta_0}\frac{d\theta}{dz}.$$

These can be used to define an approximation to the Rossby-Ertel PV Q,

$$q = f + \nabla_H^2\psi + \frac{1}{\rho_0}\frac{\partial}{\partial z}\left(\frac{\rho_0 f_0^2}{N_0^2}\frac{\partial\psi}{\partial z}\right) \tag{2.6}$$

where ∇_H^2 is the horizontal Laplacian operator and f_0 is a constant value of the f parameter. Using the streamfunction ψ the velocities u and v can be obtained by

$$(u,v) = \left(-\frac{\partial\psi}{\partial y}, \frac{\partial\psi}{\partial x}\right). \tag{2.7}$$

[1]Small Rossby number, scale of motion not being significantly larger than the deformation scale, small variations in the Coriolis parameter, and time scales advectively (Vallis, 2006). The Rossby number is the ratio of the sizes of the advective and Coriolis terms in the horizontal momentum equation, given by $Ro = U/fL$ for approximate velocity magnitude and length scale U and L respectively. If Ro is large then rotation is important at the scale of fluid motion considered, while if Ro is small then rotation is unimportant.

This is because the flow is assumed to be geostrophic, and so the anomalous pressure

$$p' = \rho_0 f \psi \tag{2.8}$$

balances with acceleration due to rotation.

A useful analogy to this definition of QGPV is electric charge and the associated electrostatic field. Bishop and Thorpe (1994) outlines how there is a close correspondence between electrical charges and QGPV anomalies, with the streamfunction in QGPV being analogous to the electric potential, and so eqn. 2.6 being equivalent to Gauss' law, see e.g. Griffiths (1998). If one knows the charge (PV) distribution, one can work out the electric (velocity) field, and furthermore a combination of point charges (PV distributions) linearly combine to form an electric (velocity) field via a superposition principle.

Both Q and q are useful ways to describe the disposition of the stratosphere which will be used extensively in later chapters. Now it is time to return to December 1984, and examine what happens when the stratospheric polar vortex is disrupted, displaced, and even splits apart.

2.3.2. Sudden Stratospheric Warmings

The stratospheric polar vortex is the largest feature of the wintertime circulation in the stratosphere, seen in fig. 2.2. Driven by the large equator to pole temperature gradient and intensified in the middle atmosphere by the thermal wind shear relation (see e.g. Andrews et al. (1987)), vortices exist in the northern and southern hemispheres during their respective winters, with the southern vortex being substantially stronger and more uniform than its northern counterpart (Waugh and Polvani, 2010). In the northern hemisphere the vortex forms in approximately November, characterised by very strong westerly winds, and extends from around 200hPa or 15km in altitude (see e.g. Randel and Boville (1987)) through into the mesosphere above the stratosphere, as seen in fig. 2.2. At the end of winter the vortex winds change direction as the stratosphere enters into the summertime easterly pattern shown in fig. 2.2. In the northern hemisphere this typically happens around April (Black and McDaniel, 2007).

There are various ways to describe the strength of the boreal polar vortex. Perhaps

the most direct is the zonal mean zonal wind at 10hPa and 60N, being approximately a measure of the windspeed at the edge of the vortex. This is sometimes known as the polar jet, or polar night jet. See, e.g., Labitzke and Naujokat (2000). Equivalent to describing the vortex as being comprised of strong westerly winds is describing the vortex as a large positive PV accumulation centred over the pole. As such, separating the PV into a climatology and anomaly, the relative strength of the vortex can be characterised by the size and sign of the PV anomaly in the polar region. Another common way to describe the strength of the vortex is to use the principal component time series of the first EOF of the geopotential field in the mid-stratosphere - the Arctic Oscillation (AO) - as an index (see section 2.4.1).

The vortex is eroded by the breaking of planetary waves that have propagated from the troposphere in the stratospheric surf zone equatorward of the polar jet, weakening the circulation. When this forcing is large enough, approximately six times each decade in the northern hemisphere, the regime of a strong westerly stratospheric polar vortex is punctuated by an extreme event known as a *sudden stratospheric warming* (SSW), from the original term used by Scherhag in his 1952 discovery of the phenomenon: *explosionsartige Stratosphärenerwarmung*. These events are accompanied by a increase in temperatures over several days of up to 80K - hence the name - in the mid to upper stratosphere, and in the most extreme cases the westerly circulation of the vortex can be reversed to a weak easterly circulation. See e.g. Quiroz (1975); Labitzke (1977); Schoeberl and Strobel (1978).

There is no one universal definition of what constitutes a SSW. Different definitions are based on different fields, allow for different maximum frequencies of SSWs, and require events to have different durations before being classified as an SSW. Butler et al. (2015) gives a review of various indices for defining a sudden warming, the most common of which are:

1. Zonal mean zonal wind at a high altitude and latitude, most notably at 10hPa and 60°N - as in Charlton and Polvani (2007) (hereafter CP07). A sudden stratospheric warming occurs when the zonal mean zonal wind here falls below 0 m/s between November and March. Events must return to westerly for at least 20 consecutive days before a new warming can be defined, and must return to westerly for at least 10 consecutive days prior to 30 April, or an event is attributed to the final breakup

of the vortex associated with the end of winter;

2. Empirical Orthogonal Functions (EOFs - see p 34) can be used to analyse fields in the winter stratosphere to find the leading order mode of variability, corresponding to the polar vortex. In Gerber et al. (2010), for example, this analysis is performed on zonal mean geopotential heights at 10hPa, weighted by the square root of the cosine of latitude, from 20-90°N. The index is then calculated by projecting the geopotential anomaly data on the calculated first EOF. Sudden warmings are defined as being when the index falls 3 standard deviations or more from the mean, at least 60 days from the most recent event. A similar index was used in Baldwin and Dunkerton (2001), as discussed more fully in section 2.5.1;

3. Vortex moments. Both of the above indices use zonally symmetric data or annular modes, ignoring zonal asymmetries, which can be highly significant during a warming. Elliptical diagnostics (Waugh, 1997) of the stratospheric PV field on a given isobaric or isentropic surface can be used to obtain time series of the vortex area, aspect ratio and centroid latitude (Mitchell et al., 2011). See Hannachi et al. (2011); Seviour et al. (2013), and Mitchell et al. (2013) (hereafter M13). For example, in M13 the centroid latitude and the aspect ratio are used: a warming occurs when the centroid latitude of the vortex is equatorward of 66°N for 7 days or more.

Each of these definitions lead to slightly different frequencies of sudden warmings in reanalysis (Butler et al., 2015).

Causation

SSWs are believed to be caused by wave-mean flow interaction, as first proposed by Matsuno (1971). In the idealised case of purely zonal flow $(\bar{u}(y,z),0,0)$, the QGPV eq. 2.6 can be linearised as

$$\left(\frac{\partial}{\partial t}+\bar{u}\frac{\partial}{\partial x}\right)q'+v'\frac{\partial \bar{q}}{\partial y}=f_0\rho_0\frac{\partial}{\partial z}\left(\frac{\rho_0 Q'}{\partial\theta_0/\partial z}\right) \tag{2.9}$$

where the fields have been decomposed into zonally averaged components, identified by overbars, and zonal eddy or anomaly components, identified by primes. Q here is the

diabatic heating rate, with $Q' = Q - \overline{Q}$ the deviation from the zonal mean. Eq. 2.9 has vertically propagating wave-like solutions, provided that the zonal wind $\bar{u}$ is within some bound. For the simple case of waves with zero phase speed relative to the ground the condition on vertical wave propagation is (see Charney and Drazin (1961))

$$0 < \bar{u} < \bar{u}_c, \quad \text{where} \quad \bar{u}_c = \frac{\beta}{k^2 + l^2 + f_0^2/4H^2N^2} \tag{2.10}$$

where H is a vertical scale height and N is the static stability, and k and l are zonal and meridional wavenumbers respectively. So for Rossby or planetary waves to propagate vertically from the troposphere into the stratosphere, the stratospheric flow must be positive, i.e., westerly, but not too strong. Longer wavelengths with smaller wavenumbers can propagate through stronger westerly flows, which explains why stratospheric asymmetries are larger scale than tropospheric ones (as can be seen in e.g. fig. 4.4), as only the lowest wavenumbers are able to propagate into the strong westerly flow. If the flow were to intensify or become easterly even this wave propagation would be inhibited. In this scenario upward propagating waves would reach a *critical surface* where either $\bar{u} = 0$ or $\bar{u} = \bar{u}_c$, and their linear propagation would break down. The waves would break and impart their momentum on the zonal flow. This occurs in the stratospheric surf zone mentioned above, and is associated with irreversible deformation of the PV field (McIntyre and Palmer, 1983).

Matsuno (1971) proposed that SSWs occur when an anomalously large level of wave activity originating from the troposphere enters the stratosphere, reaches a critical surface and breaks, decelerating the zonal flow. If the forcing is exceptionally large then this deceleration can result in a reversal of the flow from westerly to easterly. This then causes a new critical surface to form where $\bar{u} = 0$. This new critical surface then descends through the stratosphere as further waves break on the surface, causing the zonal circulation at successively lower levels to also switch from westerly to easterly. The descent of the critical surface is also associated with large-scale descent of air masses over the pole, driven by a residual circulation. Eventually the descending critical surface associated with the SSW reaches the tropopause, below which the assumption of purely zonal flow is no longer valid and this analysis breaks down. Planetary waves are effectively prevented from propagating into the stratosphere, and the vortex is left untouched by wave forcing. Radiative cooling

allows the stratosphere to relax to its initial state, the polar vortex reforms over a period of several weeks, and wave forcing is again able to propagate into the stratosphere. The question of what happens dynamically in the troposphere following a sudden stratospheric warming is still not understood (see section 2.5.3).

While all of the above theory is applicable to both hemispheres this thesis will be focusing entirely on the northern hemisphere vortex and associated coupling of events such as December 1984. While there have been several warming events every decade in the northern hemisphere, in the entire observational record there has only been one warming in the southern hemisphere, in 2002 (see *Journal of Atmospheric Science, 2005, 62(3)*). This is likely due to significantly lower wave forcing propagating up into the stratosphere in the southern hemisphere (Newman and Nash, 2005). As such for the remainder of this thesis, when referring to the polar vortex or the polar atmosphere it is implicit that the northern hemisphere is being referred to.

No two SSWs are the same however, and before discussing their influence on the troposphere the distinction between two categories of SSW are now briefly examined.

Splits and displacements

One way of categorising SSWs is into two categories: *splits* and *displacements*. There are other ways of categorising SSWs, such as into wave-1 and wave-2 events, but this thesis will not discuss these. Precisely what constitutes a split and what constitutes a displacement depends on the categorisation algorithm used, but as the name suggests there is a fundamental qualitative difference between the two. Broadly speaking a vortex split occurs when the high PV core of the polar vortex is split into two or more 'daughter' vortices with their own distinct PV cores. An example is shown in fig. 2.3b. A vortex displacement on the other hand involves the PV core of the vortex being contiguously dislocated from the pole and generally distended in some way. It should be noted however that vortex splits are also typically displaced from the pole. An example of a vortex displacement is shown in fig. 2.3c. The two types of SSW have very different evolution timescales, as well as these differences in spatial distribution (Matthewman et al., 2009). The SSW commencing December 25th 1984 is categorised as a vortex split, and two clear daughter vortices can be seen in the temperature field in fig. 1.1.

Seviour et al. (2013) compares the performance of the methods used by M13, CP07, and the simple diagnostic of zonal mean geopotential height at 10hPa at 60°N in distinguishing between splits and displacements. Each definition gives different PV fields on the 850K surface, indicating the sensitivity of distinguishing between splits and displacements. This is shown in fig. 2.4. While splits and displacements have distinct spatial and temporal evolution in the stratosphere, whether they have different signals in the troposphere is a matter of debate (see section 2.5.1).

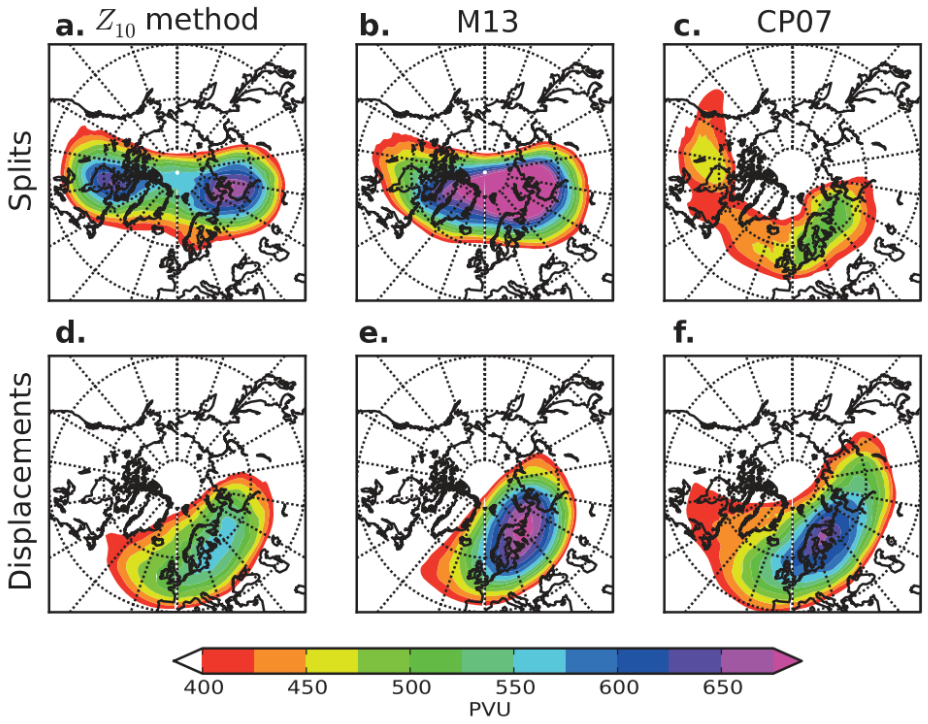

Figure 2.4.: Composites of potential vorticity on the 850K isentropic surface, at approximately 20km in altitude. Composites are taken over the 5 days following the onset date of (a, b, c) split vortex events and 7 days following (d, e, f) displaced vortex events (the difference is due to the different timescales of these events). The geopotential at 10hPa method (Figures a and d) is compared with that of M13 (Figures b and e) and CP07 (Figures c and f). Figure and description from Seviour et al. (2013).

To identify a SSW event as either a split or a displacement requires information about the two dimensional structure of the vortex, which can be described using closed contours of relative vorticity ξ within the edge of the vortex (CP07), or vortex moments (Waugh (1997); Waugh and Randel (1999); Mitchell et al. (2010, 2011), M13). The differences between these algorithms will be examined in detail in chapter 5.

This thesis is concerned with the impact of stratospheric events on the troposphere. As such, now that the dynamics of the stratosphere have been introduced, the dynamics of the troposphere are briefly reviewed before existing evidence of stratosphere-troposphere

coupling and the statistical techniques used in its analysis are covered.

2.4. The stratosphere's influence on the troposphere

The troposphere, in contrast to the stratosphere, is massive, dense, and wet. It has a global general circulation driven by differential heating of the surface (Wallace and Hobbs, 2006; Vallis, 2006). This consists of an easterly-westerly-easterly pattern of zonal winds going from the equator to the pole. In the meridional plane the general circulation is resolved into distinct cells, with the thermally forced Hadley cell consisting of warm air at the equator rising and moving poleward, then descending at approximately 30N. The midlatitudes have a similar but reversed cell, the Ferrel cell. At the approximate boundary between the Hadley cell and the Ferrel cell, and between the troposphere and stratosphere, there exists a midlatitude tropospheric jet stream consisting of a tight band of fast-moving, westerly winds (see fig. 2.2). The midlatitude jet contains large meanders known as Rossby waves (Rossby, 1939), which are driven by the north-south temperature gradient in the midlatitudes. These Rossby waves can vary in the vertical (slow-moving baroclinic waves) or be invariant in the vertical (faster-moving barotropic waves). The action of the baroclinic waves is to reduce the temperature gradient, and to dominate the midlatitude flow with large-scale features such as extratropical cyclones (large areas of low pressure) and frontal zones (narrow bands of large horizontal temperature contrasts). The mean latitude of the midlatitude jet - along with the degree of wave activity causing the jet to deviate from this mean position - can be described using indices covered in section 2.4.1.

The two major differences between the dynamics of the stratosphere and of the troposphere are attributable to the fact that the latter can be convectively unstable, and moist. As such in order to represent the troposphere via an equation of state, the equation for the stratosphere, eq. 2.1, needs to be altered to make it suitable. This can be accomplished this by introducing the virtual temperature,

$$T_v = \frac{r + \epsilon}{\epsilon(1 + r)} T, \tag{2.11}$$

where r is the mixing ratio - the ratio of water vapour mass to air mass in the atmosphere - and ϵ is the ratio of the specific gas constants of dry air and water vapour. T_v can be interpreted as the temperature which a theoretical dry parcel of air would have if it was at the pressure and density of an observed moist parcel of air. As such thermodynamic quantities in the troposphere can be related with an updated version of eq. 2.1,

$$p = \rho R T_v. \tag{2.12}$$

The large scale vertical motion made possible by static instability, and the accompanying latent heat fluxes associated with phase changes of water, cause the troposphere to have very different dynamics from the stratosphere. As these dynamics differ so greatly the boundary between the two domains - the tropopause - is of great importance when considering coupling between the layers. The tropopause has been defined in several ways: in terms of temperature lapse rate (the rate of change of temperature with altitude) (Lewis, 1991), PV (Hoerling et al., 1991), or chemical composition (Bethan et al., 1996). The most fundamental definition of the tropopause is that it separates two regions with qualitatively different dynamics, and perhaps most fundamentally, with qualitatively different heat budgets. The stratosphere is in (or is close to) radiative equilibrium, while the tropical tropopause is (mostly) dominated by convection and the extratropical troposphere by eddy heat transport (Thuburn and Craig, 2000). It should be noted that the tropopause is a very sharp boundary between the stratosphere and troposphere when viewed instantaneously, but becomes a blurry boundary extending over a finite interval when time or spatial averages are taken (Vallis, 2006).

Variations of pressure, geopotential and temperature tend to be much greater in the troposphere and vary over shorter timescales than in the stratosphere, excepting SSW events. The greater variance and chaotic internal variability in tropospheric fields makes identifying downwards stratospheric influence difficult. The problem of more generally attributing variability throughout the rest of the troposphere to stratospheric dynamics are covered more fully in section 2.5, and attempts to explain any observed coupling of dynamics in section 2.5.3.

2.4.1. Annular mode analysis

In describing the dynamics of the atmosphere it can be useful to isolate particular elements of variability rather than considering the complex system as a whole. The most common way to do this is to use *empirical orthogonal function* (EOF) analysis (Lorenz, 1956), also known as principal component analysis (PCA) (Pearson, 1901). EOF analysis transforms a set of observations into a set of linearly uncorrelated variables known as principal components. For technical details of how this is done, see Appendix A.

The first EOF of the pressure field at the surface is known as the *Arctic Oscillation* (AO) (Thompson and Wallace, 1998; Thompson et al., 2000). The AO is also known as the Northern Annular Mode (NAM) in the literature, and is closely linked to a much older index of the principle mode of variability of surface pressure in the northern hemisphere known as the North Atlantic Oscillation (NAO). The NAO was identified as an oscillation of pressure anomalies centred over the Azores and Iceland - when one experienced low pressures the other experienced high pressures, and vice versa - and widely known by the mid-18th century (and possibly as early as the 13th century (Stephenson et al., 2001)). The NAO is highly correlated with the AO (Thompson and Wallace, 1998) and possesses a spatial pattern that can be seen as a subset of the spatial pattern of the AO, although there is still no consensus over which is more physically meaningful - see e.g. Wallace (2000); Ambaum et al. (2001).

By definition, the AO/NAM and its southern counterpart the Southern Annular Mode (SAM) are the leading mode of variability in the pressure field at the surface. The AO can also be constructed using geopotential data on pressure surfaces, shown in fig. 2.5, which allows for a three-dimensional annular mode structure to be defined. As fig. 2.5 shows, this structure proves to be largely barotropic. However just because the AO spatial patterns are large scale and barotropic, this does not necessarily mean that teleconnections implied by it are coherent, as the spatial structure of EOFs have a strong tendency to take the simplest possible structure inside the domain (see Richman (1986); Deser (2000); Ambaum et al. (2001)).

While the AO pattern varies slowly in the vertical, the interpretation of the AO index (the principal component time series associated with the AO) is very different in the troposphere and in the stratosphere. In the stratosphere the AO index can be seen as a measure of the

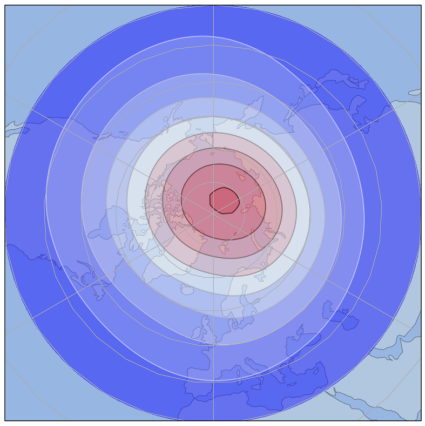

(a) 1hPa

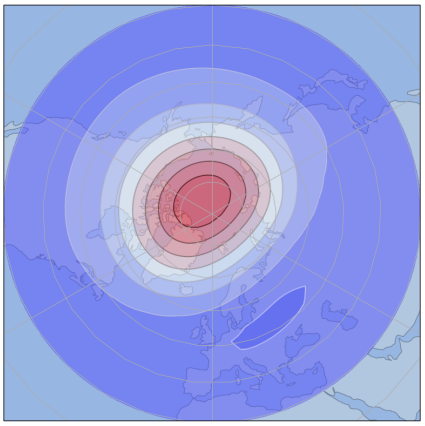

(b) 10hPa

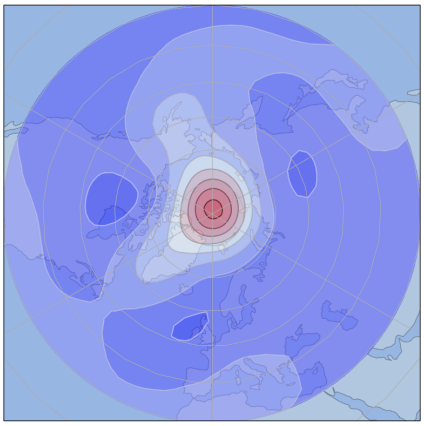

(c) 350hPa

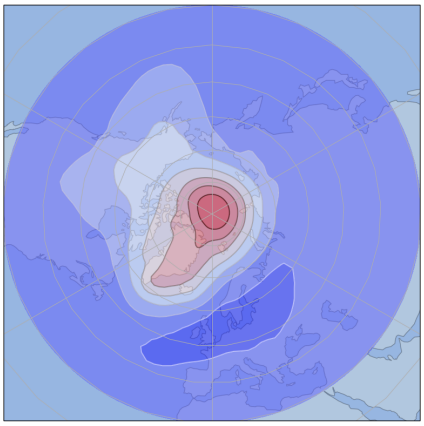

(d) 1000hPa

Figure 2.5.: The spatial pattern of the leading EOF of the geopotential field (the AO) on four pressure levels. Calculated using 33 years of ERA-Interim geopotential data (6 hour and 3°resolution) from 30°to 90°N. Note the almost total zonal symmetry in the stratosphere and the see-saw pattern over the Arctic and the north Atlantic.

strength of the polar vortex, with a very negative AO index corresponding to a SSW event. In the troposphere the AO index can be interpreted the mean latitude of the eddy-driven jet streams and so the storm track (Limpasuvan and Hartmann, 1999), however as the latitude of the jet stream is different in the Pacific and Atlantic this interpretation can be seen as overly-simplistic (Ambaum et al., 2001). As detailed in section 2.5 however, the AO index is still a valuable way of quantifying the link between dynamics in the troposphere and in the stratosphere.

2.4.2. Mass movement

Before moving on to discuss coupling of the stratosphere and troposphere in the literature, there is one simple form of stratospheric influence on the troposphere that is crucial to the rest of this thesis. As implied by the hydrostatic equation there should be a relationship between the movement of mass in the atmosphere and changes in pressure. While the equation is only precise in the case of a static fluid, hydrostatic balance approximately holds everywhere in the atmosphere where vertical accelerations are small compared to gravity.

Baldwin and Dunkerton (1999) (hereafter BD99) considered the propagation of AO index anomalies from the stratosphere to the troposphere, stating that 'elevation of polar-cap SLP [sea level pressure] implies a net transport of mass into this region and vice versa'. While this may seem trivial, it is worth considering in a little more detail.

Historically pressure is only considered at the bottom boundary of the atmospheric system; either mean sea level pressure or surface pressure. However pressure and the AO index, which can be calculated at any level in the atmosphere, can be viewed as two sides of the same coin. The pressure at a given point in the atmosphere is calculated on a given geopotential surface, with sea level simply being a special case where the geopotential is zero. When geopotential is anomalously low on a pressure surface this is equivalent to the pressure at a given geopotential (or a given geopotential height) being lowered. In the context of BD99 and related papers, examining the descent of AO index anomalies (based on geopotential anomalies) is in some sense equivalent to examining the descent of pressure anomalies from the stratosphere to the troposphere, as the AO index is constructed using geopotential anomalies on fixed pressure surfaces. While geopotential anomalies are

usually considered due to pressure being a useful vertical coordinate, considering pressure anomalies on fixed geopotential surfaces allows for an immediate calculation of mass fluxes above those surfaces, which is what much of the rest of this thesis is concerned with.

As such, extending what BD99 said above, the net transport of mass at a given altitude z above the polar region will not just increase polar SLP, but also the pressure at all altitudes less than z. Such net meridional transport of mass into the polar region takes place in a mechanism known as the wave-driven pump (Kidston et al., 2015). The particular equations of this circulation are not relevant to this thesis, but a derivation of the zonally averaged Eulerian mean equations can be found in Vallis (2006), and their subsequent manipulation found in Kidston et al. (2015).

The 'pump' refers to wave deposition of momentum decelerating the zonal circulation and inducing a mean meridional circulation. If wave forcing is increased then the zonal circulation decelerates, and the meridional circulation fluxes mass into the polar region. If this takes place in the stratosphere, where wave breaking is known to occur, then the effect is to slow the polar vortex and move mass into the polar region, forcing the tropospheric pressure field. This also forces the height of the polar tropopause. The associated residual circulation causes air to rise at low latitudes and sink at high latitudes as air is moved poleward. The opposite process takes place when wave deposition of momentum weakens - the vortex speeds up, the residual circulation transports air masses equatorward, the polar tropopause raises, and the tropical tropopause lowers.

This process of mass fluxes forcing the pressure below the location of forcing is trivial, but essential to the theory proposed in chapter 3. Now, further coupling of the stratosphere and troposphere is considered in more detail.

2.5. Stratosphere-troposphere coupling

Stratosphere-troposphere coupling can be defined as any two-way influence of stratospheric phenomena on events in the troposphere, and vice versa. As tropospheric influence on the stratosphere is better understood than stratospheric influence on the troposphere, study of stratosphere-troposphere coupling is often implicitly the study of the latter. Following Haynes (2005), stratospheric influence on the troposphere can be communicated by the following means:

1. Ozone. Changes in stratospheric ozone concentrations create changes in surface ultraviolet irradiance and flux into the troposphere, altering ozone concentrations at the surface (Zeng and Pyle, 2003) with socio-economic implications. Surface temperature variability and so surface climate is dependent on lower stratospheric ozone concentrations (Kilifarska, 2012);

2. Radiative balance of the troposphere. Further to ozone concentrations forcing the radiative balance of the surface and troposphere, varying concentrations of other greenhouse gases such as water (Mote et al., 1996) in the lowermost stratosphere directly force stratospheric temperatures and so change surface temperatures by altering the radiative equilibrium (Maycock et al., 2011) and so again alter surface climate. Surface temperatures can also be altered by aerosols in the stratosphere, such as those injected by major volcanic eruptions, see e.g. McCormick et al. (1995), which persist within the circulation on large timescales;

3. Solar variability. There are various mechanisms by which solar variability - both long- and short-term - affects tropospheric climate and dynamics, many of which are mediated by the stratosphere, as described by Gray et al. (2010) and references therein;

4. Dynamical coupling. This is the mechanical influence of stratospheric dynamics on tropospheric dynamics and what this thesis is concerned with.

2.5.1. Evidence of dynamical coupling in reanalysis

The dominant mode of variability in the stratosphere is the strength of the polar vortex (Butchart et al., 2011), rather than its mean latitude (Gerber et al., 2010). In the troposphere, however, the dominant mode of variability in the mid-latitudes is the mean latitude of the eddy-driven jet streams (Limpasuvan and Hartmann, 1999).

Kodera et al. (1990) identified coupling between the stratospheric polar jet and the strength of westerlies in the polar troposphere. This was then followed by Baldwin et al. (1994) who found that interannual variations in the boreal winter stratospheric flow were strongly correlated with variations in the 500hPa geopotential distribution closely resembling the NAO spatial pattern. The work was then further extended by BD99, which

showed that large-scale anomalies in the principle mode of variability of boreal wintertime geopotential surfaces (i.e. the AO) initiated in the stratosphere propagated downward into the troposphere with a lag of several weeks. This observation was then developed further in Baldwin and Dunkerton (2001) (hereafter BD01). They observed that when the stratospheric polar vortex was weakened, the tropospheric jet stream was displaced equatorwards, and also that when the vortex was strengthened, the jet was displaced polewards. This coupled the principal modes of variability in the stratosphere and troposphere together, and suggested a physical mechanism that dynamically coupled stratospheric variability to that in the troposphere. During the approximately 60 days following extreme stratospheric vortex events the tropospheric response closely resembled the AO spatial pattern. Associated with this AO pattern response, the large variations in the stratospheric vortex shifted the probability distributions of storm tracks in both the Pacific and the Atlantic, and the local likelihood of mid-latitude storms, as shown in fig. 2.7. The response was found to be approximately linear between weak and strong stratospheric wind cases, and present across time scales from weekly variability to multi-decadal climate change (Sigmond et al., 2008). Thompson et al. (2002) examined the surface temperature anomalies following anomalously weak or strong vortex events, as defined in BD01. The authors found that in the 60 days following a weak vortex event most mid-high latitude landmasses were anomalously cold, while extreme eastern Canada and north Africa were anomalously warm. In particular, heavily populated regions such as northern Europe, eastern North America, and east Asia were $\sim$ 1-2 K colder after a weak vortex event than after a strong vortex event. Major cities in the northern hemisphere latitudes were found to experience far more extreme cold winter days (temperature dropping more than 1.5 standard deviations from the JFM mean) in these conditions. The spatial distribution of the temperature anomalies following a SSW was found to be similar, but greater in magnitude, to that of the QBO being in an easterly phase (i.e. stratospheric equatorial winds blowing from east to west). The authors speculated that this was likely due to the effect of the phase of the QBO modulating wave forcing into the polar stratosphere. Other studies have also examined the surface effects of SSWs, with Thompson and Wallace (2001) demonstrating the equatorward shift of storm tracks in their aftermath, Woollings et al. (2010) showing an increase in high-latitude blocking, and Tomassini et al. (2012) finding an increase in cold outbreaks in northern Europe.

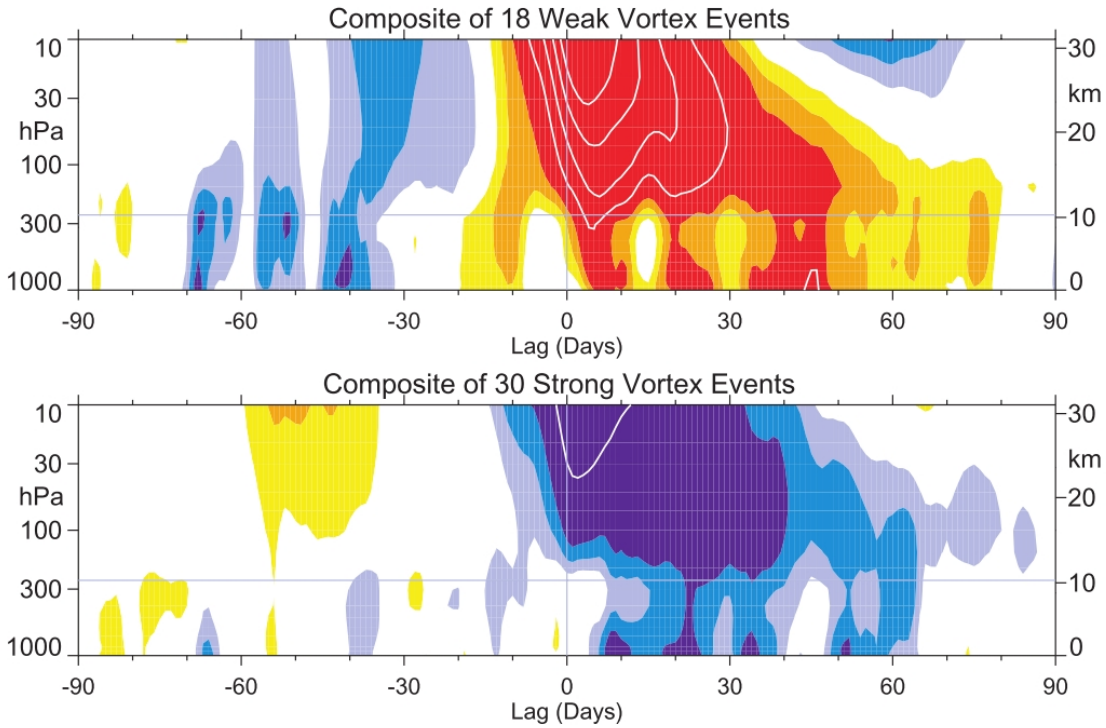

Figure 2.6.: Composite of the downward propagation of vortex anomalies, for both anomalously strong and anomalously weak vortex conditions. In this instance a strong (weak) vortex event is defined as when the 10hPa dominant annular mode crosses the +1.5 (-3) standard deviation threshold. The indices are non-dimensional; the contour interval for the color shading is 0.25, and 0.5 for the white contours. Values between -0.25 and +0.25 are unshaded. Figure from BD01.

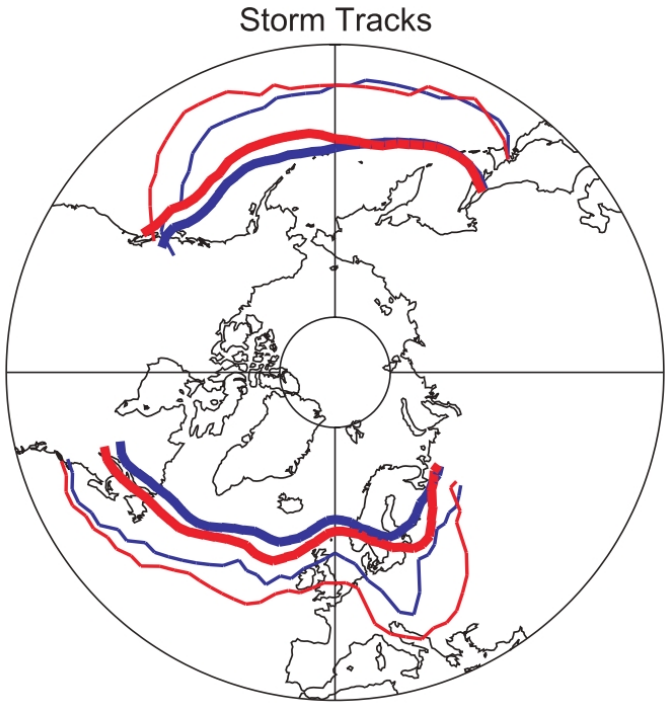

Figure 2.7.: Average latitudes of surface cyclones (defined as closed low-pressure centres less than 1000 hPa) in the Atlantic and Pacific sectors for the 1080 days during weak vortex regimes (thick red lines) and the 1800 days during strong vortex regimes (thick blue lines). The thin lines indicate the lowest latitude at which a cyclone frequency of one per two weeks is expected. Figure from BD01.

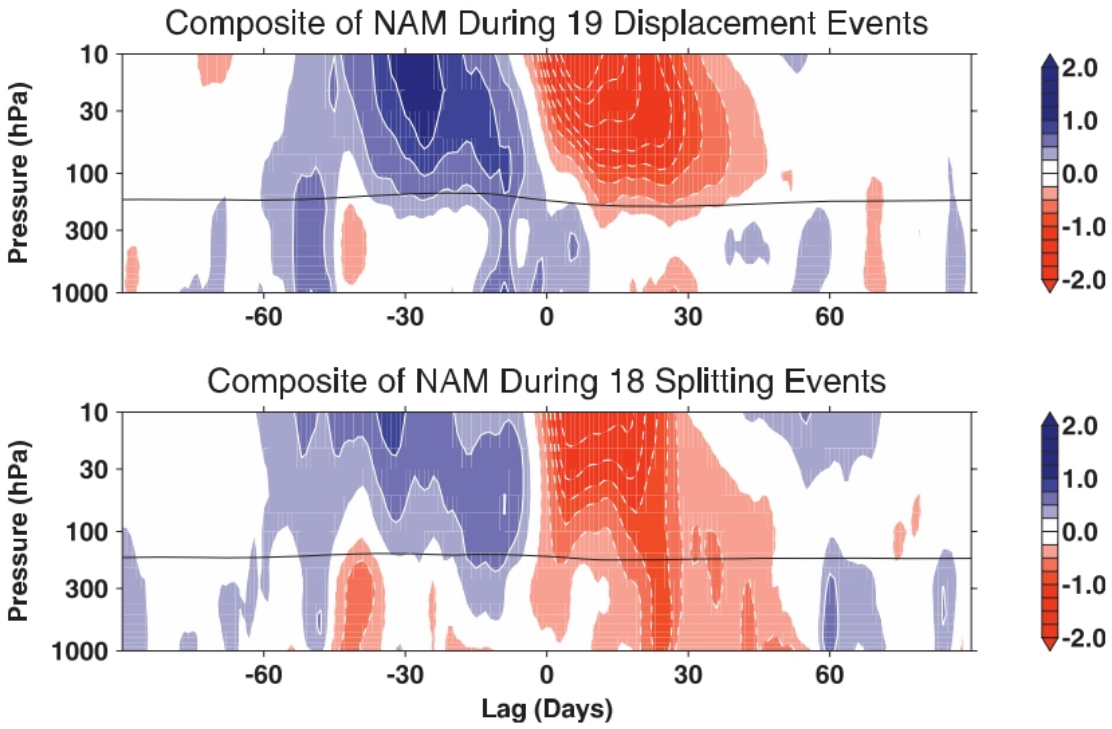

Figure 2.8.: Composites of 18 polar vortex splits and 19 polar vortex displacements and their coupling to the troposphere as a time-height plot of the Northern Annular Mode (NAM) index. Lag 0 shows the onset of an event as measured at 10 hPa. Contour intervals are 0.25 and the region between -0.25 and +0.25 is unshaded. Figure from M13.

M13 used an index based on spatial moments of the PV distribution, using the polar vortex's area, centroid latitude, and aspect ratio. M13 found that splits and displacements produced very different temperature, NAM, and mean sea level pressure (MSLP) anomaly distributions in the troposphere. Fig. 2.8 shows the difference in NAM index through the troposphere and lower stratosphere before and after vortex splits and displacements, qualitatively demonstrating that vortex splits couple to the tropospheric dynamics much more than vortex displacements. The NAM index after vortex splits was found to show a statistically significant response at the 5% level, while the surface NAM index in the aftermath of vortex splits was not found to be significantly altered.

2.5.2. Evidence of dynamical coupling in climate models

In addition to reanalysis, it is worth briefly reviewing the evidence and structure of stratosphere-troposphere coupling in numerical models. The first published study of stratospheric influence on the troposphere in a model was in Boville (1984), which used a spectral model to perform two simulations - one with consistent horizontal diffusion in the stratosphere, and one with diffusion only of certain wavenumbers. The effect of this

was to vary the structure of the stratospheric polar vortex. Between the two simulations there were significant differences in tropospheric fields such as the position and strength of stationary planetary waves, and the amount of eddy activity. Thus it was concluded that changing the structure of the stratospheric polar vortex could result in downward influence, and modification of tropospheric fields such as zonal wind.

The downward propagation of polar stratospheric circulation anomalies into the troposphere was subsequently studied in simplified models (e.g. Yoden (1987)). The first published study of this phenomena in a 3D general circulation model was in Christiansen (1999) and then Scaife and James (2000), which identified descending vacillations in the stratospheric wind field similar to the QBO but with shorter time scales. These studies however assumed a perpetual January and did not include an annual cycle, making direct comparisons to reanalysis problematic. The first paper to include the annual cycle was Christiansen (2001), which examined the downward propagation of zonal mean zonal wind anomalies from the stratosphere to the troposphere. The paper found good agreement between the model used (the ARPEGE/IFS cycle 14 GCM) and National Center for Atmospheric Research (NCAR) reanalysis, identifying such anomalies. The paper also found a statistical link between the vertical component of wave flux from the troposphere propagating into the stratosphere, and the descent of zonal wind anomalies - speculating that the downward propagation was driven by tropospheric wave activity.

A comprehensive investigation of the coupling of the stratosphere and troposphere was conducted in Hitchcock and Simpson (2014), which used a nudging technique to artificially induce a (zonally symmetric) vortex split SSW and a vortex displacement SSW in a large ensemble of runs using the Canadian Middle Atmosphere Model. By experimental design - maintaining the same zonally averaged stratospheric state across the ensemble but allowing different tropospheric regimes - the direct effect of SSWs on the troposphere could be isolated, with the models producing a tropospheric annular mode response closely analogous to that seen in reanalyses. This confirmed the downward influence of SSWs on the troposphere in a comprehensive model, and also confirmed the highly zonally asymmetric near-surface response, corresponding to a very negative phase of the NAO. The response was also found in other Coupled Model Intercomparison Project Phase 5 (CMIP5) models, though the response generally having too small an amplitude.

It should be noted that M13's conclusion that splits and displacements produce different tropospheric effects is not uniformly accepted. Maycock and Hitchcock (2015) compared the NAM signatures of splits and displacements in a 1000 year GCM run using two different algorithms for defining splits and displacements, and they found that a large (>50) number of events was required to distinguish even a small difference in the tropospheric responses. Even then the difference between the response following splits and displacements was not consistent between algorithms.

Finally there is not an absolute consensus on the existence of the downward influence of stratospheric circulation anomalies on the troposphere. Plumb and Semeniuk (2003) used 1- and 3-dimensional models to demonstrate that extratropical zonal wind anomalies in the stratosphere could descend into the troposphere naturally as a response to forcing in the lower stratosphere. This was shown to be the same mechanism as exhibited in the downward progression - but not influence - of the QBO. However, as Haynes (2005) notes, when examining the QBO the two key assumptions of small Coriolis parameter and slow varying waves involved are valid. In the polar region neither of these assumptions are valid, as the Coriolis parameter is large and the waves considered are large vertical wavelength Rossby waves, which do not vary slowly.

2.5.3. Proposed theories of dynamical coupling

Existing theories of how the stratosphere is dynamically coupled to the troposphere fall into three main groups:

Planetary waves

Given that the troposphere is known to significantly influence the stratosphere via the propagation and breaking of planetary waves, it is perhaps natural to assume that the communication could in fact go both ways. Quite how this is accomplished is a matter of some debate.

Firstly, there is one school of thought that the tropopause acts as a kind of valve for upward propagating planetary waves. Chen and Robinson (1992) found that lower stratospheric conditions - in particular the shear in zonal wind and the vertical gradient of buoyancy

frequency at the tropopause - control the transmission of planetary waves into the stratosphere. Following Charney and Drazin (1961), the 'refractive index' of the stratosphere as seen from the tropopause is highly sensitive on lower stratospheric conditions, though not on upper stratospheric conditions. Under suitable stratospheric conditions, planetary waves are reflected off some layer - either the tropopause or some higher level (approximately 5hPa according to Perlwitz and Harnik (2003)) - and propagate back through the troposphere. The reflected waves then interfere with existing waves within the troposphere, influencing the mean latitude of the midlatitude westerlies through wave-mean flow interactions (e.g. Limpasuvan and Hartmann (2000)).

A second school of thought is that downward-propagating interactions between planetary waves and the zonal mean flow, known to exist in the stratosphere and detailed in papers such as Holton and Mass (1976), continuing in some modified way below the tropopause into the troposphere. This mechanism is postulated in Hartmann et al. (2000) and Perlwitz and Harnik (2004). The former suggested that the continuation of downward propagation would be dependent on lower stratospheric conditions, and sensitive to parameters such as stratospheric ozone concentrations. The latter concluded that there are effectively two stratospheric winter states - one in which the majority of upward propagating wave momentum gets deposited in the stratosphere and wave-mean flow interaction dominates, and a second in which wave activity gets reflected down to the troposphere, as in the above. They note however that this is not a complete description of the downward propagation of information, and that other processes may 'play a role'.

Downward control

An alternative, and more mathematically formulated, hypothesis is known as downward control. Originally outlined in Haynes et al. (1991) and summarised in Haynes (2005), the hypothesis is that if anomalous wave breaking in the stratosphere is sustained for a sufficiently long time, the wave transport of PV equilibrates with creation and destruction of PV by radiative processes. In this equilibrium, the influence of the wave driving is transmitted through an induced secondary meridional circulation, which transports mass polewards and *downwards*. Crucially the influence of any region of wave breaking almost exclusively extends to levels below the region, with a weak, upward-propagating response above (Holton et al. (1995)). Downward control was not formulated with the intention

of explaining dynamical coupling of the stratosphere and troposphere, instead being motivated by examining the influence of wave forcing on vertical velocity, temperature, and chemical transport in the lower stratosphere. It has however been suggested as an explanation of observed coupling. While the underlying processes of downward control are well understood, it is not clear if the theory is capable of inducing substantial coupling to the troposphere.

Song and Robinson (2004) tested a modified version of downward control called 'downward control with eddy feedback' (DCWEF) - in which signals transmitted down into the troposphere from stratosphere wave forcing were amplified by eddies in an idealised GCM. The paper found that while the direct tropospheric response to stratospheric forcing was weak, transient eddy feedbacks amplified the response to a robust one that projects onto the model's intrinsic tropospheric modes. Furthermore the paper found that if downward-propagating planetary waves were damped in the lower stratosphere the tropospheric response to a given forcing was reduced, leading the authors to conclude that DCWEF combined with the propagation of planetary waves worked together to communicate stratospheric information to the surface.

Egger and Hoinka (2005) investigated wave forcing in ERA data and found that the structure of all observed forcing is not compatible with the assumptions of downward control, and the meridional circulation observed and associated with the forcing differs from what downward control predicts. In other words, the above studies showed that under suitable stratospheric forcing a tropospheric response is predicted, potentially explaining the downward propagation of stratospheric circulation anomalies. Egger and Hoinka (2005) however did not find evidence of such appropriate forcing existing. The study did not examine upper stratospheric fields however, and the authors did not exclude the possibility that appropriate localised forcing domains do occur.

Non-local PV effects

Another mechanism for coupling is that the far-field effects of changes in the stratospheric PV distribution communicate information to the troposphere. The mechanism is analogous to classical electrostatics, as discussed in Bishop and Thorpe (1994) - the streamfunction associated with a given PV distribution is akin to the electrostatic potential associated with an electric charge, with the velocity field being the gradient of the streamfunction as the electric field is the gradient of the potential. In this instance changes to the PV field due to wave breaking bring about changes in the far-field streamfunction in the troposphere, influencing tropospheric characteristics such as the mean latitude of the tropospheric jet.

Robinson (1988) was the first paper to use QGPV dynamics to investigate the influence of the stratosphere on the troposphere, working under the assumption that the stratospheric flow is strongly dominated by local potential vorticity. The author concluded that while the tropospheric geopotential fields did exhibit changes in the aftermath of a sudden warming in January 1979, many more events would need to be examined before any general conclusions about downward influence of stratospheric PV could be reached. Ten years later Hartley et al. (1998) had the benefit of significantly more data, and extended the use of quasi-geostrophic *piecewise potential vorticity inversion* (PPVI) analysis from the previous paper. The technique uses the linearity of the QGPV equation to allow for the streamfunctions associated with separate PV distributions to be linearly superposed (much like how electrostatic potentials associated with different electric charges can be superposed) allowing a global PV field to be separated into distinct 'pieces' or spatial regions. The study investigated the influence of stratospheric PV anomalies relative to tropospheric PV anomalies on tropopause height, and found that when the stratospheric polar vortex is distorted - as quantified by a redistribution of the stratospheric PV - there are significant perturbations in upper tropospheric fields, including the tropopause height. The influence on tropopause height of stratospheric PV was found on occasion to be as important as tropospheric influences, leading the authors to conclude that the stratosphere was a far more important influence on tropospheric fields than previously thought. This conclusion was further investigated in Black (2002), which demonstrated that large-scale potential vorticity anomalies in the stratosphere induce an annular pattern of zonal wind perturbations that extend down through the troposphere to the Earth's surface. This is

in agreement with BD01's description of descending AO index anomalies. The study also discussed two different timescales and causalities of stratosphere-troposphere coupling: if on the short scale nonlinear breaking of tropospheric waves in the stratosphere results in the redistribution of PV and changes to the AO index in the troposphere, the process can best be thought of as a dynamical feedback to the troposphere. On longer timescales, however, stratospheric radiative processes play a key role in determining the strength of the stratospheric polar vortex, suggesting a downward stratospheric forcing, rather than a two-way feedback.

Finally, and most relevantly for this thesis, Ambaum and Hoskins (2002) (hereafter AH02) investigated AO index coupling between the stratosphere and troposphere, and also investigated surface pressure changes in response to variations in polar vortex strength. The authors proposed a mechanism of stratosphere-troposphere coupling depicted in fig. 2.9: if the tropospheric AO index increases, upward-propagating planetary waves refract away from the polar region, breaking less in the stratospheric jet. This anomalously weak wave breaking in the jet results in a positive PV anomaly within the polar vortex, which raises the tropopause underneath it - leading to an enhanced cyclonic circulation over the pole. Crucially, the stretching of the tropospheric column associated with a raised tropopause results in lowered surface pressure at the pole.

It is worth discussing the language regarding causality used in many of the above studies investigating the far-field effects of PV. Spengler and Egger (2012) examined the claim that changes in the far-field are "caused" by PV anomalies, testing the attribution by seeking an unbalanced initial state containing some PV anomaly, but without a far-field from which the balanced flow can be attained by geostrophic adjustment. The paper found that the far-field can evolve from a localised anomaly without a far-field - and as such that there is no unequivocal causal relationship between the far-field of the PV anomaly and the anomaly itself. In other words it is not correct to say that a given PV anomaly "causes" changes in the far-field. This does not diminish the usefulness of PV as a diagnostic variable, or PPVI as a tool, rather it is important to stress that while there is an inherent link - under the assumptions of geostrophic and hydrostatic balance - between the far-field flow and a PV anomaly, that relationship is not causal. PV is instead a localised variable that binds much non-local information within itself, in a convenient to manipulate form.

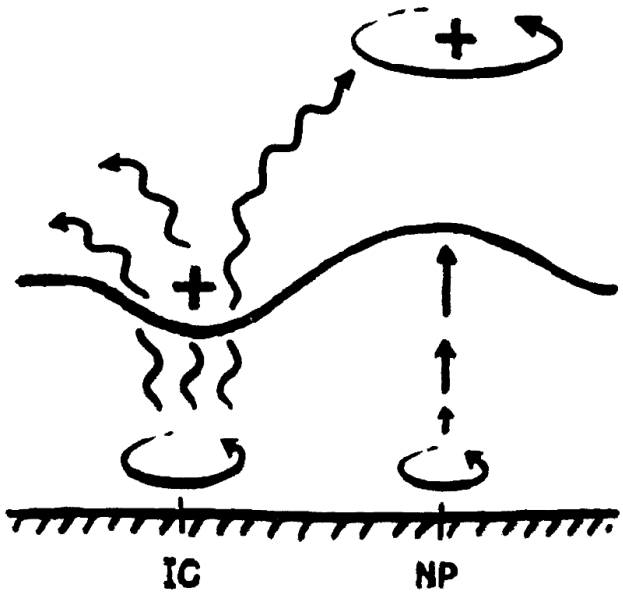

Figure 2.9.: Figure from AH02 summarising the interactions between the strength of the NAO, the height of the tropopause, and the strength of the stratospheric polar vortex. If the AO/NAO index increases, the cyclonic circulation over Iceland (IC) intensifies, lowering the tropopause there. This is then associated with a positive PV anomaly in the stratosphere above Iceland, which refracts upward propagating planetary waves more towards the equator. As a result planetary waves break less in the stratospheric jet, intensifying it and causing a positive PV anomaly over the pole (NP). This spin up then raises the polar tropopause, stretching the polar atmospheric column and enhancing the cyclonic circulation there.

2.6. Summary

The stratosphere and troposphere are two regions of the Earth's atmosphere with very different dynamics. In the stratosphere temperatures increase with altitude and the circulation is strongly dependent on the season, while in the troposphere temperatures decrease with altitude and the circulation varies on smaller temporal and spatial scales. The winter circulation in the northern hemisphere stratosphere is dominated by a polar vortex of strong westerly winds, which occasionally undergo violent events known as sudden stratospheric warmings, such as occurred on December 25th, 1984. In these events the strong winds slow or even reverse for a short time, associated with massive, rapid warming in the stratosphere. These warming events have also been associated with changes in the troposphere for a period of time following the warming, but why this happens is not yet understood.

In the following chapter a simplified model of the stratosphere-troposphere system will be proposed, and an associated new theory of the stratosphere's downward influence on the troposphere defined.

3. Theoretical work

"There is a way out of every box, a solution to every puzzle; it's just a matter of finding it."
- *(Picard, J-L)*

3.1. Aims

This chapter proposes a new view of stratospheric influence on the troposphere, making connections between the AO index, stratospheric PV, and polar pressure. The movement of mass in the atmosphere is shown to be related to changes in polar pressure, and this mass movement is related to the stratospheric PV. Mass transported into the polar region is estimated from reanalysis, and subsequent vertical redistribution of mass within the polar column examined. The mass flux associated with a given redistribution of stratospheric PV, and the resulting change in pressure throughout the polar atmospheric column, is then approximated using quasi-geostrophic theory.

3.2. The plunger hypothesis

A simple model of the polar region is a large column of air surrounded by a reservoir, as shown in fig. 3.1. Fields such as temperature, geopotential, and PV within this *polar cap* can be spatially averaged to give polar cap averages. Of these fields the polar cap pressure, evaluated on constant altitude z surfaces throughout the column, is the most important - being an index of stratospheric influence on the troposphere (see section 3.2.1). This is discussed in Baldwin et al. (2018), which proposes the so-called *plunger hypothesis*. The

eponymous plunger is the column of air discussed above, with mass transported across its boundaries causing polar cap pressure anomalies throughout the plunger. The plunger hypothesis can be summarised as follows:

1. Anomalous wave activity in the midlatitude stratosphere decelerates the zonal circulation, inducing a meridional circulation

2. This redistributes the stratospheric PV field, causing a polar stratospheric PV anomaly

3. The far field effects of these stratospheric polar PV anomalies act to anomalously flux mass into the polar region

4. This anomalous mass flux then forces pressure anomalies throughout the column of the polar atmosphere via hydrostatic adjustment.

This can be interpreted as a generalisation of the hypothesis presented in AH02. However instead of only considering the pressure response at the surface to changes in the polar stratospheric PV distribution, pressure throughout the polar column is considered. Further details of each of these points are now given.

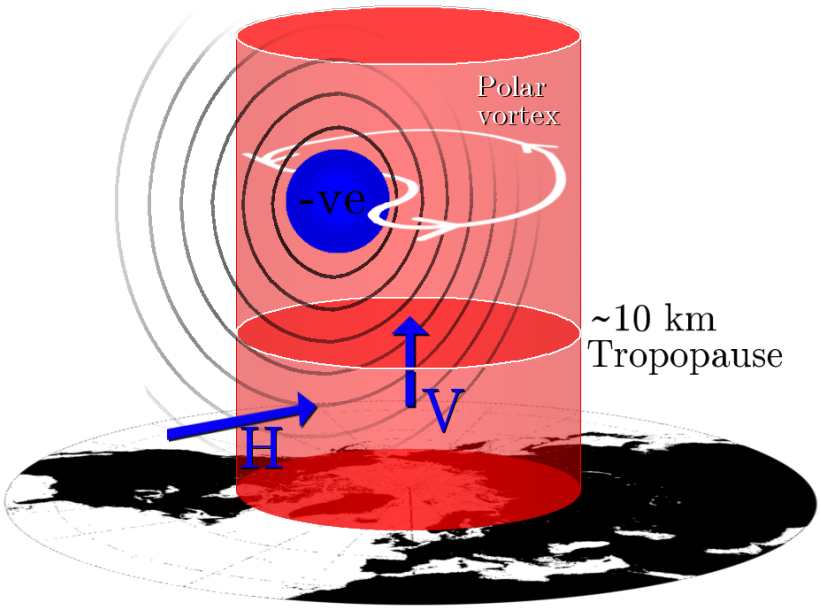

Figure 3.1.: Overview of the polar plunger. The domain considered is 30-90°N, -180-180°E. The polar cap is the red volume 65-90°N, -180-180°E, roughly encapsulating the polar vortex. The index p_i is averaged on z surfaces in this area. The far-field effect of PV anomalies in the polar stratosphere force p_i by transporting mass across the boundary at 65°N, H, and vertically moving mass within the cap, V.

3.2.1. Pressure as an index of stratosphere-troposphere coupling

Conventionally the AO index is used as a measure of stratosphere-troposphere coupling, such as in BD99 and BD01. This thesis however will not use the AO index on pressure levels as a coupling index: instead it will use spatially-averaged temporal pressure anomalies, defined later, on geopotential height levels. This is done because the mechanism of the plunger hypothesis is based on mass fluxes in the atmosphere, and as pressure is the vertical integral of mass in the atmosphere it is the logical choice for monitoring fluxes of mass. Unless otherwise specified, for the remainder of this thesis the vertical coordinate used will be geopotential height, $z = \phi/g$.

Any new index used to identify coupling should demonstrate similar behaviour as previously used indices, such as the AO index. As shown in fig. 2.5, the spatial patterns of the AO vary as the vertical coordinate is increased. However, it is consistently pole-centred with an annular structure, where broadly speaking if geopotential is anomalously high over the pole the geopotential will be anomalously low over the midlatitudes, and vice versa. As such, on a given pressure level, the gross structure of the AO index can be captured by considering the average geopotential anomaly over some area centred over the pole. When this anomaly is positive, the AO is in a positive state, and the larger the geopotential anomaly, the larger the AO index. Baldwin and Thompson (2009) found that zonally averaged geopotential anomalies correlate highly with the NAM index. However, from hydrostatic balance $\delta p = -\rho g \delta z$, and so pressure anomalies are proportional to geopotential anomalies. As such, considering the average geopotential anomaly on p surfaces in the polar cap is equivalent to considering anomalies of the polar cap pressure on z surfaces, up to a constant of proportionality. The behaviour of the AO index can then be approximated by the behaviour of the polar cap pressure.

Using fig. 2.5 as a reference, a reasonable area to consider for the polar cap is 65-90°N, across all longitudes, as found to be optimal by Baldwin and Thompson (2009). This area bounds the positive node of the AO on all levels shown, and so the average pressure within this area is expected to correlate well with the value of the AO index. A pressure index can be defined as:

$$p_i = \frac{\int_A p' \, dS}{\int_A dS} \tag{3.1}$$

where A is the polar cap north of 65°N, and dS is the associated surface integral element. Latitude 65°N approximately corresponds to the so-called stratospheric surf zone (see p24) and as such can be viewed as the approximate horizontal edge of the vortex. The p' in eq. 3.1 is the pressure anomaly - the deviation from the deseasoned and demeaned pressure on a given height surface.

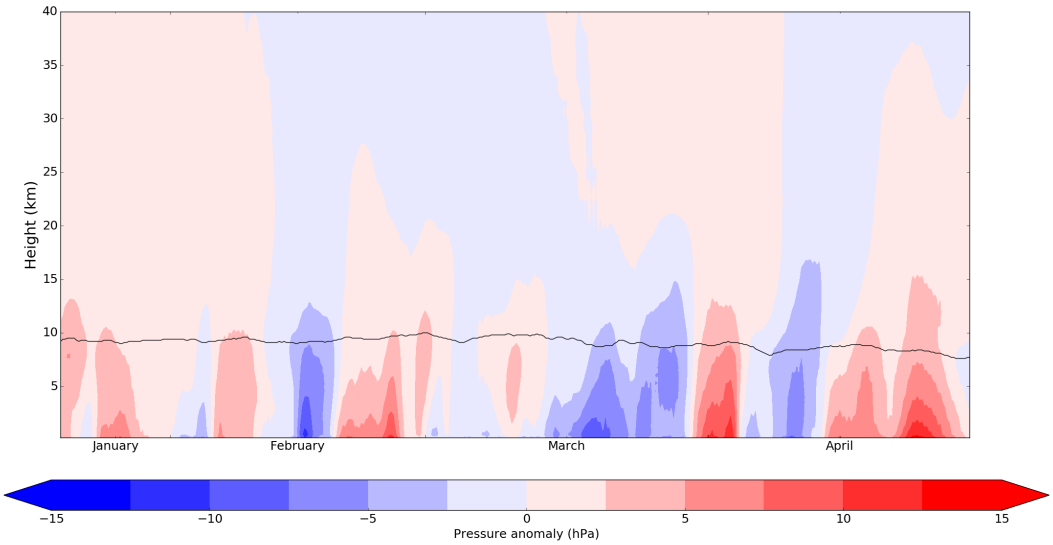

Figure 3.2.: One hundred days of pressure index data on constant height surfaces from 1981. The black line indicates the location of the thermally-defined tropopause, defined as the lowest level at which the polar cap lapse rate decreases to $2K/km$ *and* the mean lapse rate of all higher levels within 2km does not exceed $2K/km$. Data from ERA-Interim.

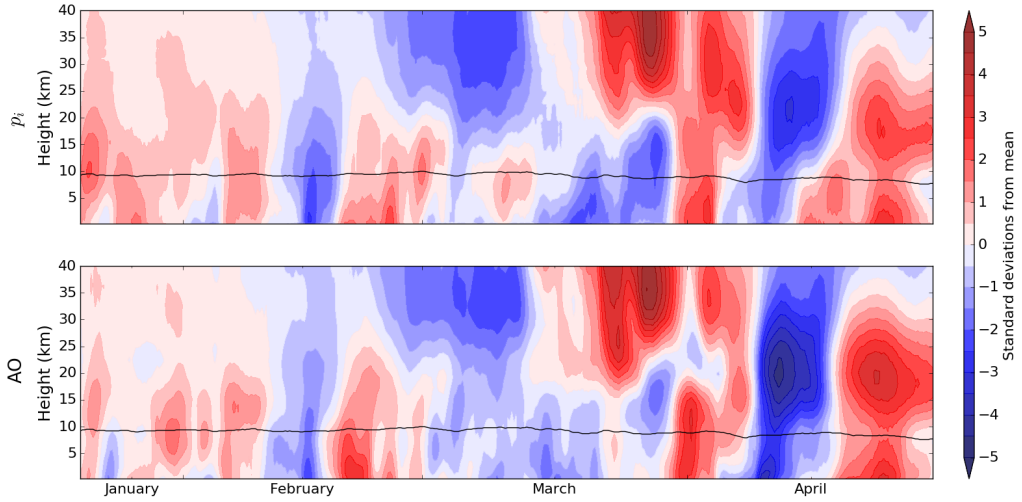

Figure 3.3.: As fig. 3.2 but plotting the standardised pressure index and directly comparing to the AO index by resampling the AO index on z surfaces. The standardised pressure index is plotted on top, and the AO index below.

The pressure index p_i then consists of pressure anomaly averaged within a cylinder of air centred over the pole and approximately encompassing the vortex, as in fig. 3.1. Figure 3.2 shows how p_i varies over 100 days.

To make the index more revealing it can be standardised by dividing by the standard deviation at each height, to give a dimensionless index, as shown in fig. 3.3. Fig. 3.3 shows that the standardised pressure index closely resembles variations seen in the AO index. By linearly interpolating the AO index on z surfaces quantitative comparisons can also be performed. As shown in fig. 3.4 the AO and pressure indices have high correlations in the troposphere that increase to greater than 0.9 in the stratosphere.

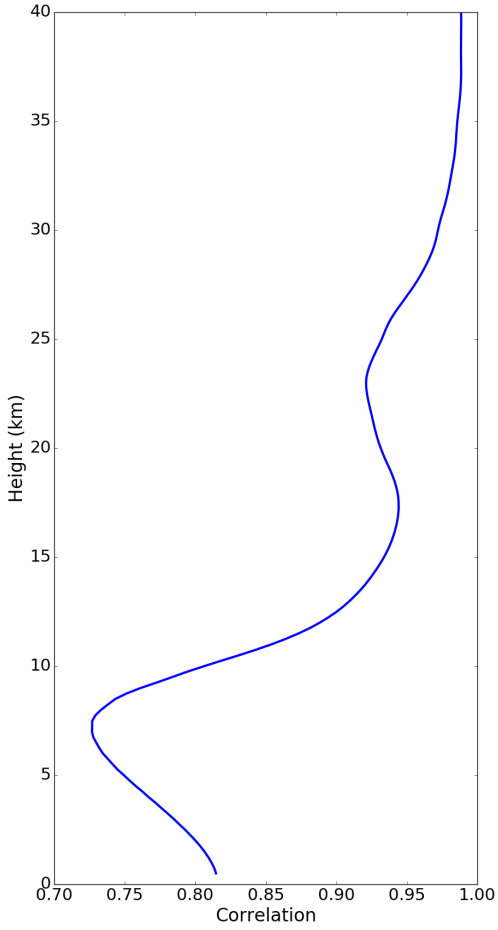

Figure 3.4.: The correlation of the pressure index and the AO index (interpolated on z surfaces) as a function of height, vertical resolution of 250m. Geopotential data from ERA-Interim (1979-2012).

Using the standardised pressure index the downward propagation of extreme stratospheric events can be considered. Following BD01, an extreme event is defined to begin when the magnitude of the pressure index at 25km, or the AO index at 10hPa, exceeds +3.5 or -2 standard deviations. Fig. 3.5 shows the composite index plots of these events for both the AO index and the normalised pressure index. 33 years of ERA-Interim data were used (1979-2012). Events defined using the pressure index on the 25km surface (top row) yielded 15 positive events and 39 negative events, while events defined using the AO index on the 10hPa surface (bottom row) yielded 11 events positive events and 48 negative events. The standardised pressure index shows the same qualitative behaviour as the AO index, recreating the same result as seen in BD01. Based on figs. 3.3-3.5 then it is not unreasonable to suggest that the pressure index can be used to investigate stratosphere-troposphere coupling as a coupling index, as has been done previously with the AO index.

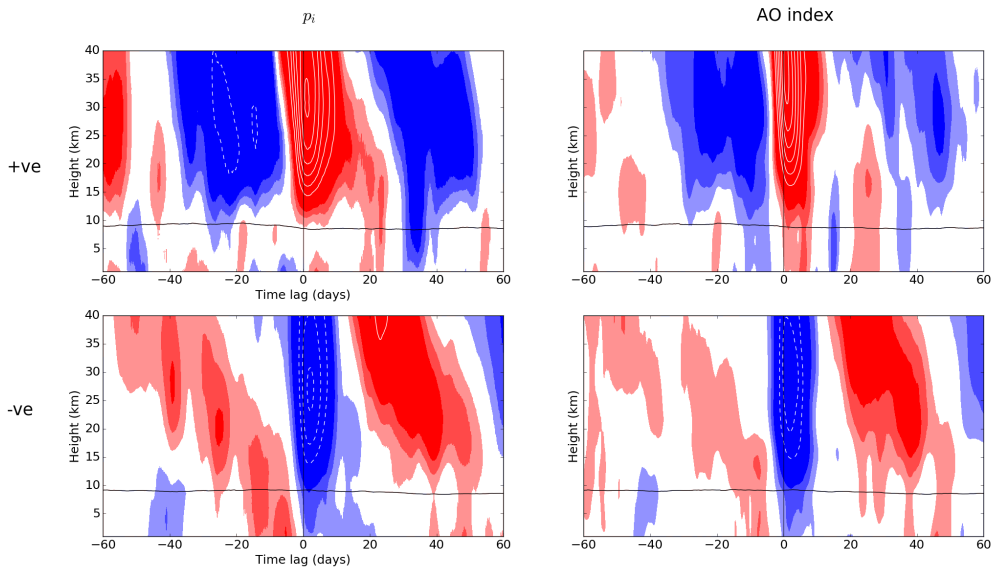

Figure 3.5.: Dripping paint plots as in fig. 2.6, reconstructed using the pressure index in the left column and the AO index in the right column. Contour intervals for the colour shading is 0.25, and 0.5 for the white contours. Index values from -0.25 to +0.25 are unshaded.

3.2.2. The polar plunger

In the plunger hypothesis (Baldwin et al., 2018) the polar region is imagined as a large plunger filled with air, surrounded by a reservoir (fig. 3.1). The plunger has fixed vertical boundaries at 65°N and the top of the plunger is sealed with a moveable impermeable lid.

In the case of a simple plunger with impermeable walls the pressure response throughout the column to a mass forcing at the top of the column is simple: uniformly linear as no air can escape. This is obviously not a realistic model of the polar atmosphere. If however some air is allowed to flow through the walls of the plunger into the reservoir of air then its response becomes more interesting, though still governed by eq. 2.4.

Of course while the polar atmosphere does not have fixed vertical boundaries to prevent air flowing in and out of the region, p_i does have an artificial hard boundary, at 65°N. As such the dynamics of p_i will have some similarities to the pressure within a plunger, with the pressure at some level - itself the vertical integral of all mass above that level - forcing the column of air underneath.

There are two governing equations for this interaction,

$$\text{Hydrostatic balance:} \quad \frac{\partial p}{\partial z} = -g\rho \tag{3.2}$$

$$\text{Conservation of mass:} \quad \frac{\partial \rho}{\partial t} + \nabla \cdot (\rho \underline{u}) = 0, \tag{3.3}$$

The hydrostatic response of the plunger system to mass fluxes can be derived by integrating eq. 3.2 vertically and taking the time derivative:

$$\frac{\partial p}{\partial t}(z) = g \int_z^\infty \frac{\partial \rho}{\partial t}\, dz', \tag{3.4}$$

where g has been assumed to not vary in time or height on the time and vertical scales considered. However to evaluate the evolution of p_{av}, a spatially-averaged pressure field, using eq. 3.4 requires a spatially-averaged density,

$$\frac{\partial p_{av}}{\partial t}(z) = \frac{g}{A} \int_z^\infty \int_S \frac{\partial \rho}{\partial t}\, dS\, dz', \tag{3.5}$$

where

$$A = \int_S dS, \tag{3.6}$$

with S as the area of the polar cap and $dS = \cos(\varphi) d\varphi d\lambda$ the associated surface element. It will be shown later that $p_{av} \simeq p_i$ in this study. Substituting in eq. 3.3 to eq. 3.5 yields

$$\frac{\partial p_{av}}{\partial t}(z) = -\frac{g}{A} \int_z^\infty \int_S \nabla \cdot (\rho \underline{u})\, dS\, dz', \tag{3.7}$$

which is equivalent to the volume integral of the divergence of momentum in the polar cap bounded vertically by height z and infinity. As such by the divergence theorem

$$\int_V \nabla \cdot (\rho \underline{u})\, dV = -\int_S \rho \underline{u} \cdot \underline{dS} \tag{3.8}$$

for momentum $\rho \underline{u}$ in a volume V bound by a surface S with surface vector $\underline{dS}$ pointing inwards, the integral is given by the total flux into the polar cap. For a given height this can be separated into flux across the low latitude limit of the cap φ_b, i.e. horizontal flux,

and vertical flux across the low z limit of the cap:

$$\frac{\partial p_{av}}{\partial t}(z) = \frac{g}{A}\left(\int_z^\infty \oint_{\varphi_b} \rho v \; a \; \cos(\varphi_b) \; d\lambda \; dz' + \int_S \rho w \; dS\right) \tag{3.9}$$

For the rest of this thesis this is notated as

$$\frac{\partial p_{av}}{\partial t}(z) = \frac{g}{A}\left(H(z) + V(z)\right). \tag{3.10}$$

where

$$H(z) = \int_z^\infty \oint_{\varphi_b} \rho(\lambda, \varphi_b, z') \; v(\lambda, \varphi_b, z') \; a \; \cos(\varphi_b) \; d\lambda \; dz' \tag{3.11}$$

$$V(z) = \int_S \rho_i(z) w_i(z) \; dS. \tag{3.12}$$

The assumption has been made in eq. 3.12 that there is no vertical mass flux at the top of the domain. The expressions 3.10-3.12 can be interpreted as the sum of vertical integral of the horizontal mass flux above z and the total vertical mass flux across the surface z forcing the evolution of the polar cap pressure at height z.

3.3. Mass fluxes in reanalysis

As stated in point 4 on page 50, anomalous mass transport into the polar region forces anomalies in the polar cap pressure index, p_i. This has now been quantified for given horizontal and vertical mass fluxes H and V in eq. 3.10. This result can be tested using mass flux data calculated from reanalysis, comparing the observed evolution of p_i to that predicted by eq. 3.10.

To obtain H, the density ρ at the latitude boundary $\varphi_b = 65$ N is calculated using eq. 2.12, accounting for the effect of moisture on tropospheric density, and multiplied by v at φ_b. Six hourly ERA-Interim fields for v, T, and r, the mixing ratio, were used from 1979 to 2016. To compare mass transport to the evolution of p_i, H and V must be split into anomaly and background terms, as p_i is constructed using pressure anomalies (eq. 3.1). After filtering H and V can then be compared to the observed $\partial p_i/\partial t$, obtained by finite differencing p_i.

Note that p_i is constructed using pressure anomalies, while H and V force the gross pressure, and so are filtered before being compared to $\partial p_i/\partial t$. This assumes that the operations of filtering and taking the time derivative are commutative, which is not necessarily true. This assumption can be tested by considering the difference between $filter(\partial p/\partial t)$ and $\partial/\partial t(filter(p))$, where $filter$ is the operation of applying a 90-day low-pass filter, as shown in figure 3.6. Details of the low-pass filter used for all timeseries in this thesis are given in appendix C. Clearly the two time series are very similar, with the residual being approximately 10^4 times smaller than the data. The standard deviation of the anomaly across 36 years of data was 3.22×10^{-6} hPa. This smallness is to be expected, as by construction the pressure climatology will vary significantly slower than the pressure anomaly p'. As such in the following $\partial p_{av}/\partial t$ has been replaced by $\partial p_i/\partial t$.

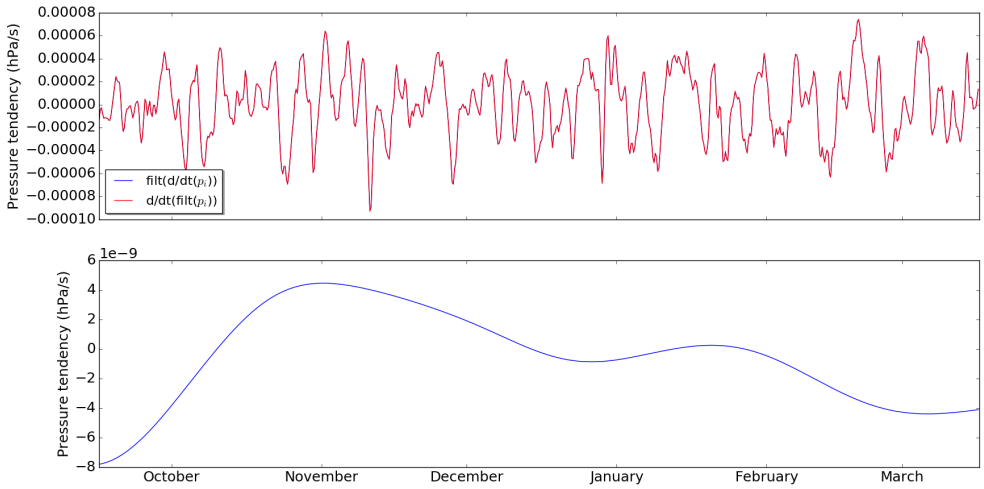

Figure 3.6.: Comparison between $filter(\partial p/\partial t)$ and $\partial/\partial t(filter(p))$, above, and the residual of the two time series, below. Data from ERA-Interim, considering 1982-1983.

To isolate H, and remove the dependence of eq. 3.10 on V, the boundary case $z = 0$ can be considered. Six months of such analysis is shown in fig. 3.7. Across the 37 year dataset there was high correlation between the observed $\partial p_i/\partial t$ at the surface and the vertical integral of H ($r = 0.81$), and fig. 3.7b clearly shows the accumulated surface anomaly to vary very similarly to reanalysis.

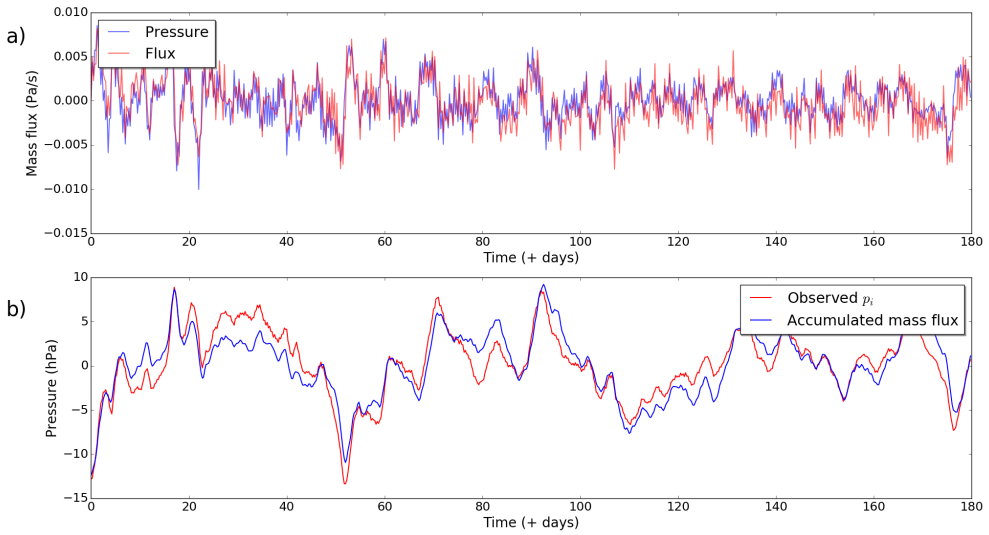

Figure 3.7.: a) Comparison of the finite difference change in surface polar pressure (6 hour resolution) with that predicted by the vertically integrated mass flux into the polar region. Both are calculated using 90-day low-pass filtered data. b) Reconstruction of the p_i calculated by the vertically integrated flux, i.e. the accumulated variable in a). Also plotted for comparison is the observed average surface pressure anomaly. Initialised on December 1st 1979, a randomly chosen date.

Away from the surface it is necessary to also consider V. To calculate this the vertical velocity $\omega = \partial p/\partial t$ is interpolated on z surfaces. This is the velocity of pressure surfaces, and so in (x,y,z)-coordinates is given by the Laplacian derivative of p:

$$\frac{Dp}{Dt} = \omega = \frac{\partial p}{\partial t} + u\frac{\partial p}{\partial x} + v\frac{\partial p}{\partial y} + w\frac{\partial p}{\partial z}.$$

Substituting in the hydrostatic relation, eq. 2.4, for $\partial p/\partial z$ this can be rearranged as

$$w\rho = \left(\frac{\partial p}{\partial t} + u\frac{\partial p}{\partial x} + v\frac{\partial p}{\partial y} - \omega\right)/g,$$

which can be integrated over the area of the polar cap A to give V at a given z. This is done by averaging the right hand side, weighting each datapoint by the cosine of its latitude to produce an area-weighted mean. The magnitude and variance of V relative to H are plotted in fig. 3.8. Clearly V is a large contribution to eq. 3.10, being approximately equal in magnitude and variance to H. While ρw may be significantly smaller than ρv at a given location, the former is integrated over the area of the polar cap, while the latter is integrated over the latitude boundary to the polar cap. As such, the two components contribute approximately equally to $\partial p/\partial t$ in eq. 3.10.

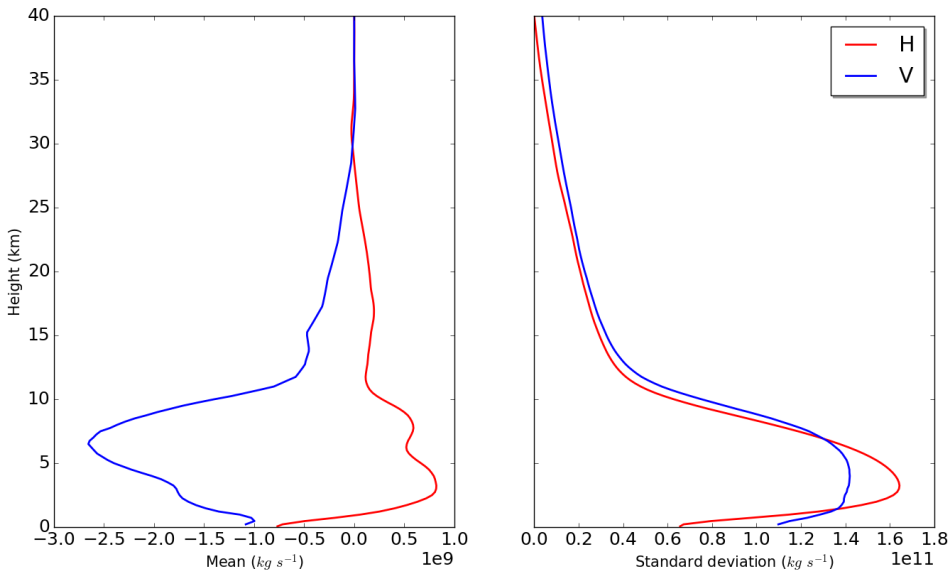

Figure 3.8.: Comparing the magnitude and variance of horizontal and vertical mass fluxes in the polar atmosphere. Data constructed from ERA-Interim, 1979-2016.

It should be noted that V does not go to zero at the surface, as is expected. This is also apparent in fig. 3.9, which shows the correlation of polar pressure index tendencies in reanalysis and as calcuated using H and V in eq. 3.10. Clearly there is an anomaly in the graph between the surface and approximately 2km in altitude. This is likely due to the poor calculation of V from reanalysis fields, owing to both a low spatial resolution and the effects of topography, notably the Greenland ice-sheet and the Chersky range in eastern Russia. As such in the analysis of the following two chapters, it is worth remembering that there is a substantial systematic error associated with the calculation of polar pressure changes using mass fluxes in the lower troposphere, even when said fluxes are calculated from reanalysis.

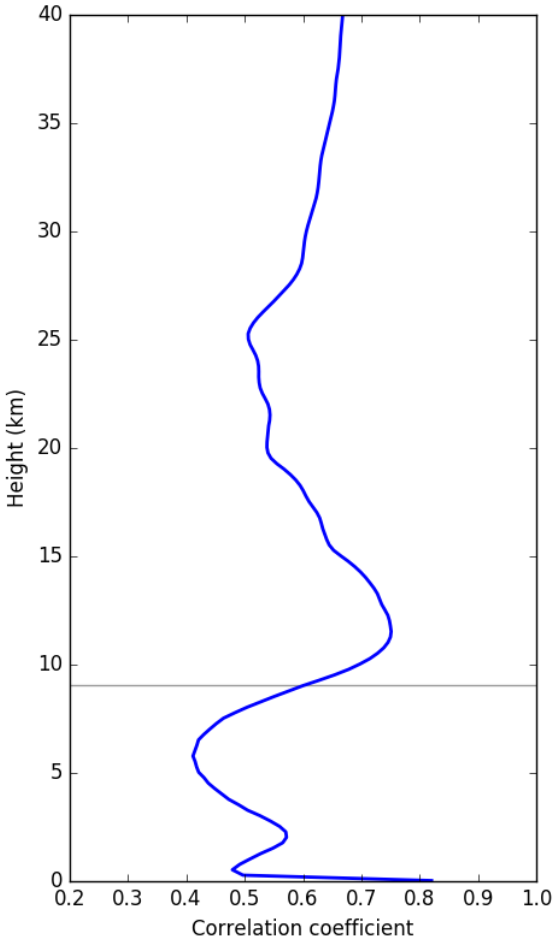

Figure 3.9.: The correlation of the pressure tendency on z predicted by eq. 3.10 and that observed in reanalysis. Data from ERA-Interim 1980-1985.

3.4. Approximating the mass flux

The purpose of this thesis is to investigate a first order explanation of the response of the polar atmosphere to stratospheric events such as SSWs. This is done using the plunger hypothesis and the assumption that the streamfunction associated with the stratospheric PV field fluxes mass into the polar region. As such associated with this framework will be expressions approximating the mass fluxes H and V given a streamfunction ψ associated with a PV field Q. These expressions can be derived using various assumptions to calculate the quantities in eqs. 3.11 and 3.12. Two sets of assumptions are explored in the following sections.

It is not expected that any mass fluxes approximated by this method will exactly correspond to those seen in reanalysis, nor perfectly approximate observed pressure tendencies. The objective is to provide a first order estimate of the pressure tendency, and in the case of extreme events such as SSWs, capture the gross scale of the atmospheric response in time and height. In the following sections this is done geostrophically and quasi-geostrophically. It should be noted however that even if a full ageostrophic result could be obtained it would not perfectly approximate pressure tendencies due to the limitations outlined in section 3.3, and further, the limitations of the data available. The highest temporal resolution available for reanalysis is 6-hourly data, which will not account for processes with shorter timescales. The limitations of the data are discussed further in section 6.1.1.

3.4.1. Geostrophy

The simplest approximation is that of geostrophic flow, defined as the balance of the rotation and pressure terms in the primitive equations:

$$\underline{f} \times \underline{u}_g = -\frac{1}{\rho}\nabla_h p. \tag{3.13}$$

This gives a dH/dz, the horizontal mass flux at a given z,

$$\frac{dH}{dz} = \oint_{\varphi_b} \rho\ v\ a\ \cos(\varphi_b) d\lambda = \oint_{\varphi_b} \frac{1}{f}\frac{\partial p}{\partial \lambda} d\lambda = \frac{1}{f}\oint_{\varphi_b} \frac{\partial p}{\partial \lambda} d\lambda = 0. \tag{3.14}$$

Clearly, assuming geostrophy does not allow for the calculation of H. While it is con-

ceivable that a geostrophic expression for V could be derived, as shown in section 3.3 both H and V contribute approximately equally to dp/dt. As such geostrophy will not be sufficient to predict changes in pressure over the polar cap.

3.4.2. Quasi-geostrophy

Geostrophy results from the exact balance of the pressure and rotation terms in the primitive equations, so the next logical step is consider these terms being approximately in balance. It is reasonable to assume that the Rossby number is small, and inertial forces are an order of magnitude smaller than rotation and pressure forces, i.e. quasi-geostrophy (Vallis, 2006).

Within quasi-geostrophy, pressure and density fields are split into mean and anomaly fields, $p(z,t) = p_0(z) + p'(z,t)$ and $\rho(z,t) = \rho_0(z) + \rho'(z,t)$, as in section 2.3.1. The two mean fields p_0 and ρ_0 satisfy their own mean hydrostatic relation, eq. 2.4, with the anomaly fields related by

$$\frac{\partial p'}{\partial z} = -g\rho'.$$

From eq. 2.8, $p' = \rho_0(z) f\psi$ and so

$$\rho' = \frac{1}{g}\frac{\partial}{\partial z}\left(\rho_0(z) f\psi\right) \tag{3.15}$$

$$= -\frac{f}{g}\left(\frac{d\rho_0}{dz}\psi + \rho_0\frac{\partial\psi}{\partial z}\right). \tag{3.16}$$

Substituting this into eq. 3.11 along with $v = (1/a\cos\varphi_b)\partial\psi/\partial\lambda$ gives

$$\frac{dH}{dz} = \frac{1}{a\cos\varphi_b}\oint_{\varphi_b}\left(\rho_0 - \frac{f}{g}\left(\frac{d\rho_0}{dz}\psi + \rho_0\frac{\partial\psi}{\partial z}\right)\right)\frac{\partial\psi}{\partial\lambda}a\cos\varphi_b d\lambda \tag{3.17}$$

$$= \rho_0\oint_{\varphi_b}\frac{\partial\psi}{\partial\lambda}d\lambda - \frac{f}{g}\frac{d\rho_0}{dz}\oint_{\varphi_b}\psi\frac{\partial\psi}{\partial\lambda}d\lambda - \frac{f\rho_0}{g}\oint_{\varphi_b}\frac{\partial\psi}{\partial z}\frac{\partial\psi}{\partial\lambda}d\lambda \tag{3.18}$$

which simplifies to:

$$\frac{dH}{dz} = -\frac{f\rho_0}{g}\oint_{\varphi_b}\frac{\partial\psi}{\partial z}\frac{\partial\psi}{\partial\lambda}\,d\lambda. \tag{3.19}$$

The mass flux is given by the product of the vertical and zonal derivatives of the streamfunction, so proportional to the product of the eddy temperature field and the eddy meridional velocity field. Anomalous mass flux into the polar region only occurs where theta surfaces are anomalously separated *and* where there exists an anomalous meridional

velocity. This corresponds to the streamfunction at the boundary to the cap varying in both longitude and height simultaneously - it is not enough for the field to vary horizontally or vertically in isolation to flux mass. Constant ψ surfaces must twist in a manner similar to a skirt on a spinning dancer in order for H to be non-constant.

An expression can also be derived for the vertical mass flux $\rho(z)w(z)$ using QG assumptions. From the continuity equation in (x, y, p) coordinates,

$$\nabla \cdot \mathbf{u_g} = \frac{\partial u_g}{\partial x} + \frac{\partial v_g}{\partial y} + \frac{\partial \omega_g}{\partial p} = 0, \tag{3.20}$$

and by construction the horizontal geostrophic velocities u_g, v_g are non-divergent, so $\partial\omega_g/\partial p = 0$. Therefore if $\omega_g = 0$ anywhere, such as at the surface, then $\omega_g = 0$ everywhere. Assuming this to be the case, ω_g can be expressed in (λ, φ, z) coordinates as

$$\omega_g = \frac{Dp}{Dt} = \frac{\partial p}{\partial t} + \frac{u_g}{a\cos\varphi}\frac{\partial p}{\partial \lambda} + \frac{v_g}{a}\frac{\partial p}{\partial \varphi} + w_g\frac{\partial p}{\partial z}. \tag{3.21}$$

By construction, p in the first three terms on the right hand side can be replaced by the pressure anomaly p', as the background pressure profile p_0 depends on z only. As such the expression for geostrophic balance, eq. 2.8, can be substituted in these terms. Also substituting hydrostatic balance and expressions for the horizontal geostrophic velocities,

$$\rho_0 f\frac{\partial \psi}{\partial t} - \frac{1}{a^2\cos\varphi}\frac{\partial \psi}{\partial \varphi}\frac{\partial}{\partial \lambda}(\rho_0 f\psi) + \frac{1}{a^2\cos\varphi}\frac{\partial \psi}{\partial \lambda}\frac{\partial}{\partial \varphi}(\rho_0 f\psi) - w_g\rho g = 0. \tag{3.22}$$

A further approximation of QG theory is that the Coriolis parameter varies linearly in space about the value at a given location such that $f(\varphi) = f_0 + a\beta\varphi$, where $\beta = 1/a\ df/d\varphi$. Substituting this in,

$$\rho_0 f\frac{\partial \psi}{\partial t} - \frac{\rho_0 f}{a^2\cos\varphi}\frac{\partial \psi}{\partial \varphi}\frac{\partial \psi}{\partial \lambda} + \frac{\rho_0}{a^2\cos\varphi}\frac{\partial \psi}{\partial \lambda}\left(f\frac{\partial \psi}{\partial \varphi} + a\psi\beta\right) - w_g\rho g = 0, \tag{3.23}$$

and as the horizontal terms cancel,

$$\rho_0 f\frac{\partial \psi}{\partial t} + \frac{\rho_0\psi\beta}{a\cos\varphi}\frac{\partial \psi}{\partial \lambda} = w_g\rho g, \tag{3.24}$$

and so

$$\rho w_g = \frac{\rho_0}{g}\left(f\frac{\partial \psi}{\partial t} + \frac{\partial \psi}{\partial \lambda}\frac{\psi\beta}{a\cos\varphi}\right). \tag{3.25}$$

This is then integrated over the area of the polar cap, A, to give the total vertical mass

flux $V(z)$ at a given height z

$$V(z) = \frac{\rho_0}{g} \int_z^{\pi/2} \oint_\varphi \left(f \frac{\partial \psi}{\partial t} + \frac{\partial \psi}{\partial \lambda} \frac{\psi \beta}{a \cos \varphi} \right) a \cos \varphi_b d\lambda \; d\varphi, \tag{3.26}$$

however the second term will not net contribute over a closed contour of λ and so

$$V(z) = \frac{\rho_0}{g} \int_{\varphi_b}^{\pi/2} (f_0 + a\beta\varphi) \oint_\varphi \frac{\partial \psi}{\partial t} \; a \cos \varphi_b \; d\lambda \; d\varphi. \tag{3.27}$$

Combining eqns. 3.10, 3.19, and 3.27, the QG approximation of the pressure tendency over the polar region bounded by latitude φ_b given a streamfunction ψ associated with a stratospheric PV distribution is

$$\frac{\partial p_i}{\partial t}(z) = \frac{\rho_0}{A} \left(\int_{\varphi_b}^{\pi/2} (f_0 + a\beta\varphi) \oint_\varphi \frac{\partial \psi}{\partial t} \; a \cos \varphi_b \; d\lambda \; d\varphi - f \int_z^\infty \oint_{\varphi_b} \frac{\partial \psi}{\partial z} \frac{\partial \psi}{\partial \lambda} d\lambda \; dz' \right). \tag{3.28}$$

3.5. Summary

This chapter has attempted to construct an explanation for observed downward influence of extreme stratospheric events on the troposphere, as defined in the previous chapter. The main results from this chapter are:

- The coupled stratosphere-troposphere system has been simplified by considering a column of air over the polar region. The average pressure over this polar cap, p_i, behaves very similarly to the AO index;

- The pressure index p_i changes due to mass horizontally transported into and out of the polar region, H, and subsequent vertical redistributions of mass over the polar cap, V. Eq. 3.10 has been derived to describe the response of the index to given mass forcing, and tested using data from reanalysis;

- The assumptions associated with quasi-geostrophic balance are met in the stratosphere, and an equation predicting H given information about the PV distribution in the atmosphere has been derived, shown in eq. 3.19;

- Furthermore, the QG assumptions have been used to derive an expression predicting V given information about the PV distribution in the atmosphere, shown in eq. 3.27.

These two QG expressions for H and V are now tested using data from reanalysis. The performance of the plunger hypothesis in predicting changes in p_i using information about the PV field will be tested in chapter 4. Extreme values of the pressure index associated with SSWs, and the associated mass fluxes predicted by QG theory, are then examined in detail in chapter 5.

4. Evaluating the quasi-geostrophic plunger hypothesis

"I refuse to answer that question on the grounds that I don't know the answer."
- *(Beeblebrox, Z)*

4.1. Aims

In the previous chapter a quasi-geostrophic (QG) theory of the coupling of stratospheric circulation anomalies and pressure tendencies in the troposphere was developed. This QG theory was built on the plunger hypothesis - that changes to the stratospheric PV distribution flux mass into and within the polar region. These mass fluxes then force pressure tendencies through conservation of mass and the hydrostatic relation. This chapter tests the QG plunger hypothesis.

This hypothesis involves a two-step process. Firstly a QG streamfunction ψ is obtained from the inversion of reanalysis data. Secondly this streamfunction is used in QG mass flux eqns 3.19 and 3.27, derived in the previous chapter, to calculate mass fluxes which then force polar cap pressure tendencies, as described by eq. 3.28. Thus, to disentangle any errors which arise in this calculation of pressure tendencies, these two steps will be evaluated individually before comparing calculated pressure tendencies to those observed in reanalysis. Firstly in section 4.2 the equations describing mass flux under QG assumptions, eqns 3.19 and 3.27 are examined using an established streamfunction from reanalysis, and calculated mass fluxes compared to those calculated directly from reanalysis fields.

Then in section 4.3 the accuracy of the technique used to invert QGPV is evaluated by comparing the inverter's output to the established reanalysis streamfunction. Piecewise inversion is also used to obtain the streamfunction associated with two different distributions of QGPV: that of the whole atmosphere, and that of the stratosphere alone, and variance of these streamfunctions compared to reanalysis.

With these two steps individually evaluated and errors quantified, QG mass fluxes are then calculated and compared to reanalysis fluxes in section 4.4, and used to approximate the polar pressure tendency in section 4.5. Finally, the point of constructing the plunger hypothesis was to estimate the tropospheric impact of extreme stratospheric events such as sudden stratospheric warmings. As such this section will conclude by evaluating the performance of the QG plunger hypothesis in approximating extreme values of the polar pressure tendency.

4.2. Evaluating the QG mass flux equations

The objective in deriving eqns 3.19 and 3.27 was to calculate mass fluxes, and hence polar cap pressure changes, in response to a streamfunction associated with a QGPV distribution. Before considering a streamfunction derived from inverting a QGPV distribution however, a 'true' reanalysis streamfunction ψ can be obtained by inverting the equation $\nabla^2\psi = \zeta$, where ζ is the vertical component of the reanalysis vorticity field. This calculation of ψ was performed using ERA-Interim data on isobaric surfaces by the Centre for Environmental Data Analysis (CEDA). Any inversion process has associated errors, hence referring to the streamfunction calculated by the CEDA being 'true' rather than *true*. However irrespective of not being exact, this streamfunction is accepted as the correct reanalysis streamfunction for ERA-Interim, and so makes for a useful tool in evaluating both steps involved in the plunger hypothesis: by calculating mass fluxes, evaluating of the validity of eqns 3.19 and 3.27, and by direct comparison to the streamfunction calculated by the QGPV inversion process used in this thesis.

The two streamfunctions - obtained from the inversion of QGPV, and obtained from reanalysis by the CEDA - will hence be notated as ψ_{QG} and ψ_{ERA} respectively.

Anomalous horizontal and vertical mass fluxes $H'(\psi_{ERA})$ and $V'(\psi_{ERA})$ were calculated across 33 years of reanalysis data, being anomalous fluxes as ψ_{ERA} is defined using ERA-Interim streamfunction data which has been filtered, as outlined in Appendix C. Equivalent anomalous horizontal and vertical mass fluxes were also calculated directly from reanalysis fields - the density anomaly ρ' is calculated using eq. 2.4 and the velocity anomalies v' using eq. 2.7. Vertical flux was then calculated using eq. 3.21. These fields were calculated on height surfaces rather than isobaric surfaces, as outlined in section 3.2.2, achieved by resampling isobaric ψ_{ERA} data on height surfaces using reanalysis geopotential fields.

The correlations of these equivalent fluxes were calculated and are displayed as a function of height in fig. 4.1. The correlation of fluxes during the winter months of December, January and February (DJF) only, and during the summer months of June, July, and August (JJA) only are also shown. The correlation of horizontal flux across all months is moderate at $\sim$0.25 and largely barotropic, though decreasing towards the surface in the troposphere. By contrast the correlation of vertical flux is $<$0.25 until $\sim$25km above the surface, above which it increases to a maximum of $\sim$0.5. For both horizontal and vertical fluxes the correlation is substantially lower in the summer months, while being marginally higher than the gross correlation in the winter months.

This evaluation indicates that eqns 3.19 and 3.27 do not produce mass fluxes which correlate well with mass fluxes calculated directly from reanalysis, particularly in the troposphere. Does this indicate then that the QG mass flux equations 3.19 and 3.27 are invalid? If making justifiable assumptions and using a streamfunction calculated directly from reanalysis fields, the mass fluxes should correlate very well with observations. However there are several reasons why this might not be the case.

One such reason is demonstrated in fig. 4.2, showing the zonal profile of observed and calculated meridional velocities on several height surfaces at 65N on a randomly selected day, the 3rd of January 1996. While the meridional velocities calculated from ψ_{ERA} on each level are a reasonable approximation of the velocities observed in reanalysis, the zonal profile of these velocities consists of many large positive and negative eddies. As such, failure to accurately calculate a single positive or negative eddy, of many, along the zonal profile results in a substantial error in the integral. Furthermore, closer to the surface the number of eddy terms increases markedly, making the problem more sensitive to error in the approximation of eddies in the troposphere than in the stratosphere. Comparing with

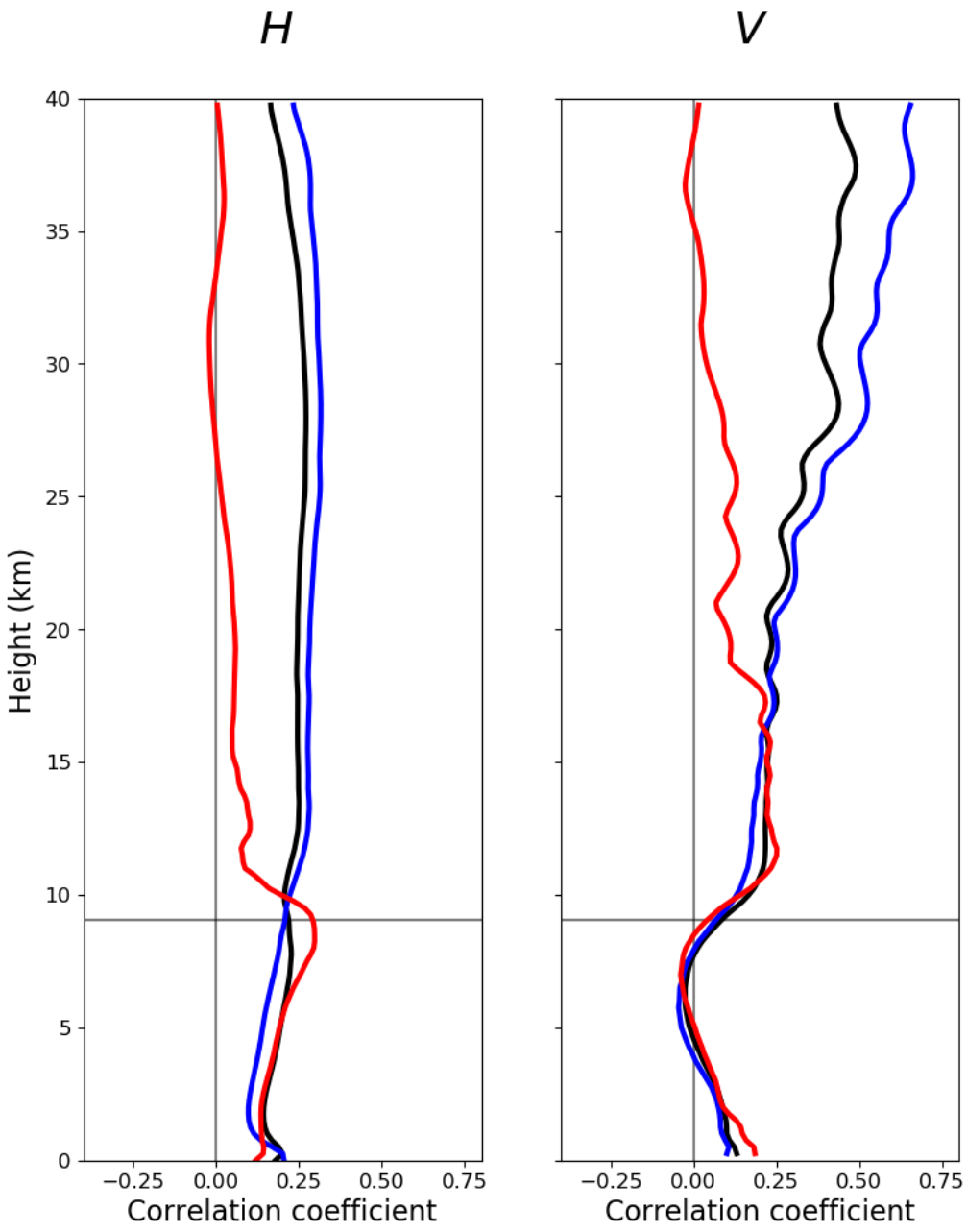

Figure 4.1.: Correlation of mass fluxes H and V calculated from reanalysis density and velocity fields with mass fluxes calculated from ψ_{ERA} using eqns 3.19 and 3.27 respectively. The black curve shows the correlation of these fields across all months, the red curve shows the correlation during JJA only, and the blue curve shows the correlation during DJF only. The horizontal line indicates the mean altitude of the polar tropopause across the whole dataset, defined as in fig. 3.2. Data is from ERA-Interim, ψ_{ERA} is calculated by CEDA using ERA-Interim data.

fig. 4.1, this would explain the weaker performance of $H(\psi_{ERA})$ and $V(\psi_{ERA})$ closer to the surface and the improved performance in the polar stratosphere when the number of eddy terms is lowest. Compounding this issue is the fact that ψ_{ERA} is calculated by the CEDA on a 0.75° latitude and longitude grid, while due to hardware limitations the fields considered in this thesis were calculated and evaluated on a 3° latitude and longitude grid. As such in resampling the streamfunction, defined to calculate observed velocities exactly on a 0.75° grid, on a coarser 3° grid information is lost, and small-scale velocity features, such as zonal eddies, will not be recreated accurately.

The ultimate purpose of calculating these mass fluxes, however, is to calculate changes in anomalous polar cap pressure. Combining the fluxes $H'(\psi_{ERA})$ and $V'(\psi_{ERA})$ using eq. 3.10 and comparing with polar cap pressure tendencies seen in reanalysis produces a mean correlation of 0.52 throughout the atmospheric column, as seen in fig 4.3. This indicates that the calculation of polar cap pressure changes through mass fluxes is 'greater than the sum of its parts'. While the correlation of horizontal and vertical mass fluxes with their respective fluxes in reanalysis may be low, their sum correlates moderately with the sum of fluxes in reanalysis. As with the component fluxes there is a strong seasonality to this correlation, with the changes in polar cap pressure calculated from mass fluxes correlating well in the winter months but performing substantially worse in the summer throughout the column, notably so in the mid stratosphere. Unlike the individual flux components however, the correlation of polar cap pressure changes is almost entirely barotropic, indicating that the errors in calculating pressure changes are systemic, such as outlined previously. The notable departure from the correlation being wholly independent of height is a sharp increase away from the

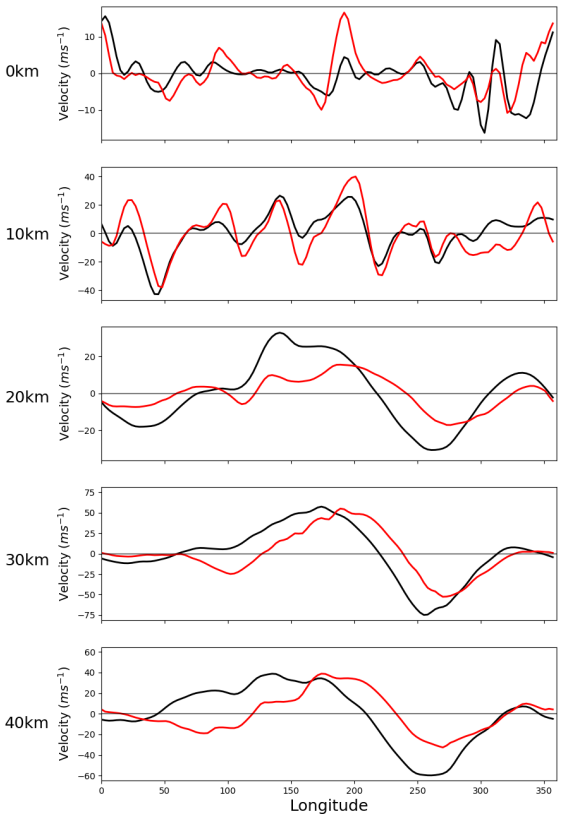

Figure 4.2.: Meridional velocity at 65N on a number of height surfaces on 3/1/1996. Observed velocities in ERA-Interim are shown in black, velocities calculated from ψ_{ERA} using eq. 2.7 are shown in red. ψ_{ERA} is calculated from ERA-Interim fields by CEDA.

surface. This is possibly due to the effects of topography on the calculation of vertical mass flux.

If considering the correlation of all reanalysis polar cap pressure tendencies with those calculated using ψ_{ERA} then the mean correlation is 0.52, as previously shown. If however only reanalysis pressure tendencies more than one standard deviation from their mean are considered in the calculation, then the mean correlation increases to 0.72. Further, if pressure tendencies are only considered if more than two standard deviations from the mean then this correlation increases again to 0.81. In both these cases (not plotted) the correlation remains largely barotropic, indicating that the mass flux framework has systematic flaws but that these flaws become less important as the magnitude of the pressure tendency, and so mass flux, increases.

Overall, while eqns 3.19 and 3.27 evaluated using ψ_{ERA} on a 3° latitude and longitude grid do not produce mass fluxes which correlate well with those seen in reanalysis, their sum does correlate moderately well with the sum of reanalysis fluxes. Changes in anomalous polar cap pressure are therefore recreated with moderate accuracy using the mass flux framework associated with the plunger hypothesis outlined in chapter 3, though with notable errors. Some of these errors are systematic to the framework, notably the dependence of net anomalous mass flux on large eddy terms, but others are specific to the use of ψ_{ERA} as calculated by CEDA. The plunger hypothesis in practice then cannot be expected to exactly replicate observed polar pressure tendencies as seen in reanalysis. However if an appropriate streamfunction is used, such as one defined on a 3° grid with an accurate inversion process, then the mass flux framework may still provide a useful insight into the phenomenon of stratosphere-troposphere coupling. This may especially be the case when considering extreme wintertime events, such as SSWs, due to correlations of both mass fluxes and pressure tendencies being highest in the winter months, and the performance of the plunger hypothesis being greatest when considering extreme events.

In the next section such a streamfunction will be obtained, and the accuracy of its inversion process assessed, before it is used to calculate mass fluxes and hence polar cap pressure tendencies in sections 4.4 and 4.5.

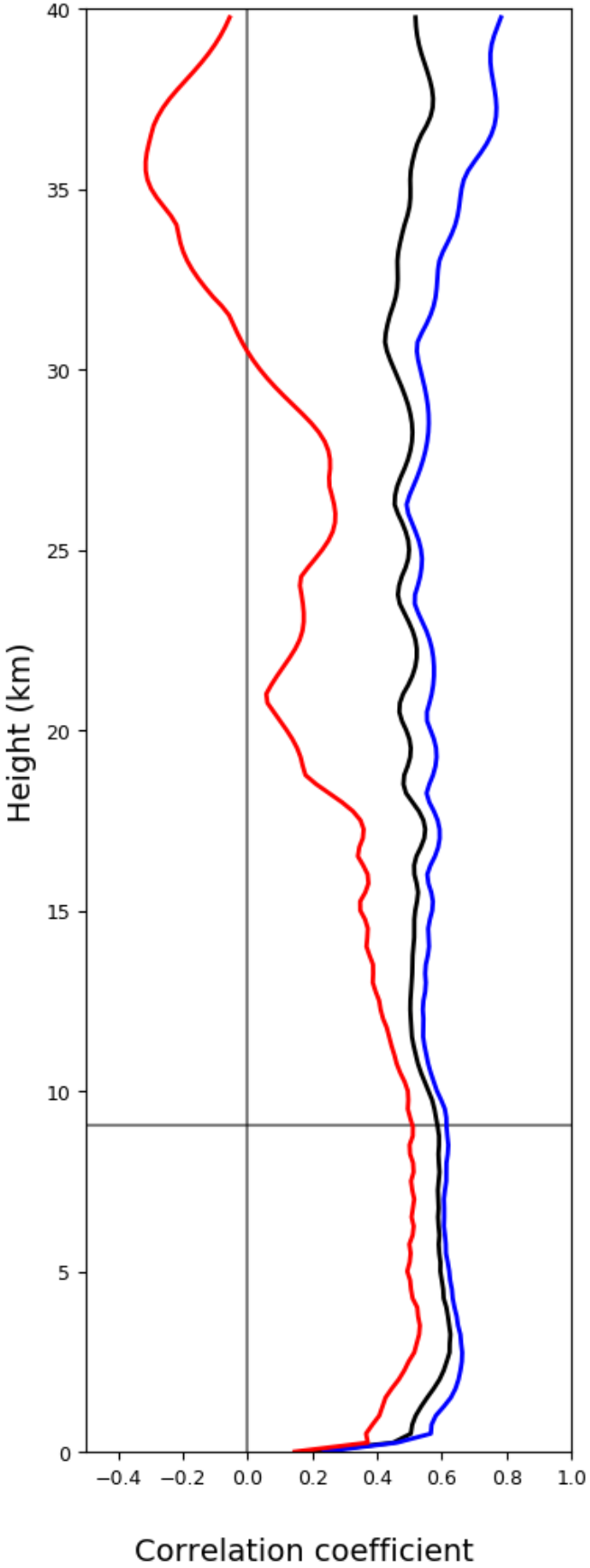

Figure 4.3.: Correlation of polar cap pressure anomalies observed in reanalysis, and those calculated using eq. 3.10 and reanalysis streamfunction ψ_{ERA}. The black curve shows the correlation of these fields across all months, the red curve shows the correlation during JJA only, and the blue curve shows the correlation during DJF only. The horizontal line indicates the mean altitude of the polar tropopause across the whole dataset, defined as in fig. 3.2. Reanalysis data is from ERA-Interim, ψ_{ERA} is calculated by CEDA using ERA-Interim data.

4.3. Evaluating the inversion of quasi-geostrophic potential vorticity

A QGPV distribution q can be calculated from eq. 2.6 using temperature and velocity fields from reanalysis. Any such QGPV field has an associated streamfunction ψ_{QG} related by the equation $q = \mathcal{L}\psi_{QG}$, where $\mathcal{L}$ is a linear operator consisting of the derivatives in eqn. 2.6. The streamfunction ψ_{QG} can be found by inverting this equation. Details of how q is calculated and of this inversion are given in Appendix B.

An assessment of the accuracy of the inversion technique used in this thesis is to compare its output ψ_{QG} to the equivalent 'true' reanalysis streamfunction ψ_{ERA} calculated by the CEDA. Such a comparison is shown on several pressure surfaces on a randomly selected day - again, the 3rd of January 1996 - in fig. 4.4. The inverter output is spatially very similar to the exact reanalysis streamfunction throughout the atmospheric column, though the fields differ substantially on the 1000hPa surface. The magnitude of inverter output is similar to that seen in reanalysis in the stratosphere and upper troposphere, though again there are substantial discrepancies on the 1000hPa surface, with the inverter output being much too large, and the magnitude of a large positive feature substantially underestimated on the 10hPa surface.

Also plotted in fig. 4.4 is the streamfunction associated with the inversion of stratospheric QGPV only, ψ_S. Previously the QGPV associated with the whole atmosphere has been inverted to give a streamfunction. However as the equation $q = \mathcal{L}\psi_{QG}$ is linear, a field q can be split into multiple components and each inverted separately to give associated streamfunctions. These streamfunctions then sum to give the streamfunction associated with the inversion of the total field. For example,

$$q = q_T + q_S = \mathcal{L}\psi_T + \mathcal{L}\psi_S, \tag{4.1}$$

where q_T and q_S are the QGPV in the troposphere and stratosphere respectively. The streamfunctions ψ_T and ψ_S are then, respectively, the components of ψ_{QG} associated with the tropospheric and stratospheric QGPV only, but are defined throughout the entire domain. They also sum to give the streamfunction $\psi_{QG} = \psi_T + \psi_S$ associated with inversion of QGPV through the whole atmosphere. The boundary conditions applied to

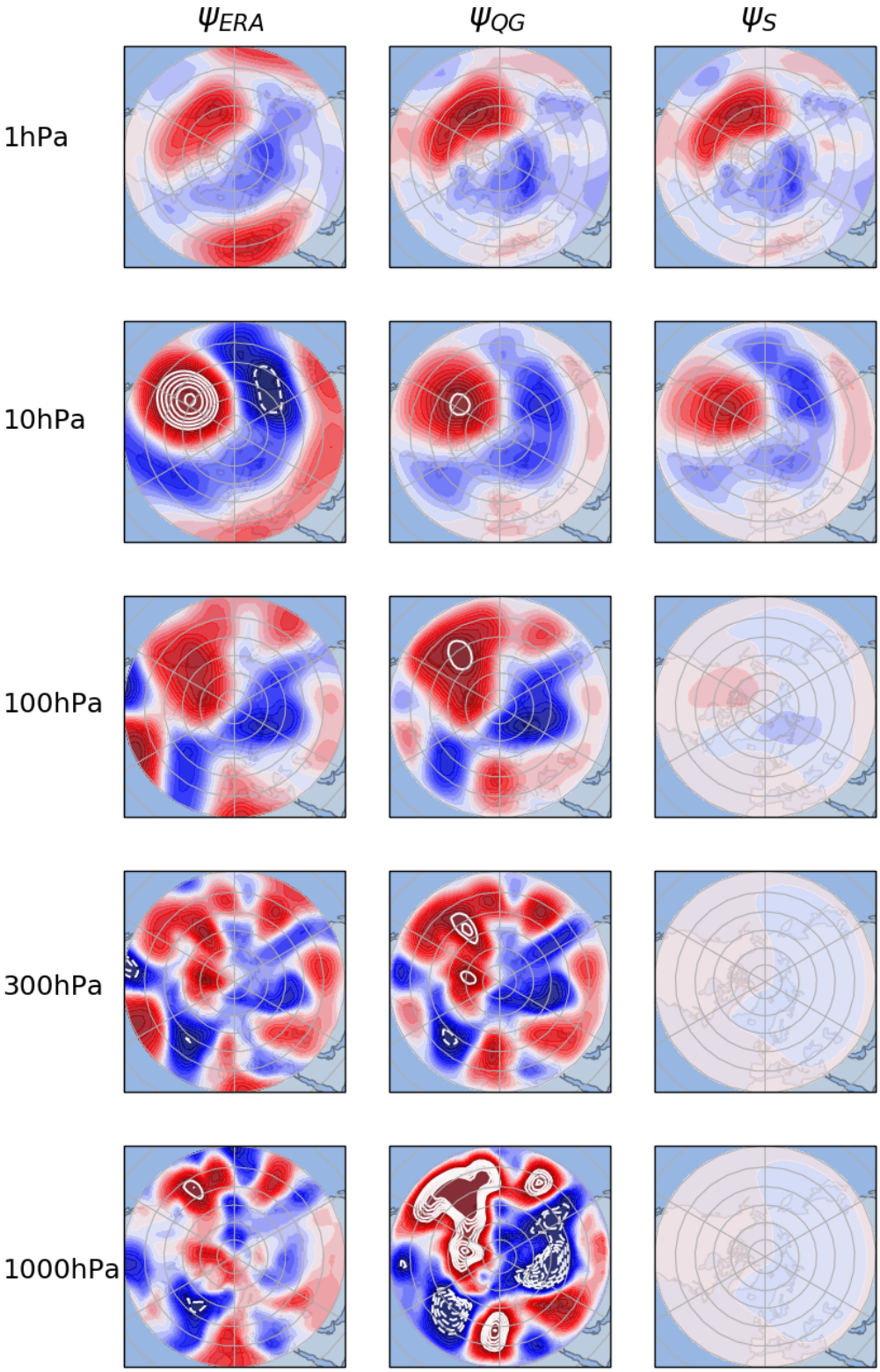

Figure 4.4.: Comparison of the established reanalysis streamfunction ψ_{ERA}, streamfunction output from the QGPV inverter considering all information, ψ_{QG}, and streamfunction output from the QGPV inverter considering stratospheric information only, ψ_S. Data is from 3/1/1996. All fields are standardised by the standard deviations of streamfunction anomalies seen in reanalysis on each p surface. Contour intervals for the colour shading are 0.25, and 0.5 for the white contours.

each independent inversion, however, must sum to the boundary conditions applied to the inversion of the entire field. For example, when considering the tropospheric and stratospheric QGPV separately appropriate boundary conditions on the vertical gradient of the streamfunction would be:

- q_T: At the surface $\partial\psi_T/\partial p$ forced by T_{surf}, at the top of the atmosphere $\partial\psi_T/\partial p = 0$
- q_S: At the surface $\partial\psi_S/\partial p = 0$, at the top of the atmosphere $\partial\psi_S/\partial p$ forced by T_{top},

where T_{surf} and T_{top} are the temperature fields at the surface and the top of the domain in the inversion, respectively. Separating the q field in this way allows for the influence of the stratospheric QGPV on the streamfunction, and so on the QG mass fluxes, in the troposphere to be isolated.

For the purposes of this division, for the remainder of this thesis unless otherwise specified the tropopause is defined as being at 100hPa. This is done as the reanalysis data used (ERA-Interim) is supplied on isobaric surfaces. While this data could be interpolated onto constant geopotential surfaces, allowing the use of thermally-defined tropopause height data as a time-varying boundary, this would introduce additional errors into the calculation of the QGPV. As such a single value pressure boundary was chosen. The 100hPa surface was chosen specifically as a high tropopause, ensuring that no tropospheric information is included in the stratospheric component of QGPV.

Returning to fig. 4.4, as might be expected ψ_S closely matches both ψ_{ERA} and ψ_{QG} in the upper- and mid-stratosphere, as local QGPV information dominates the inverter output. However from 100hPa down to the surface, ψ_S decreases in magnitude, leaving only a weak dipole similar in structure to the stratospheric streamfunction at the bottom of the domain. This is of course a consequence of the boundary condition requiring no vertical gradient in ψ_S at the 1000hPa surface. As such, based on this one case study, ψ_S is broadly equivalent to ψ_{QG} in the stratosphere, and so compares favourably with the accepted reanalysis streamfunction ψ_{ERA}, but does not capture tropospheric information in either spatial structure or magnitude. A more general evaluation of the inverter output is the correlation of ψ_{QG} and ψ_{ERA}, and ψ_S and ψ_{ERA}, as a function of height, shown in fig. 4.5. In this figure the correlation of ψ_{QG} and ψ_{ERA} is seen to increase from around 0.3 at the surface to $\sim$0.75 at the tropopause, then increase more slowly to around 0.9 in the mid stratosphere. This correlation is slightly higher when considering the winter

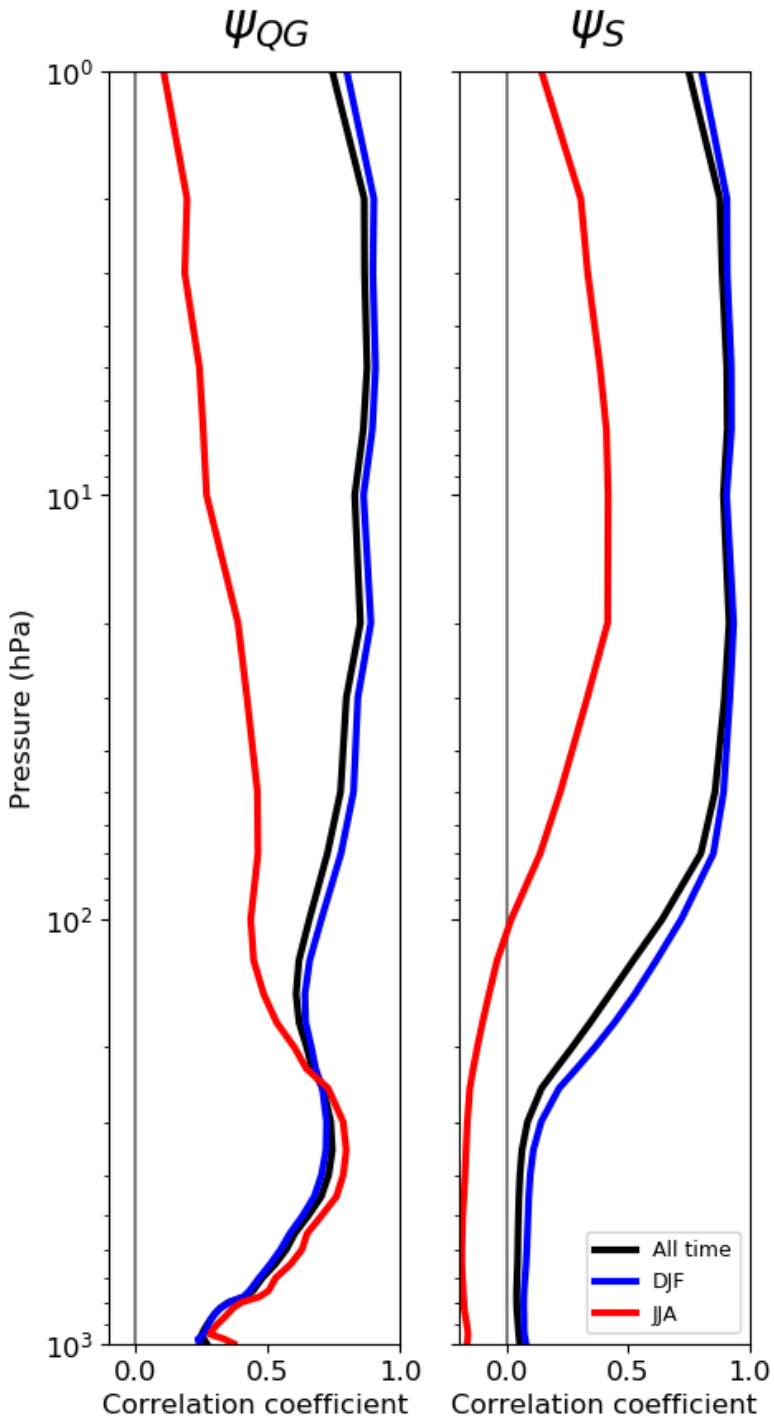

Figure 4.5.: Correlation of the established reanalysis streamfunction with a) streamfunction output from the QGPV inverter considering information from the whole atmosphere, ψ_{QG}, and b) streamfunction output from the QGPV inverter considering stratospheric information only, ψ_S, from 1979 to 2012 as a function of pressure. The correlation of the two variables was calculated at each gridpoint on a pressure level and then averaged. The black curve shows the correlation of these fields across all months, the red curve shows the correlation during JJA only, and the blue curve shows the correlation during DJF only. Data is from ERA-Interim.

months only, while in the summer months tropospheric correlations are approximately the same but stratospheric correlations are substantially lower, tending towards zero at 1hPa from a maximum of ∼0.8 at the tropopause. By contrast the correlation of ψ_S and ψ_{ERA} is near zero throughout the troposphere but then increases to ∼0.9 at 50hPa, staying approximately constant up to 1hPa. This correlation is slightly higher when considering winter months only, and while substantially lower when considering summer months only is still higher in the mid-stratosphere than the correlation of ψ_{QG} and ψ_{ERA}. This appears to indicate that tropospheric information reduces the accuracy of the QGPV inverter's output in the stratosphere in the summer months. More broadly, as seen in fig. 4.4, while ψ_{QG} recreates ψ_{ERA} with moderate accuracy in the troposphere and well in the stratosphere, ψ_S compares favourably in the stratosphere with ψ_{ERA} but fails to do so in the troposphere. Further, the inversion process is substantially more accurate in the winter months than the rest of the year both when considering information from the entire atmosphere and from the stratosphere only.

An alternative evaluation of the inverter's performance is to examine the spatial distribution of correlations of ψ_{ERA} with ψ_{QG} and ψ_S, as shown in fig. 4.6. The correlation of ψ_{ERA} and ψ_{QG} is inhomogeneous, notably so in the troposphere, where the correlation on the 1000hPa surface is higher over the Pacific and Atlantic ocean basins (∼0.6) than over central Asia and North America (∼0.2). This contrast between ocean basins and continental areas is also seen to a lesser extent on the 300hPa surface, while in the stratosphere the correlation is largely zonally symmetric. As areas of low correlation in the troposphere are co-located with large mountain ranges (the Rocky Mountains and the Himalayas) it appears that a notable source of local error in the inversion process is topography. A further source of error appears to be the handling of the high latitude boundary, evidenced by the decreased correlation over the North Pole on all surfaces. As expected from fig. 4.5, the spatial pattern of the correlation of ψ_S and ψ_{ERA} is very similar to the correlation of ψ_{QG} and ψ_{ERA} in the upper stratosphere. On the 1hPa surface the two patterns are nearly identical, while on the 10hPa surface the correlation for ψ_S is marginally higher. On the 100hPa surface, the artificial boundary between the stratosphere and the troposphere considered in this thesis, the correlation of ψ_S and ψ_{ERA} is greater than 0.6 in the high latitudes, decreasing to being weakly negative by 30N. In the troposphere the correlation is weak, though weakly positive in the higher latitudes and weakly negative in the lower latitudes.

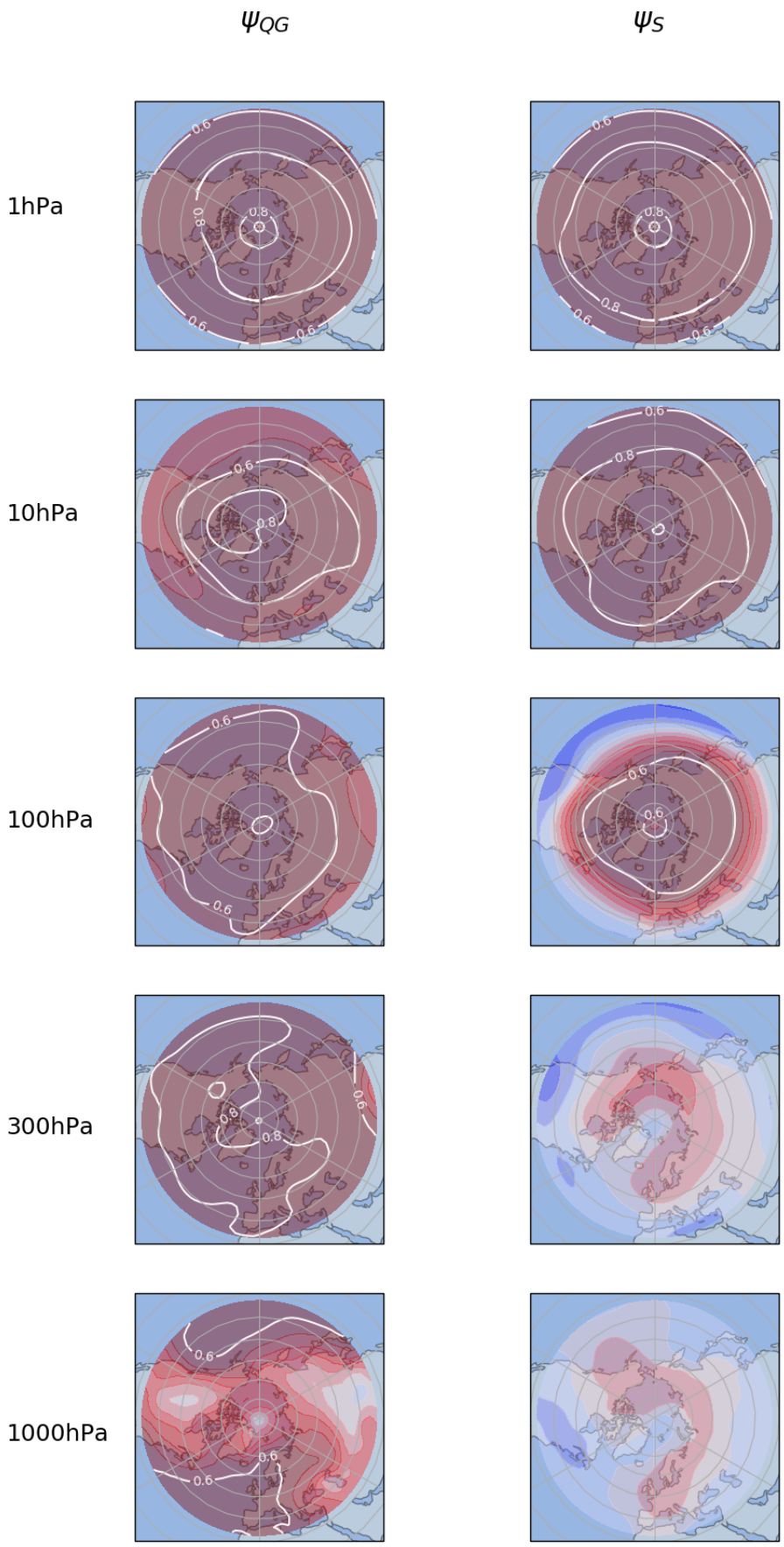

Figure 4.6.: Correlations of the established reanalysis streamfunction ψ_{ERA} with the streamfunction output from the QGPV inverter considering all information, ψ_{QG}, and streamfunction output from the QGPV inverter considering stratospheric information only, ψ_S, from 1979-2012. Contour intervals for the colour shading are 0.1 from -0.6 to +0.6. Data is from ERA-Interim.

To summarise, the inversion process used in this thesis produces a ψ_{QG} which is similar to the reanalysis streamfunction ψ_{ERA} when considering QGPV information from the whole atmosphere. This is especially true in the winter months, and less so in the summer months. The streamfunction output correlates well with ψ_{ERA} in the stratosphere, though less well above continental areas in the lower troposphere. If inverting using only QGPV data from the stratosphere, the output streamfunction ψ_S correlates well with ψ_{ERA} in the stratosphere, though poorly in the troposphere. While the inverter output does have associated errors, considering that this thesis will use the streamfunction output in the mid- to high-latitudes, and in wintertime when considering SSWs, the output will be used when these errors are at a relative minimum. As such the QGPV inverter used in this thesis appears to be an appropriate tool for this investigation, with the caveat that lower tropospheric output has notable errors.

4.4. Quasi-geostrophic mass fluxes

In the previous section the QG streamfunctions ψ_{QG} and ψ_S were compared to the reanalysis streamfunction ψ_{ERA}. The objective of inverting the QGPV distributions q and q_S however is to calculate horizontal and vertical mass fluxes using eqns. 3.19 and 3.27 which can then be used to calculate polar pressure tendencies. These equations both use gradients of the calculated streamfunctions. As such before calculating horizontal and vertical fluxes H and V in the following subsections, the fields constructed from gradients of the streamfunction - namely, ρ and v' - are compared to those seen in reanalysis.

4.4.1. Horizontal flux

The anomalous horizontal flux at given z, dH/dz, is the product of the density and the meridional velocity fields at the boundary to the polar region, 65N. The QG approximations of these boundary fields calculated from ψ_{QG} and ψ_S are compared to reanalysis for in fig. 4.7 as a function of height and longitude January 3rd 1996. Here the density anomaly ρ' is calculated using eq. 2.4 and the velocity anomaly v' using eq. 2.7. Also included in this figure are the mass fluxes calculated from reanalysis and from these streamfunctions - note that this is not the product of the ρ' and v' fields shown. The mass flux is the product of the velocity anomaly v' (shown) and the sum of the density anomaly ρ' (shown) and the density background state ρ_0 (calculated from reanalysis).

On this particular date ρ' is accurately approximated from the QG streamfunction ψ_{QG} on all z surfaces shown, though least well approximated at 10km. The ρ' calculated from ψ_S is small compared to reanalysis in the troposphere but by 30km is almost indistinguishable from the anomaly calculated from ψ_{QG}. Large density anomaly features in the stratosphere - co-located with the stratospheric streamfunction (and so pressure) dipoles seen in fig. 4.4 - are accurately recreated by those calculated from QG streamfunctions. However in the lower stratosphere, as in fig. 4.4, the ρ' calculated from ψ_S varies approximately correctly in longitude but with a magnitude that is too small.

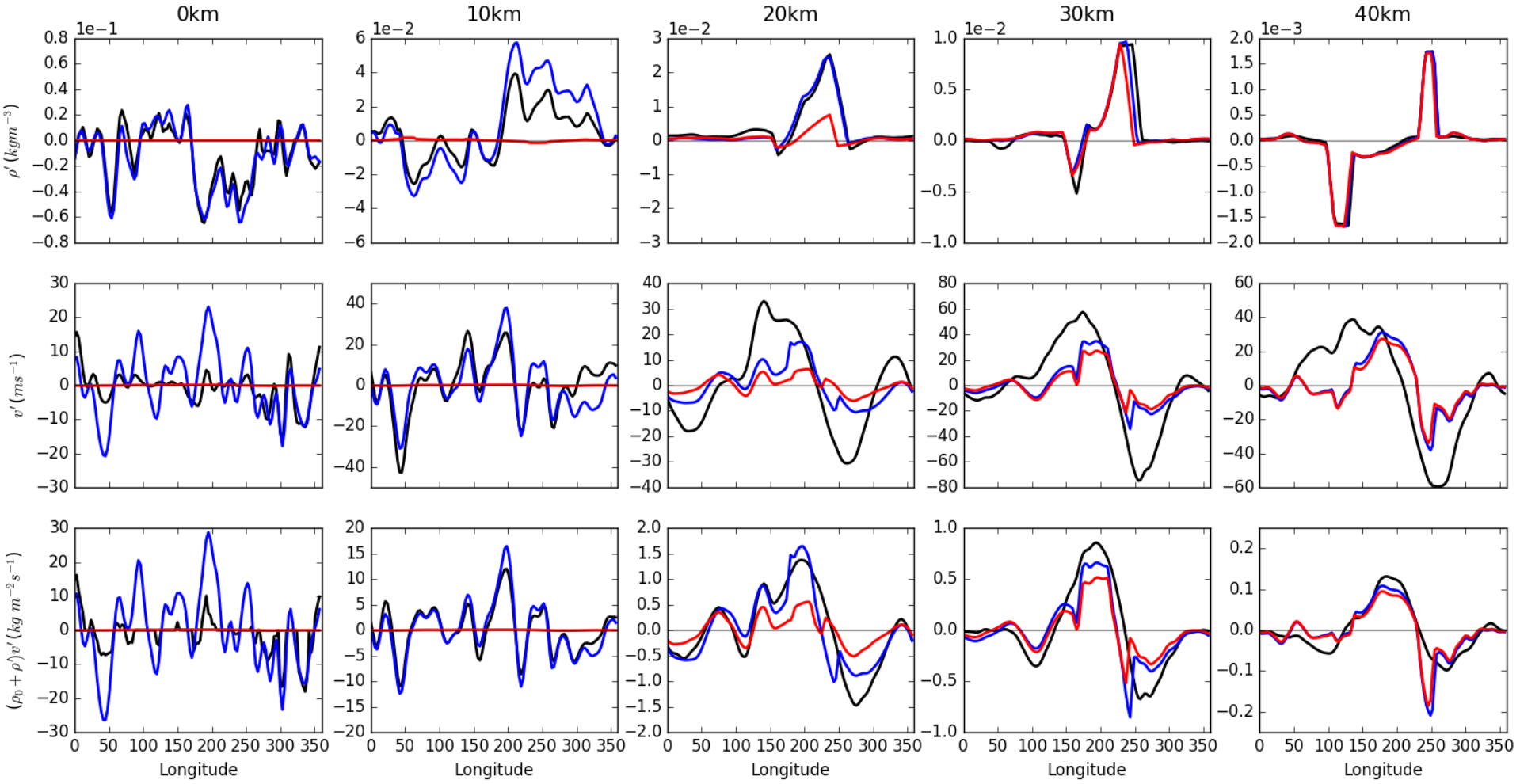

Figure 4.7.: The density anomaly ρ', velocity anomaly v', and anomalous horizontal mass flux dH'/dz at 65N on 3/1/1996 as a function of longitude and height. The fields as seen in reanalysis (ERA-Interim) are shown in black, the fields calculated from ψ_{QG} are in blue, and the fields calculated from ψ_S in red.

While the density anomaly field is mostly well approximated from the QG streamfunctions, the meridional velocity anomaly v' is not. As implied by fig. 4.4 and eq. 2.7 the surface v' calculated from the QG streamfunction ψ_{QG} is significantly too large, though has approximately the correct profile in longitude. The velocity anomaly is best approximated at 10km, with the stratospheric v' containing significant errors. This is likely because the v' in reanalysis includes ageostrophic components, particularly in the troposphere, which the velocity calculated from a QG streamfunction will not be able to recreate. The v' calculated from ψ_S, similarly to the density anomaly field, is vanishingly small in the troposphere and extremely close to the anomaly field calculated from ψ_{QG} in the upper stratosphere. This can also be seen in the RMS error/signal ratio of the ρ' and v' fields, shown in fig. 4.8-4.9. In these figures the RMS error/signal ratio is calculated by dividing the residual of the fields and their reanalysis counterparts by the magnitude of the reanalysis field, for each longitude point and then averaged across all longitudes. While the density and velocity profiles in longitude shown in fig. 4.7 look reasonably accurate, the zonal average of these fields are shown to have significant errors relative to reanalysis. This is because, as previously discussed, the zonal mean is the sum of many large components which sum to approximately zero.

The error in the final row of fig. 4.7, the calculated anomalous horizontal mass flux $(\rho_0 + \rho')v'$, comes mostly from the calculated velocity anomaly field rather than the density anomaly field, although as shown in fig. 4.8 the density anomaly is generally poorly approximated from QG theory in the upper troposphere. As $\rho' << \rho_0$, however, this will contribute a smaller fraction of the error to the mass flux than the velocity. At the surface the calculated mass flux is substantially too large, though by 10km this is no longer the case and the flux distribution closely matches that calculated from reanalysis. Surprisingly in the mid-stratosphere the error between fluxes calculated from ψ_{QG} and ψ_S and that calculated from reanalysis is substantial, and larger than at 10km. As with the velocity anomaly field, the mass flux calculated using stratospheric QGPV, i.e. from ψ_S, is vanishingly small in the troposphere.

The horizontal mass flux into the polar cap on this date is shown as a function of longitude and height in fig. 4.10. As already seen in fig. 4.7 the large-scale features seen in reanalysis are also present in the mass flux field calculated from ψ_{QG}. The flux calculated from ψ_S also does this to an altitude of approximately 15km, but below this very little mass is

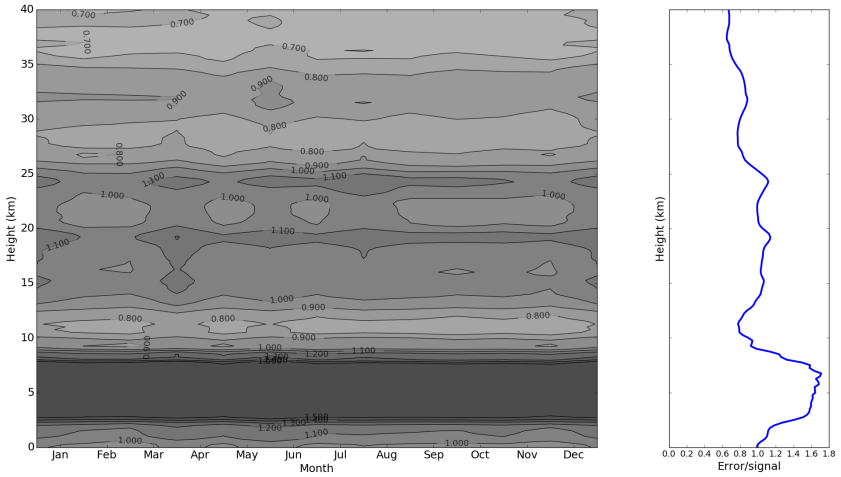

(a) ψ_{QG}

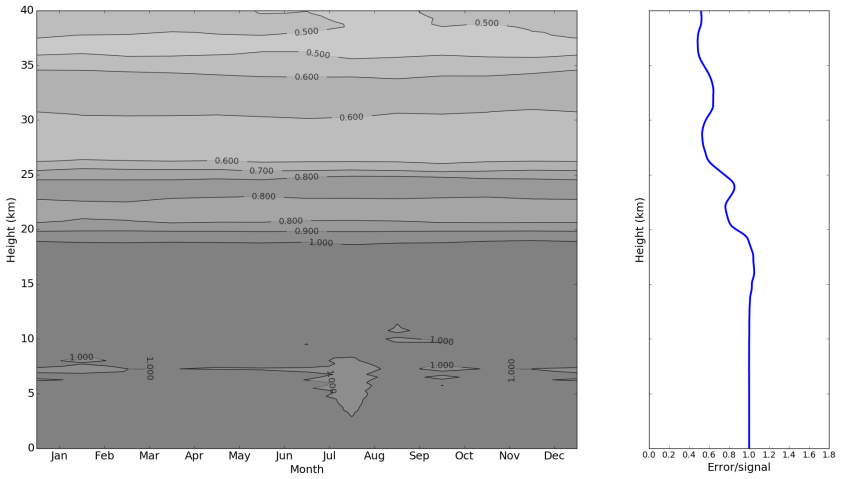

(b) ψ_S

Figure 4.8.: The RMS error/signal ratio of the density anomalies ρ' at 65N calculated from a) ψ_{QG}, and b) ψ_S, relative to reanalysis. On the right is an average across all months as a function of height.

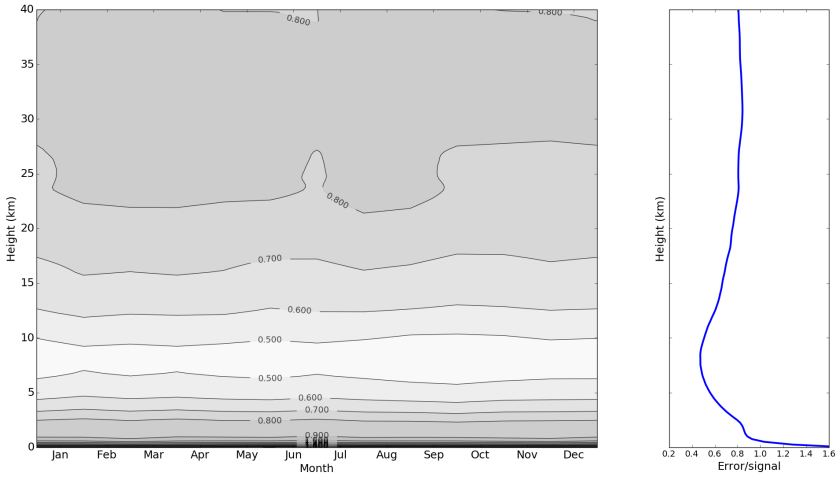

(a) ψ_{QG}

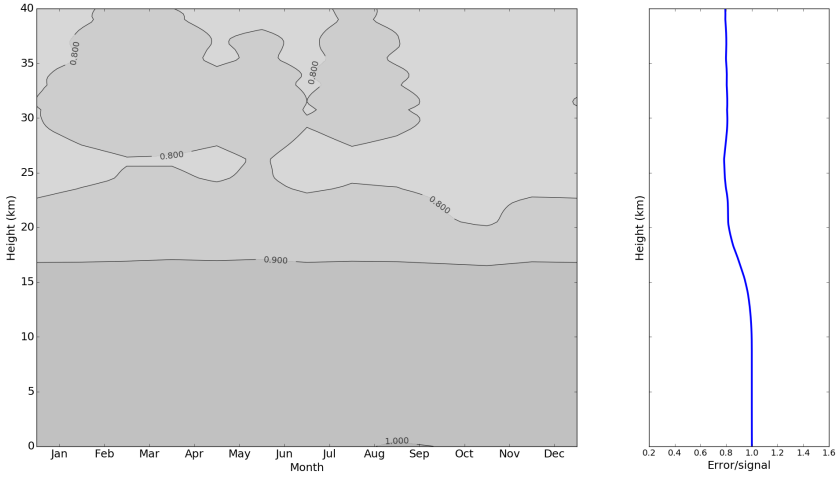

(b) ψ_S

Figure 4.9.: The RMS error/signal ratio of the meridional velocity anomalies v' at 65N calculated from a) ψ_{QG}, and b) ψ_S, relative to reanalysis. On the right is an average across all months as a function of height.

fluxed. There are clear striations in the fields calculated from ψ_{QG} and ψ_S. This is likely due to the approximation of derivatives in eqns. 2.4 and 2.7 as finite differences, as these striations are present in the ρ' fields calculated from both reanalysis and QG streamfunctions.

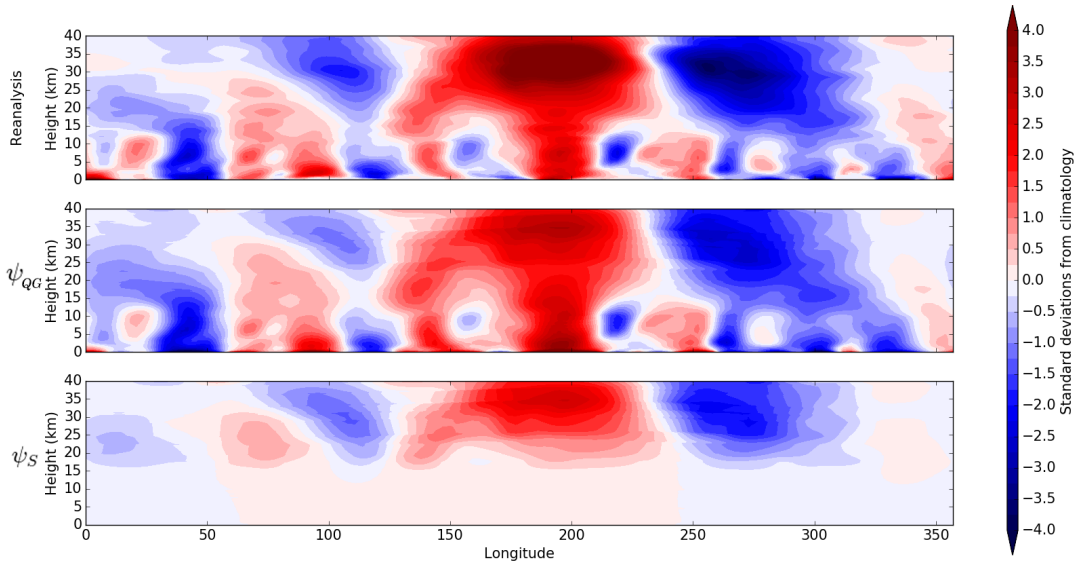

Figure 4.10.: Horizontal mass flux $(\rho_0 + \rho')v'$ at 65N on 3/1/1996. Fluxes are standardised by the standard deviations of horizontal mass flux seen in reanalysis on each z surface.

The variable which contributes to forcing the polar cap pressure, however, is the boundary mass flux at each z integrated across all longitudes, dH/dz. From QGPV theory this is calculated to be given by eq. 3.19, reproduced here:

$$\frac{dH}{dz} = -\frac{f\rho_0}{g} \oint_{\varphi_b} \frac{\partial \psi}{\partial z} \frac{\partial \psi}{\partial \lambda} \, d\lambda.$$

This equation is not a linear function of the streamfunction used. If splitting the streamfunction into tropospheric and stratospheric contributions, $\psi_{QG} = \psi_T + \psi_S$, the horizontal mass flux at a given z is a combination of three terms,

$$\frac{dH}{dz} = -\frac{f\rho_0}{g} \oint_{\varphi_b} \left(\underbrace{\frac{\partial \psi_T}{\partial z}\frac{\partial \psi_T}{\partial \lambda}}_{\substack{\text{tropospheric} \\ \text{influence}}} + \underbrace{\frac{\partial \psi_S}{\partial z}\frac{\partial \psi_S}{\partial \lambda}}_{\substack{\text{stratospheric} \\ \text{influence}}} + \underbrace{\frac{\partial \psi_T}{\partial z}\frac{\partial \psi_S}{\partial \lambda} + \frac{\partial \psi_S}{\partial z}\frac{\partial \psi_T}{\partial \lambda}}_{\text{interference}} \right) d\lambda. \tag{4.2}$$

Each of these three terms are calculated for the first three months of 1996 - including the previous randomly selected case study of January 3rd - and shown in fig. 4.11. A single vertical cross-section of this figure therefore corresponds to the longitudinal integral of fig. 4.10, except now with the tropospheric, stratospheric, and interference terms separated. As such, it is no surprise that the total flux calculated from the QG stream-

functions is significantly too small, as was the case in fig. 4.10. Additionally, while the mass flux distribution calculated from QG streamfunctions in fig. 4.7 appeared to closely resemble that seen in reanalysis, the flux calculated from ψ_{QG} in fig. 4.11 notably differs from reanalysis. Some features are recreated, for instance a large negative anomaly at 20km in early March, a positive anomaly at the tropopause in early February, and a descending stratospheric positive anomaly in mid-February, but the two distributions have substantial differences. As expected the mass flux calculated from ψ_S is localised to the stratosphere, with the flux calculated from ψ_T localised to the troposphere but extending into the lower stratosphere. The interference between these two streamfunctions is shown in the final plot of fig. 4.11 being significant at around 20km in altitude, and particularly contributing to the large negative anomaly seen in early March. As with the density and velocity anomaly fields, while the longitudinal distribution of the QG horizontal mass flux in fig. 4.10 appears to be a good approximation of the flux seen in reanalysis, the zonal average of the QG field is substantially different from the zonal average of the reanalysis flux.

So far the anomalous horizontal mass flux at given z, dH'/dz, has been shown. However the horizontal contribution to eq. 3.28 is the vertical integral of this field, H'. This is also shown for the first three months of 1996 in fig. 4.12. This figure is similar in many ways to fig. 4.11, showing QG horizontal mass flux which is too small in magnitude but with passing similarity in temporal and spatial structure to reanalysis. The magnitude of the calculated mass flux in the troposphere is greater for H' than for dH'/dz however. Interestingly, while the direct influence of the stratospheric QGPV (i.e. the mass flux solely attributable to q_S) extends to approximately 15km in this example, the interference between ψ_S and ψ_T is significant at the tropopause and into the troposphere, being of a comparable magnitude to the direct contribution of q_T.

This is only for one case study, the start of 1996, however. To examine the general performance of QG theory in approximating the horizontal mass flux H, and the influence of ψ_S on this, correlations of the calculated QG mass fluxes and those calculated from reanalysis are shown in fig. 4.13. In this figure the correlations are shown for the entire dataset; for the winter months of December, January, and February; and the summer months of June, July, and August. A strong seasonal dependence of the performance of the QG theory is shown, with the correlation of the observed flux and that calculated from both ψ_{QG} and

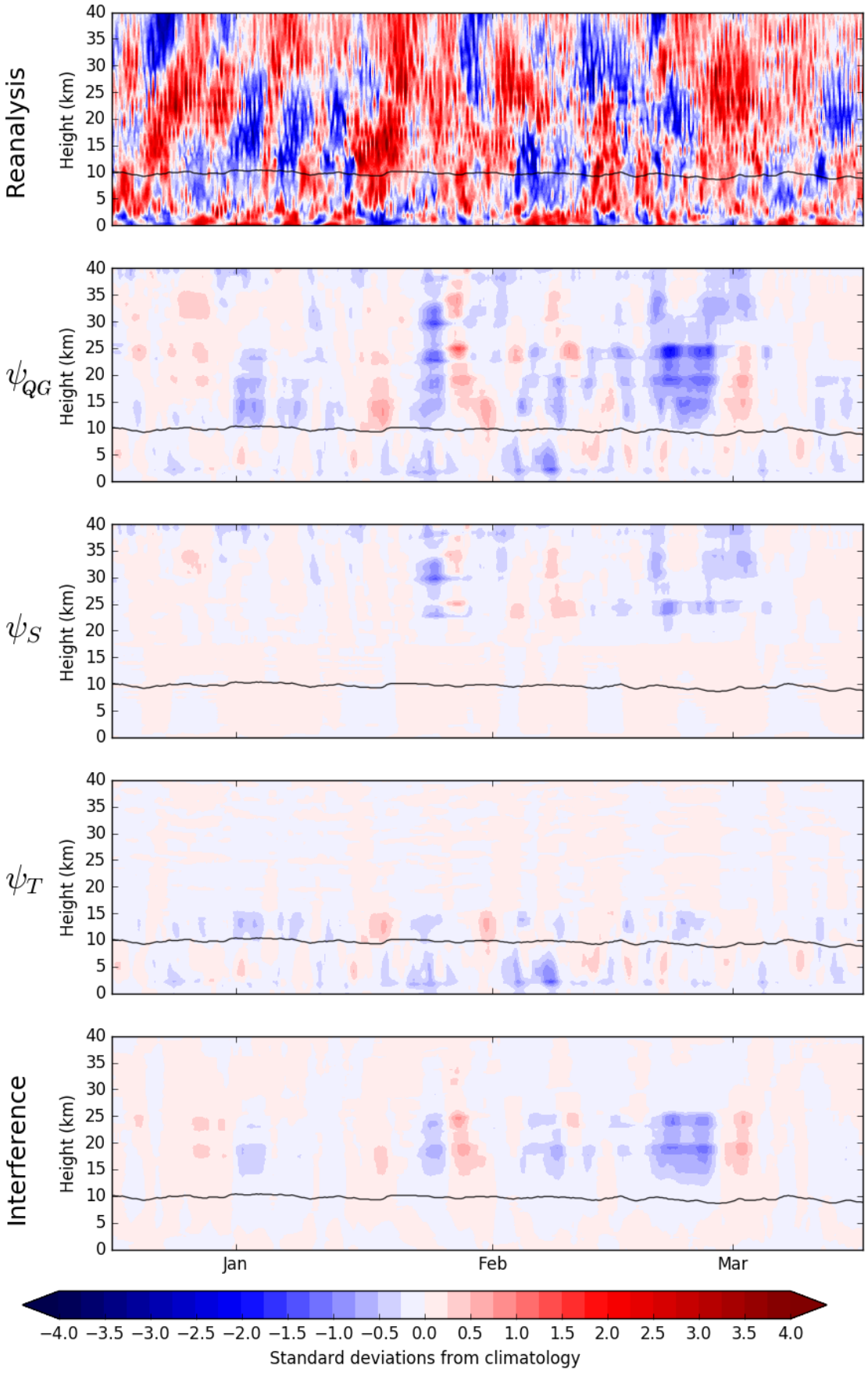

Figure 4.11.: Horizontal mass flux dH/dz at 65N from 1/1/1996 to 1/4/1996, as predicted by eq. 3.19. The streamfunction used in this equation is shown on the left of the figure, with stratospheric, tropospheric, and interference terms as introduced in eq. 4.2. Fluxes are standardised by the standard deviations of horizontal mass flux seen in reanalysis (ERA-Interim) on each z surface. The black line is the approximate location of the tropopause, defined as in fig. 3.2.

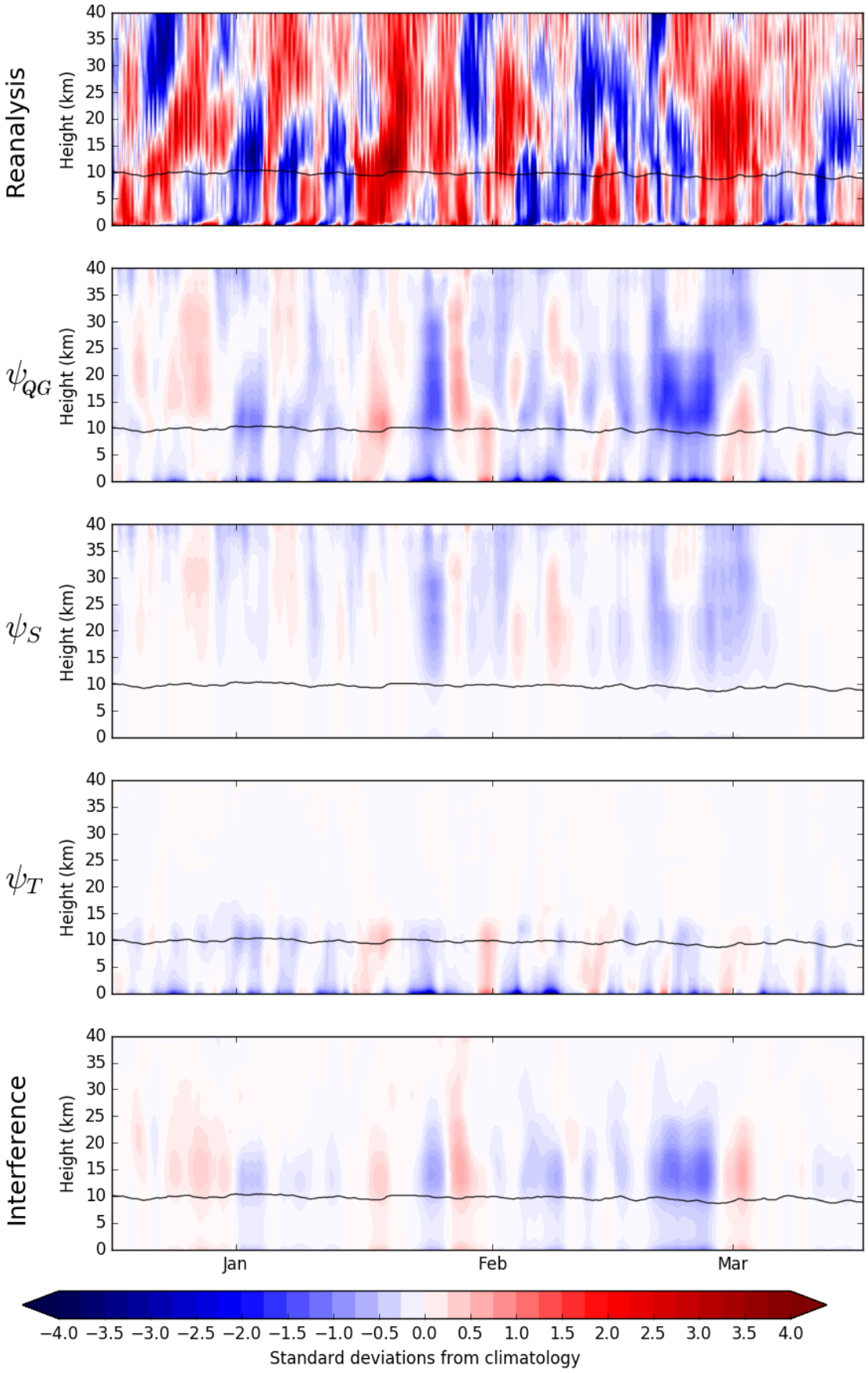

Figure 4.12.: Vertically integrated horizontal mass flux H at 65N from 1/1/1996 to 1/4/1996, as predicted by vertical integration of eq. 3.19, as seen in eq. 3.28. The streamfunction used in this equation is shown on the left of the figure, with stratospheric, tropospheric, and interference terms as introduced in eq. 4.2. Fluxes are standardised by the standard deviations of vertically integrated horizontal mass flux seen in reanalysis (ERA-Interim) on each z surface. The black line is the approximate location of the tropopause, defined as in fig. 3.2.

ψ_S effectively zero in the stratosphere during the summer months but around 0.3 in the winter. These features, and the magnitudes of the correlation, are comparable to when the reanalysis streamfunction ψ_{ERA} was used, as shown in fig. 4.1. Interestingly, similar to the reanalysis case, the highest correlation between the variables is seen at the summer tropopause, where the correlation of the H calculated from ψ_{QG} and that from reanalysis is around 0.5. As this is not seen in the flux calculated from ψ_S or in the interference terms, this is associated with tropospheric information included in ψ_T. As indicated in fig. 4.12 the H associated with interference of ψ_S and ψ_T in eq. 4.2 correlates with the H from reanalysis with a similar magnitude as the H calculated from ψ_S alone. This correlation, however, extends through the tropopause down to the surface, though not during the summer months.

In summary, the stratospheric information encoded in q_S, and represented after inversion of this QGPV field by ψ_S, contributes to QG horizontal mass fluxes throughout the polar atmospheric column. In the mid-stratosphere this is primarily through mass flux directly associated with ψ_S, however in the lower stratosphere and troposphere this is primarily through interaction of ψ_S and the streamfunction associated with tropospheric information, ψ_T.

4.4.2. Vertical flux

The vertical mass flux V is approximated in QG theory by eq. 3.27, being the area integral of the streamfunction tendency weighted by the local value of the Coriolis parameter. This equation is linear in the streamfunction used, with the vertical mass flux being the sum of the mass flux calculated using the streamfunction associated with stratospheric QGPV only and the streamfunction associated with tropospheric QGPV only, $V(\psi_{QG}) = V(\psi_T)+V(\psi_S)$. As a companion to fig. 4.12, fig. 4.14 shows the anomalous vertical flux for the beginning of 1996 using QGPV data from the whole atmospheric column, encoded in ψ_{QG}, and using QGPV data from the stratosphere only, encoded in ψ_S. It is clear from this figure that there are substantial differences between the V' calculated from QG theory and that calculated from reanalysis. In particular the flux predicted in the mid-stratosphere is significantly too small, and the evolution of the mass flux in time takes place over much shorter timescales than seen in reanalysis. Furthermore, the flux calculated from ψ_S is

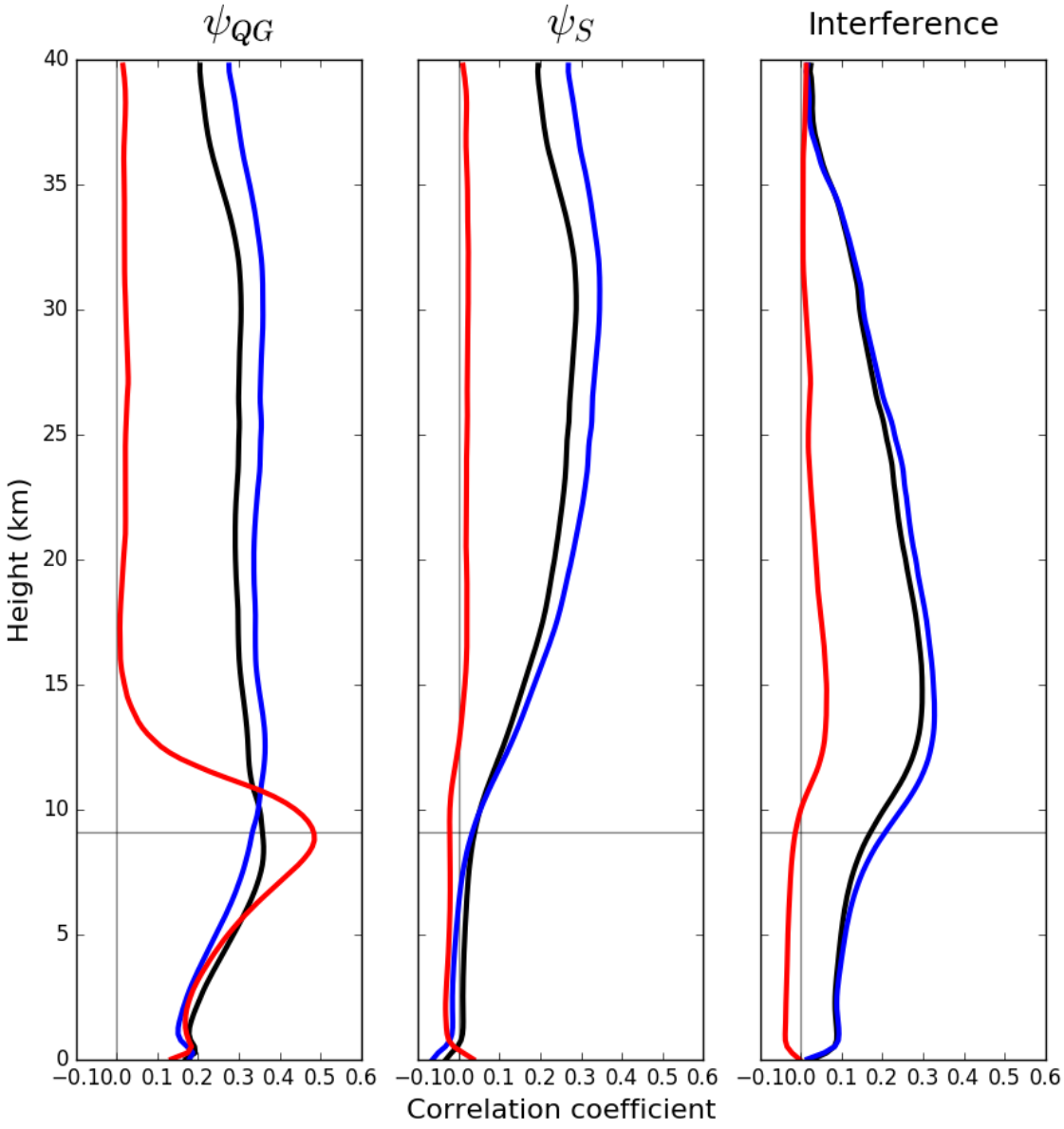

Figure 4.13.: The correlations between H' calculated from ERA-Interim and that predicted by various QG streamfunction, as a function of height. The correlations are calculated with H' calculated using ψ_{QG}, with QGPV information from the whole atmospheric column; with H' calculated using ψ_S, with QGPV information from the stratosphere only; and with the H' arising from interference of ψ_S and ψ_T, as defined in eq. 4.2. Calculated for the whole dataset 1979-2016 (in black); for the winter months of December, January, and February of those years (in blue); and for the summer months of June, July, and August of those years (in red). The horizontal line indicates the mean altitude of the polar tropopause across the whole dataset, defined as in fig. 3.2.

significantly smaller again than that calculated from ψ_{QG}, indicating that stratospheric information did not contribute substantially to the QG V' on these dates.

The general performance of eq. 3.27 can be examined by calculating the correlation of V' calculated from reanalysis with that calculated from ψ_{QG}. The stratospheric influence on the QG V can also be considered by calculating the correlation between the V' calculated using ψ_S and the V' in reanalysis. These are both done in fig. 4.15 for the whole dataset, and also for the summer and winter months alone. The calculated correlations are very small in the troposphere, increasingly modestly in the stratosphere, particularly above 30km in altitude. As seen in fig. 4.13, there is also a strong seasonal dependence of the correlation, being < 0.2 in the summer months but increasing to 0.6 in the winter stratosphere. In the wintertime stratosphere there is little difference between the correlation of the flux calculated using ψ_{QG} and ψ_S. In fact in the lower stratosphere and troposphere the V' calculated from ψ_S correlates better with the flux from reanalysis than the flux calculated from ψ_{QG}. While the correlations in fig. 4.15 are again moderate though comparable to the correlations of observations and V(ψ_{ERA}), the magnitude of the QG fluxes, particularly in the stratosphere, are significantly too small. This can be clearly seen in the scatter plots in fig. 4.16, where in the stratosphere in particular the correlation of the fluxes may be large, but the magnitudes are clearly mismatched.

Compared to the QG horizontal flux H', the QG vertical flux V' correlates better with reanalysis but has magnitudes which are too small, particularly in the stratosphere. Both horizontal and vertical QG fluxes calculated using a QG streamfunction correlate with their reanalysis counterparts comparably to the use of ψ_{ERA} in the stratosphere, and barely at all in the troposphere. In both cases, the fact that ageostrophic velocities cannot be recreated from a QG streamfunction likely reduced performance, particularly in the troposphere. Further, if the stratospheric streamfunction ψ_S is considered in isolation then the QG vertical and horizontal mass fluxes in the troposphere bear no relation to those seen in reanalysis. QG horizontal fluxes in the troposphere correlate slightly better with reanalysis if the interaction between ψ_S and the streamfunction associated with q_T only, ψ_T, is included. Based on these comparisons however, it appears stratospheric QGPV information alone is not sufficient to accurately approximate tropospheric mass fluxes. What remains to be seen is how these mass fluxes combine to produce approximations of tropospheric pressure tendencies. This is done in the following section.

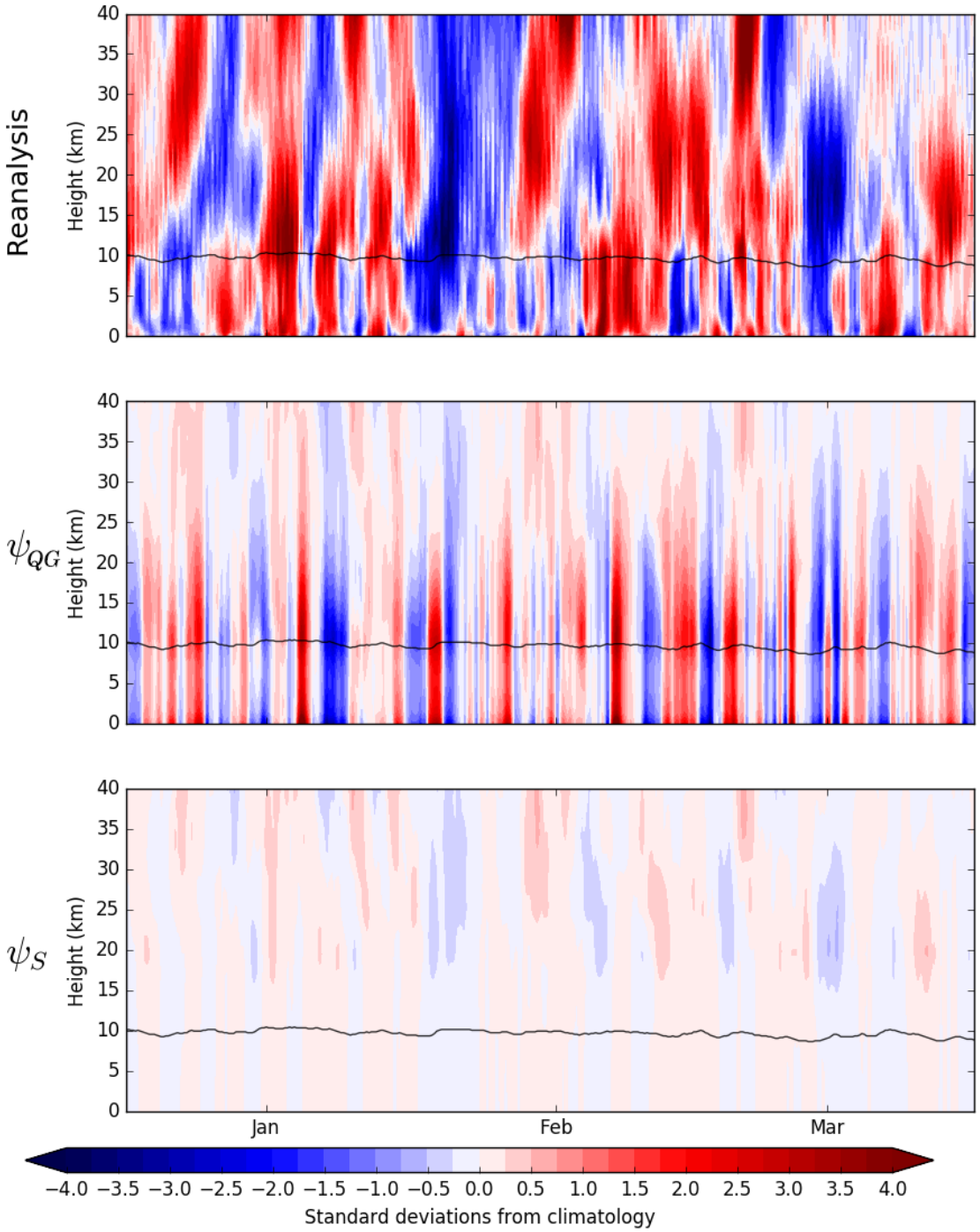

Figure 4.14.: Anomalous vertical mass flux V' averaged over 65-90N from 1/1/1996 to 1/4/1996, as calculated from eq. 3.27. The streamfunction used in this equation is shown on the left of the figure. Fluxes are standardised by the standard deviations of vertical mass flux seen in reanalysis (ERA-Interim) on each z surface. The black line is the approximate location of the tropopause, defined as in fig. 3.2.

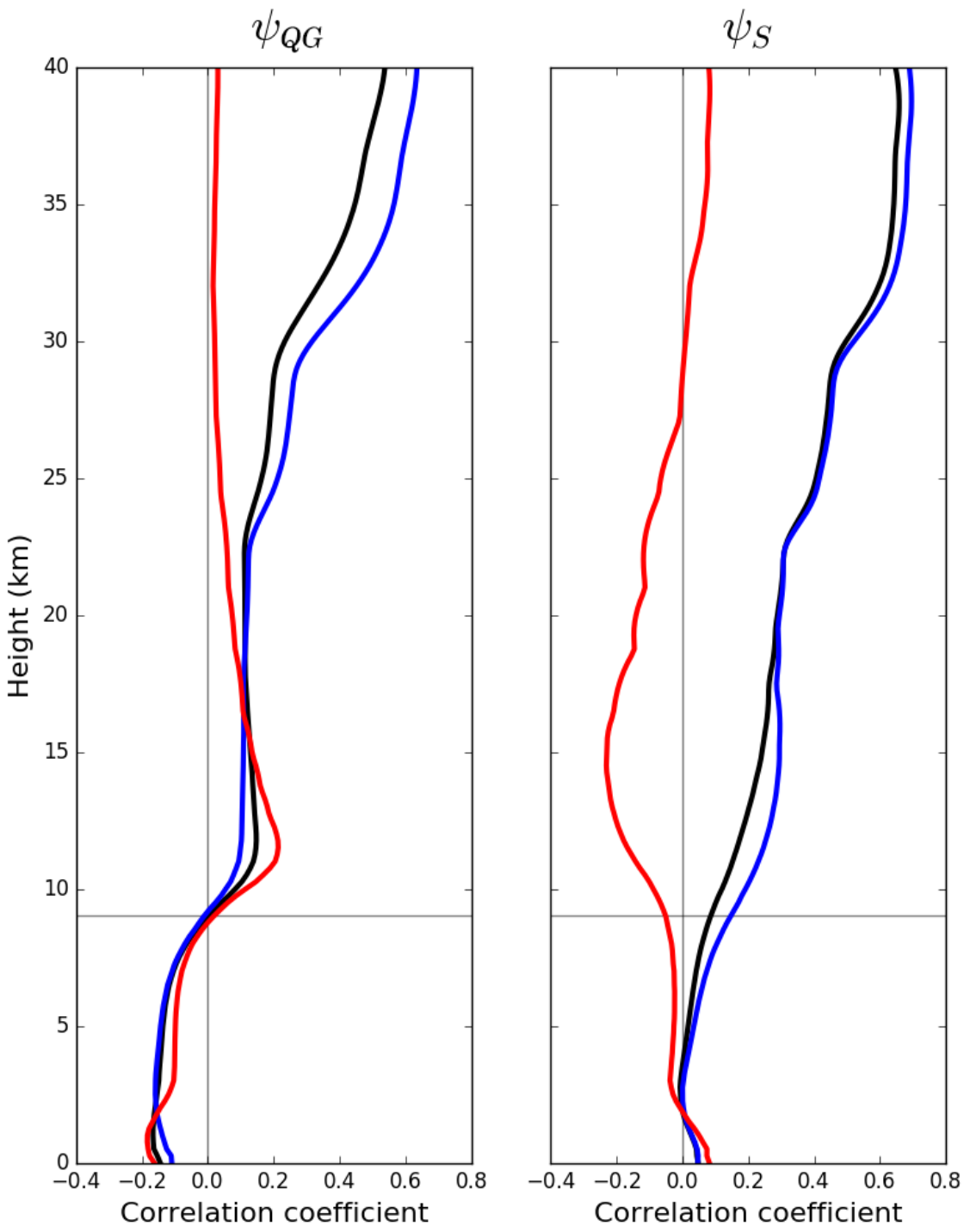

Figure 4.15.: The correlations between anomalous vertical mass flux V' calculated from ERA-Interim and that calculated using ψ_{QG}, with QGPV information from the whole atmospheric column; and with V' calculated using ψ_S, with QGPV information from the stratosphere only. Calculated for the whole dataset 1979-2016 (in black); for the months of December, January, and February of those years (in blue); and for the months of June, July, and August of those years (in red). The horizontal line indicates the mean altitude of the polar tropopause across the whole dataset, defined as in fig. 3.2.

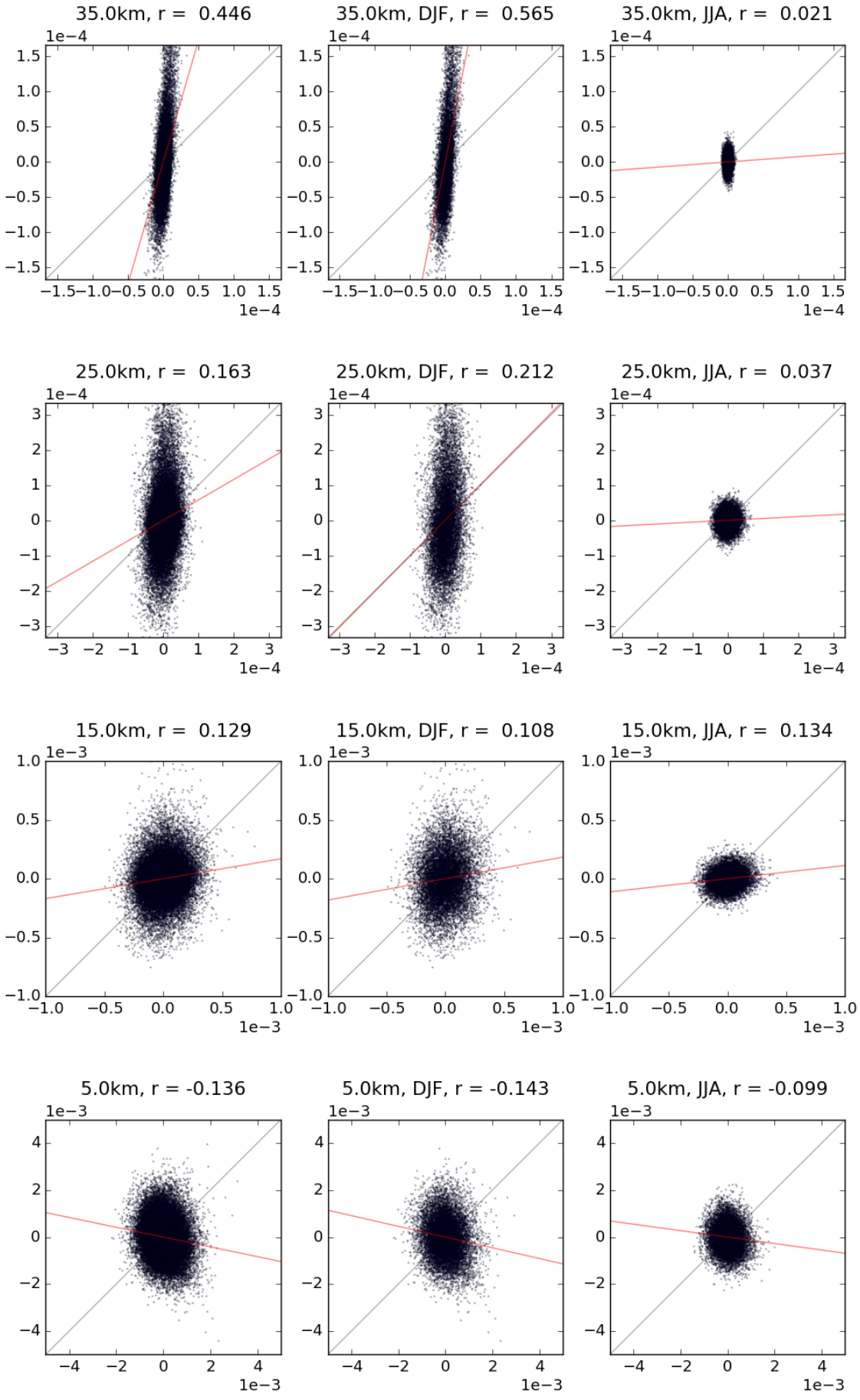

Figure 4.16.: Comparison of anomalous vertical mass flux V' calculated from ERA-Interim and that calculated using ψ_{QG}, with QGPV information from the whole atmospheric column. Calculated for the whole dataset 1979-2016; for the months of December, January, and February of those years; and for the months of June, July, and August of those years. The grey line indicates a 1:1 relationship, the red line indicates the least-square best fit of the data.

4.5. Quasi-geostrophic pressure tendencies

The two expressions for horizontal and vertical QG mass fluxes, eqs. 3.19 and 3.27, are combined to approximate a QG polar pressure tendency in eq. 3.28. As with the QG mass fluxes in section 4.4 this tendency can be calculated using a streamfunction associated with the QGPV in the entire atmosphere or in a limited region of it. This is done using ψ_{QG}, the streamfunction associated with QGPV q in the entire northern hemisphere, and shown for the first three months of 1996 in fig. 4.17. Also shown are the pressure tendencies calculated using ψ_S and ψ_T, the streamfunctions associated with the inversion of the stratospheric and tropospheric QGPV only, q_S and q_T respectively. As eq. 3.28 contains the non-linear eq. 3.19 however, the interference between any ψ_S and ψ_T, described in eq. 4.2, also contributes to the pressure tendency calculated. This term also contains stratospheric information, and so to fully examine stratospheric influence on the polar pressure tendencies approximated using QG theory this term is also included in the tendencies labelled with ψ_S^*.

In the three months shown in fig. 4.17 the QG polar pressure tendencies calculated using ψ_{QG} bear a clear resemblance to those in reanalysis. Large positive features in late February and a large negative feature in early February are clearly reproduced in the tendency timeseries. The agreement between the tendencies in reanalysis and calculated from ψ_{QG} for these dates appears to be much greater than for either the associated horizontal or vertical mass fluxes. The tendencies calculated using ψ_S recreate some of the large-scale features seen in reanalysis, notably negative features in early February and mid-March, but are substantially too small in the troposphere. Including the interference between ψ_S and ψ_T however, as denoted by streamfunction ψ_S^*, extends the influence of stratospheric information into the troposphere and down to the surface, notably in the mid-March negative event. The tendencies calculated using ψ_T clearly contribute a large fraction of the tendencies calculated using ψ_{QG}, both in the troposphere and stratosphere. This contribution is almost entirely barotropic and has a shorter timescale than the contribution from the stratosphere.

A comparison of the polar pressure tendencies calculated from reanalysis and from the whole atmosphere QG streamfunction ψ_{QG} is shown in fig. 4.18. As expected from comparisons of the horizontal and vertical mass fluxes, the magnitude of the QG pressure

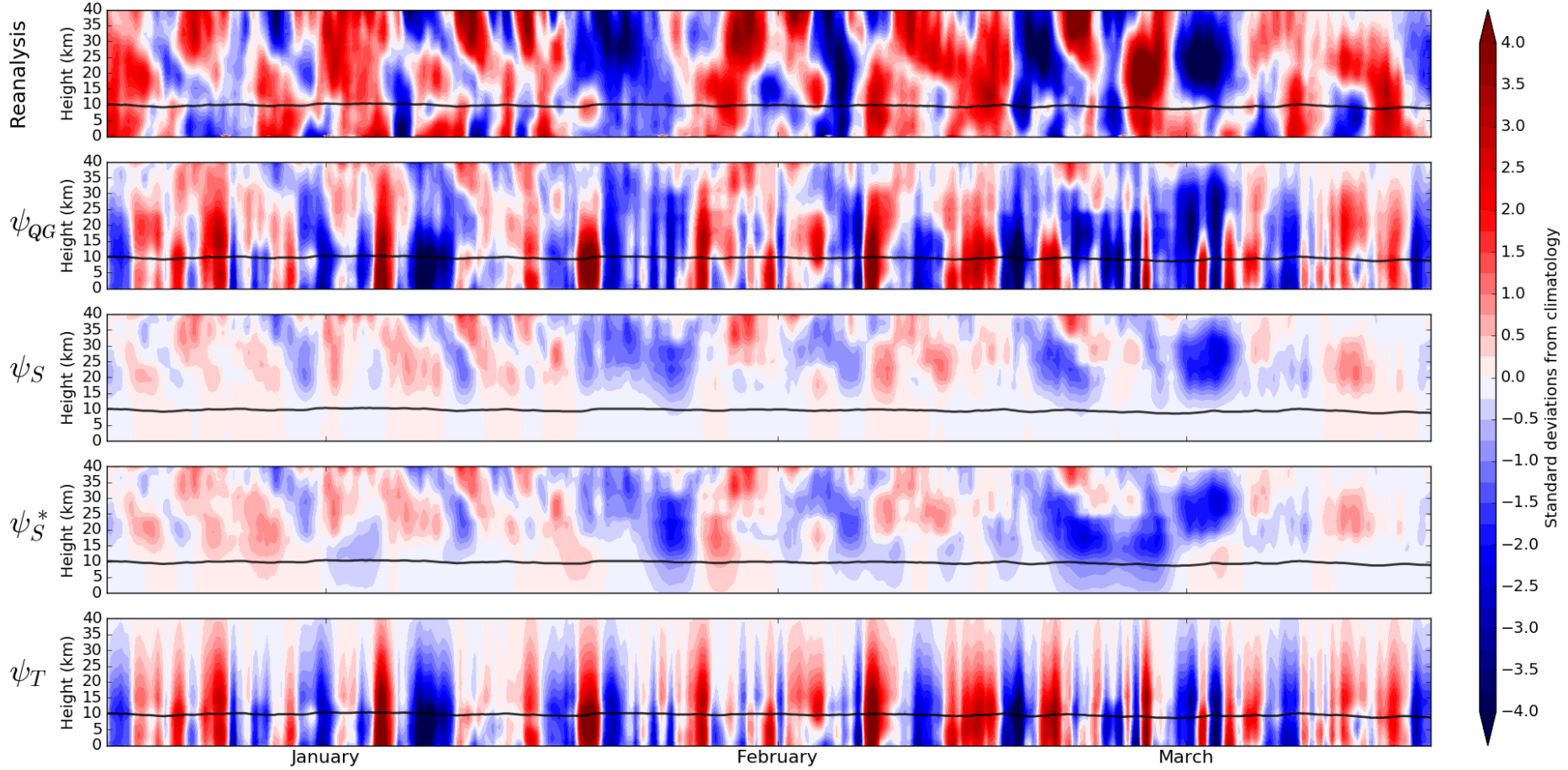

Figure 4.17.: Anomalous polar pressure tendencies relative to climatology, calculated from reanalysis, and calculated using the QG result, eq. 3.28. The streamfunction used in the QG calculation is indicated on the left: ψ_{QG} is the streamfunction associated with inversion of the whole atmosphere q, ψ_S is the streamfunction associated with inversion of the stratospheric QGPV q_S only, ψ_S^* is as ψ_S but also including the interference term as defined in eq. 4.2, and ψ_T is the streamfunction associated with inversion of the tropospheric QGPV q_T only. All tendencies have been standardised by the anomalous pressure tendencies seen in reanalysis.

tendencies is consistently too small, though improves higher in the atmosphere. This is most pronounced in the summer months, when the QG tendency is an order of magnitude smaller than that in reanalysis. Also included in this figure is the correlation of the reanalysis and QG pressure tendency on each height surface considered. This is generalised to all levels in fig. 4.19, where the correlations during the winter and summer months are also shown. The correlation of reanalysis pressure tendencies and those calculated from ψ_{QG} increases with altitude up to the tropopause, where it remains at approximately 0.4 until approximately 30km, after which it increases with altitude again to the top of the region where it peaks at around 0.8. This represents a greater correlation between the QG and reanalysis pressure tendencies than either the vertical or horizontal flux and their respective reanalysis fields. As such eq. 3.28 can again be viewed as 'greater than the sum of its parts', with the QG approximation of pressure tendencies more accurate than the QG approximation of component mass fluxes. Overall, comparing with the results of section 4.2, the error associated with the QG approximation of anomalous polar pressure tendencies within the plunger hypothesis framework is considerable but not substantially greater than when ψ_{ERA} is used to calculate pressure tendencies. Both ψ_{ERA} and ψ_{QG} produced mass fluxes which correlate moderately and barotropically in the stratosphere, however ψ_{QG} correlates increasingly poorly closer to the surface in the troposphere. Considering the errors in the QGPV inversion method used, highlighted in section 4.3, this is likely a result of inaccuracies in ψ_{QG} in the troposphere, specifically over landmasses.

The influence of stratospheric information on the QG approximation of pressure tendencies is also shown in fig. 4.19 by the correlation of tendencies approximated using ψ_S and ψ_S^*. These represent, respectively, the QG pressure tendencies forced by mass fluxes associated with stratospheric QGPV q_S only, and the pressure tendencies forced by q_S *and* including the non-linear interaction between ψ_S and ψ_T. While both of these pressure tendencies correlate better with reanalysis data than the pressure tendencies calculated using ψ_{QG} in the stratosphere, in the troposphere this correlation is practically zero. As seen in the last panel of fig. 4.19, the information contributed by tropospheric QGPV q_T to ψ_{QG} accounts for the observed tropospheric correlation between pressure tendencies in reanalysis and those calculated using ψ_{QG}.

As such across the whole dataset it can be concluded that stratospheric information does not, directly or through interaction with tropospheric information, substantially influence

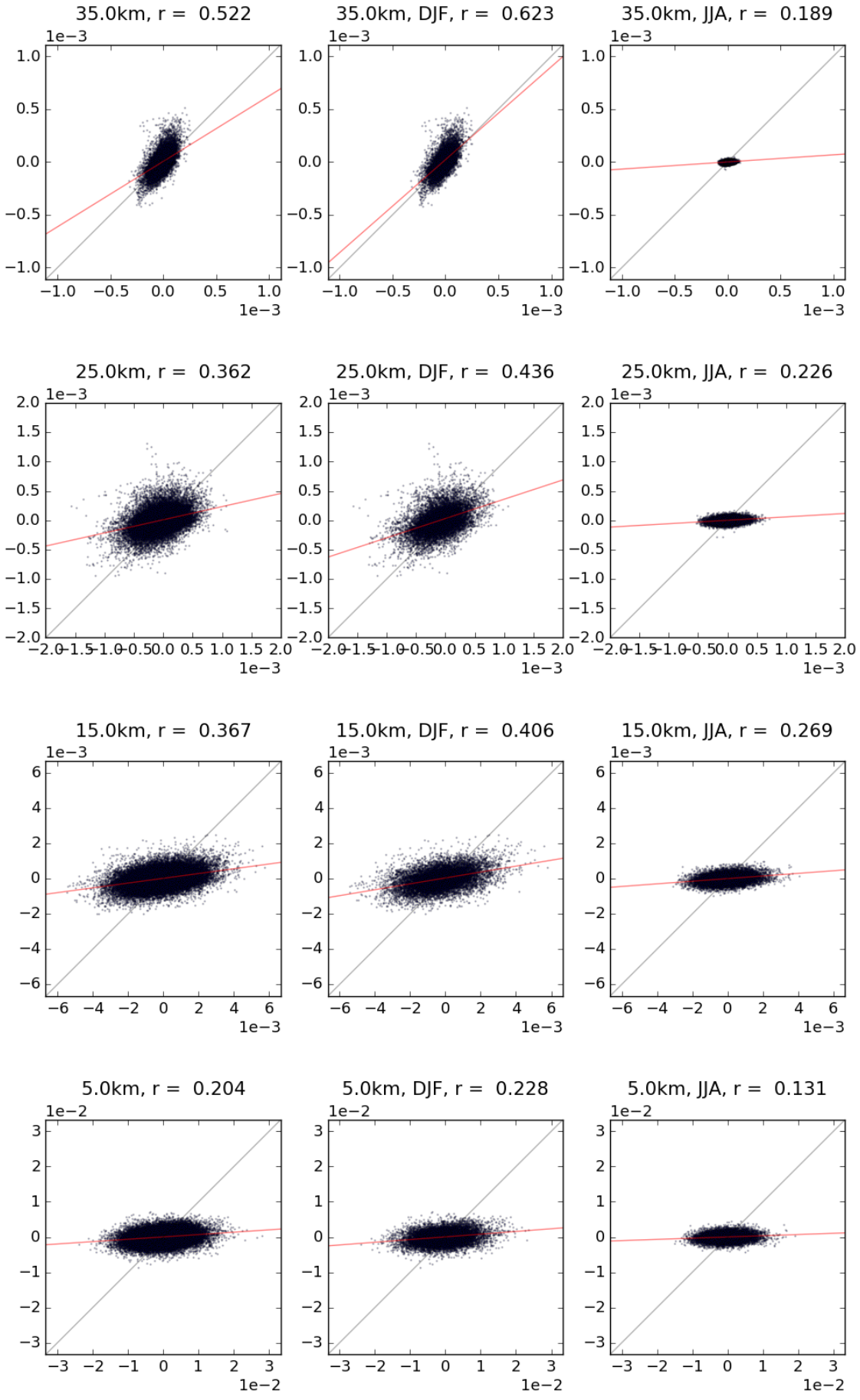

Figure 4.18.: Scatter plots comparing the anomalous polar pressure tendency predicted by QG theory using streamfunction ψ_{QG} (horizontal axis) and that observed in ERA-Interim (vertical axis). Data in the left column is from 1979 to 2016. Data in the middle column is from the winter months of December, January, and February of these years. Data in the right column is from the summer months of June, July, and August in these years. The red lines indicate the least-squares best fit. Units are Pa/s.

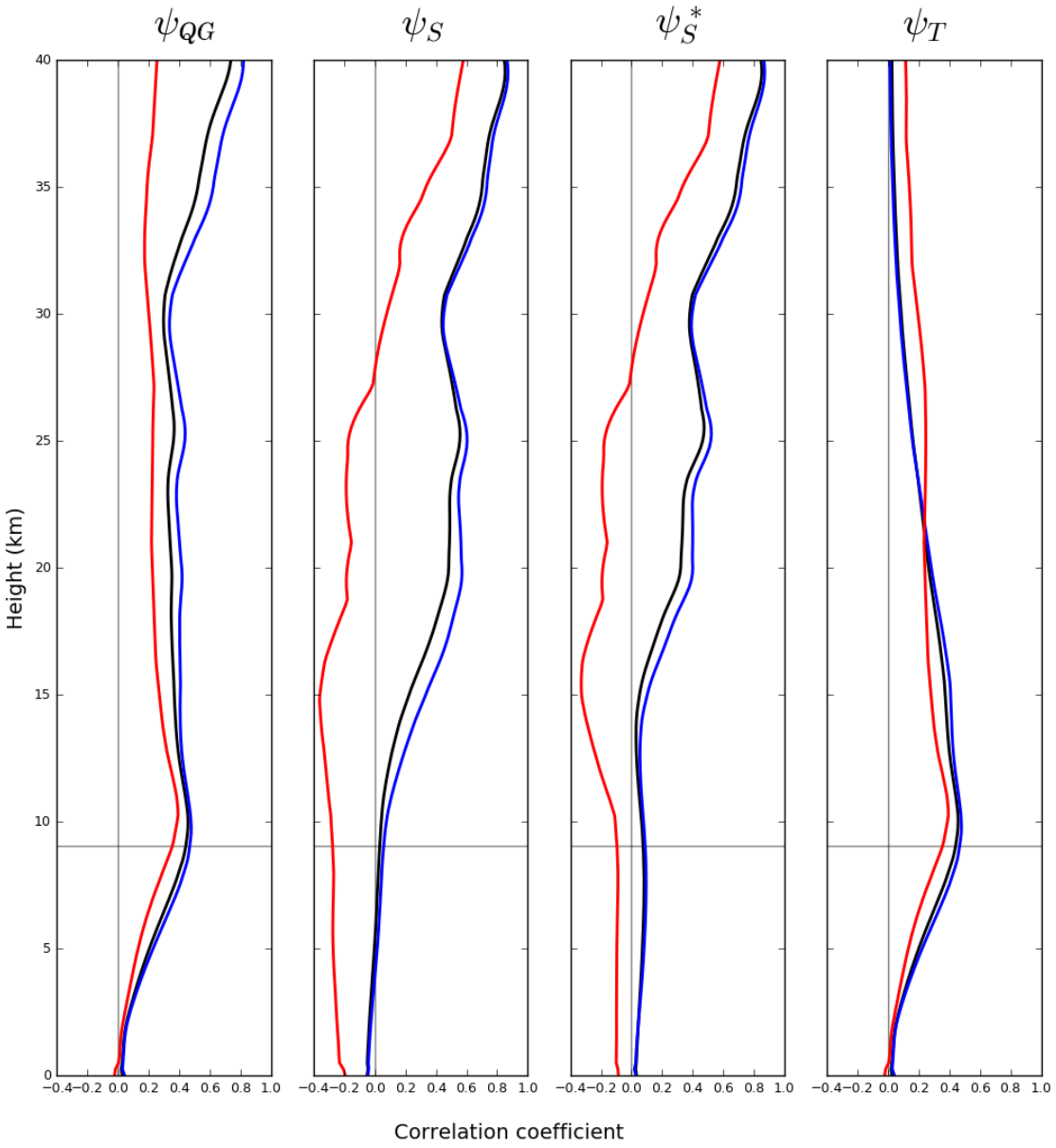

Figure 4.19.: The correlation coefficient between anomalous polar pressure tendencies approximated by QG theory, using eqs. 3.28, and calculated using data from ERA-Interim. Data is from 1979 to 2016. The streamfunction used in the calculation is shown above the subplot: ψ_{QG} is the streamfunction associated with the inversion of QGPV in the entire atmospheric column, q; ψ_S is the streamfunction associated with inversion of stratospheric QGPV q_S only; ψ_S^* is as ψ_S but also including the interference between ψ_S and ψ_T term in eq. 4.2; and ψ_T is the streamfunction associated with inversion of tropospheric QGPV q_T only. Black lines show the correlation across all months during these years; blue lines show the correlation during the winter months of December, January, and February; red lines show the correlation during the summer months of June, July, and August. The horizontal line shows the mean height of the tropopause, defined as in fig. 3.2.

tropospheric pressure tendencies. The correlation of the non-linear interference term in eq. 4.2 with observed horizontal mass fluxes in the troposphere is not seen in the correlation of QG and reanalysis pressure tendencies. However, as seen in fig. 4.17 the stratospheric influence on tropospheric pressure tendencies seems largest during extremely large disturbances to the stratospheric field. This, combined with the strong annual cycle shown in fig. 4.19, suggests that perhaps the QG pressure tendencies perform better around extreme events in the pressure field, such as SSWs. This is explored in the following section.

4.5.1. Extreme events

Given that pressure tendencies in reanalysis are largest in winter, it is possible that the ability of QG theory to approximate mass fluxes, and thus predict pressure tendencies, is proportional to the magnitude of the mass flux. This can be tested by comparing the correlation of extreme values of the pressure tendency in reanalysis and those predicted by quasi-geostrophy. This analysis is shown in fig. 4.20.

The correlation of pressure tendencies in reanalysis and those calculated using ψ_{QG} across the whole dataset is shown to increase with altitude from around zero at the surface to approximately 0.4 at the tropopause, and then gradually increase to approximately 0.8 at 40km. If however pressure tendencies at altitude z are considered only if more than one standard deviation from the mean at z (in reanalysis), then the correlation is greater, with a value of approximately 0.6 at the tropopause increasing to $\sim$0.85 at 40km. Further, if tendencies are considered only if more than two standard deviations from the mean, as might be a definition of an 'extreme event', then this correlation increases further still, being greater than 0.7 at the tropopause and 0.9 at 40km. If stratospheric information alone is considered, and so ψ_S is used to calculate the tendencies, a similar increase in correlation at a given z is seen when considering successively more extreme values. This only applies to the stratosphere however: in the troposphere the correlation remains approximately the same. If the interference between ψ_S and ψ_T is accounted for as well as the direct stratospheric influence, however, then the correlation in the mid-troposphere does increase to a moderate 0.2.

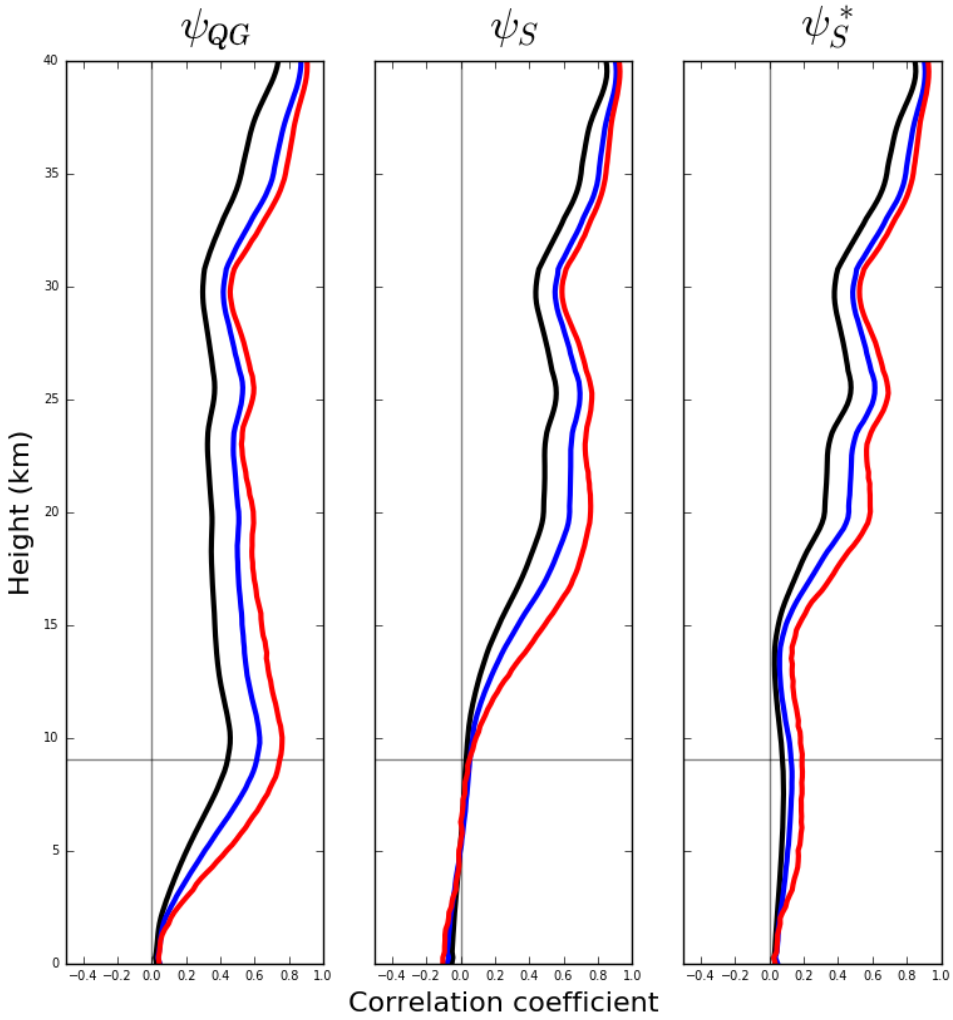

Figure 4.20.: The correlation of pressure tendencies observed in ERA-Interim and those approximated by QG theory using various streamfunctions. The correlation is calculated for all values of the reanalysis pressure tendency (in black), for those dates on which the tendency was greater than one standard deviation from the mean tendency at height z (in blue), and for those dates on which the tendency was greater than two standard deviations from the mean tendency at height z (in red). The streamfunction used in the calculation is shown above the subplot: ψ_{QG} is the streamfunction associated with the inversion of QGPV in the entire atmospheric column, q; and ψ_S is the streamfunction associated with inversion of stratospheric QGPV q_S only; ψ_S^* is as ψ_S but also including the interference between ψ_S and ψ_T term in eq. 4.2.

	Gross error	Tropospheric error	Stratospheric error
ψ_{QG}, All	2.88	3.08	0.92
ψ_{QG}, σ	0.95	1.65	1.28
ψ_{QG}, 2σ	1.09	1.18	0.91
ψ_S^*, All	1.03	1.01	1.06
ψ_S^*, σ	0.97	0.99	0.93
ψ_S^*, 2σ	0.95	0.99	0.88

Table 4.1.: The mean RMS error to signal ratio of the observed pressure tendency in ERA-Interim and the tendency approximated by QG theory, for the whole atmosphere, and for the troposphere and stratosphere individually. This is calculated using QGPV data from the whole atmosphere, represented by ψ_{QG}, and using QGPV from the stratosphere only (also accounting for the interaction of the stratospheric and tropospheric streamfunctions), represented by ψ_S^*. This is done for all dates, dates when the reanalysis pressure tendency exceeded one standard deviation from the mean, and dates when the tendency exceeded two standard deviations from the mean. The tropopause is defined daily, as in fig. 3.2.

An alternative quantitative assessment of the QG result eq. 3.28 is the RMS residual of the observed and predicted pressure tendencies, as introduced in section 4.4.1. The previous sections have shown that QG results for the horizontal mass flux, vertical mass flux, and pressure tendency perform distinctly in the troposphere and for the stratosphere. As such average RMS residuals for the troposphere and stratosphere are considered. Of course when considering extreme values of the pressure tendency, defined by being above a certain number of standard deviations from the reanalysis mean, the residual between prediction and observation will increase as the magnitude of the observed tendency increases. To enable comparison between different definitions, the RMS error is normalised by the magnitude of the pressure tendency seen in reanalysis. This forms a RMS error to signal ratio. This ratio is shown in table 4.1. Again, as seen in fig. 4.20, as the magnitude of the pressure tendency in reanalysis increases, the relative error of the tendency approximated by QG theory decreases. This is true for both the troposphere and stratosphere, but is particularly noticeable in the troposphere. When stratospheric information only is used, the RMS error still decreases, though not as substantially.

4.6. Summary

This chapter examined the performance of the QG plunger hypothesis. This was done first by separating the two steps of the hypothesis - a QGPV inversion followed by use of derived mass flux equations - and evaluating them individually using reanalysis data. QG estimates of horizontal and vertical mass fluxes, H and V, and the resulting QG polar pressure tendencies were then calculated using eq. 3.28 and a QG streamfunction. Two different QGPV distributions were inverted to produce associated streamfunctions: one using data from the whole atmosphere, and one using data from the stratosphere only, in order to isolate stratospheric contributions to QG pressure tendencies in the troposphere. The key results from this chapter were:

- The mass flux framework of the plunger hypothesis has intrinsic errors, notably in calculating zonal average mass fluxes, but calculations made using equations of the theory do broadly compare favourably with observations. The mass flux framework performs best in the winter months and worst in the summer months;

- The method used to invert QGPV in this thesis works well in the stratosphere but less well in the troposphere. The streamfunction field itself, and associated velocity and density fields, calculated from the inversion of QGPV from the whole atmosphere correlated well with reanalysis fields, though less well above landmasses in the lower troposphere. By construction however ageostrophic velocities were not recreated using this methodology. Fields calculated from the inversion of only stratospheric QGPV correlated well in the stratosphere but barely at all in the troposphere;

- Eddy horizontal mass fluxes into the polar region are approximated with good accuracy throughout the atmospheric column by QG theory. The zonal mean horizontal mass flux is not however, being uniformly predicted with mediocre accuracy in the stratosphere, and most accurately predicted at the summer tropopause. If only using stratospheric information then horizontal mass flux is not predicted with any accuracy in the troposphere;

- If the non-linear interaction of stratospheric information with tropospheric information is accounted for, outside the summer months horizontal mass fluxes are predicted with greater accuracy in the troposphere, indicating that this non-linear interaction

is substantial;

- Vertical mass fluxes are approximated with less accuracy, but if only using stratospheric information outside the summer months are predicted with moderate accuracy in the stratosphere;

- Polar pressure tendencies approximated by these QG fluxes are of the correct order of magnitude, but do not correlate with reanalysis tendencies in the troposphere. This is partly due to errors associated with the QG streamfunction, and the pressure tendency itself being a small residual of two large fluxes. As altitude increases the correlation increases, but only moderately. As such the QG plunger hypothesis does not accurately account for changes in the lower polar atmosphere, but does so to an accuracy in the stratosphere comparable to when an established reanalysis streamfunction is used. Also similar to the result using a reanalysis streamfunction, the QG framework demonstrates a strong seasonal dependence, predicting most accurately in the winter and least accurately in the summer;

- If using stratospheric information alone, even accounting for the interference of stratospheric and tropospheric information, polar pressure tendencies are not approximated with any degree of accuracy in the troposphere according to correlation statistics. However, a randomly chosen case study does show large features descending from the stratosphere into the troposphere, matching reanalysis, using stratospheric information alone;

- As the magnitude of the polar pressure tendency in reanalysis increases, the relative error in the QG approximation of the tendency decreases in both the stratosphere and troposphere. Combined with a strong seasonal dependence of the performance of the mass flux framework, this implies that the theory may be most appropriate in considering SSWs.

5. The quasi-geostrophic influence of sudden stratospheric warmings

"Success seems to be in short supply lately"
- *(Janeway, K)*

5.1. Aims

In the previous two chapters a new way of looking at stratospheric influence on the troposphere has been introduced, and an associated theory developed: changes in the stratospheric PV field remotely, quasi-geostrophically, flux mass into the polar region, forcing the polar cap pressure index. This mass flux framework has been shown to have associated errors when calculating fluxes using an established reanalysis streamfunction, but calculated pressure index tendencies which compared favourably with reanalysis throughout the atmospheric column. When using a streamfunction obtained through the inversion of QGPV the theory was shown to perform substantially worse in the troposphere, in part due to tropospheric errors in the inversion process, but comparably to when a reanalysis streamfunction was used in the stratosphere. As obtained through inversion of stratospheric QGPV only, stratospheric information appears to contribute significantly to mass fluxes in the stratosphere, but this influence decreases beneath the tropopause.

In this chapter the extreme events known as sudden stratospheric warmings (SSWs) are examined using this plunger hypothesis. First the event introduced in chapter one - beginning on December 25th 1984 - is investigated, comparing observed horizontal mass fluxes and polar pressure tendencies seen in reanalysis to those calculated from QG theory. In

the following section all SSWs defined by two different algorithms have their mass fluxes and associated polar pressure tendencies examined. Within these algorithms the tropospheric pressure response to split and displacement SSWs are compared to determined if, as has been speculated, there is a difference in how the two classifications influence the troposphere.

Finally the QG theory is applied to SSW events defined by the two algorithms, approximating mass fluxes and associated pressure tendencies using QGPV information from the whole atmospheric column, and from the stratosphere alone. The objective is to determine if stratospheric information, encoded in QGPV and communicated by the associated streamfunction, substantially influences tropospheric pressure in the aftermath of SSWs. And, further, if this influence differs when the SSW is a split or displaced vortex.

5.2. December 25th, 1984

The algorithms used in both CP07 and DM13 categorise December 25th 1984 as the onset of a vortex split event. The details of these algorithms will be reviewed in the following section. The horizontal and vertical mass fluxes associated with this event can be calculated using the QG eqns. 3.19 and 3.27. These QG-approximated fluxes are presented in figs. 5.2-5.3 from one month before to one month after December 25th, alongside the equivalent fluxes seen in reanalysis. Combined these fluxes allow for the calculation of QG-approximated polar cap pressure tendencies, via eq. 3.28. The pressure tendencies calculated using this equation are shown first in fig. 5.1.

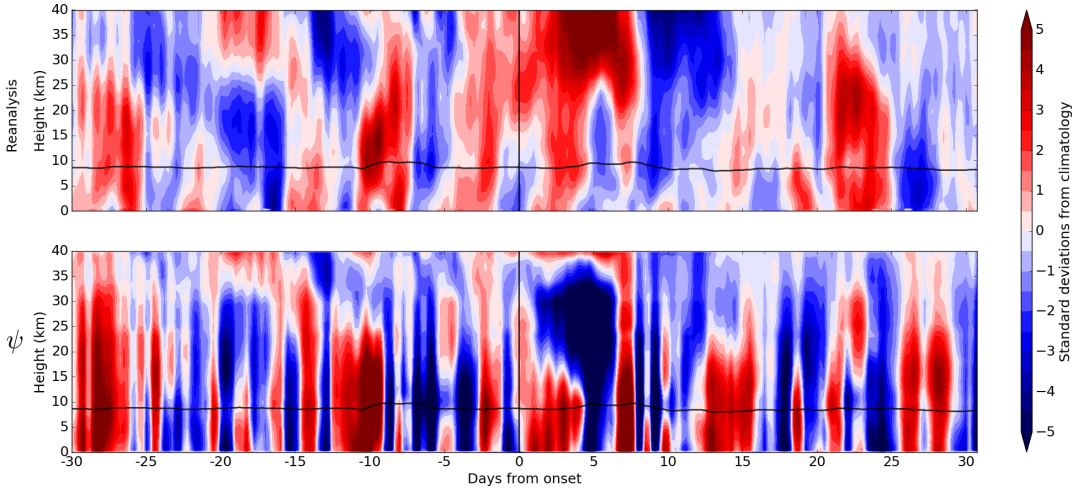

Figure 5.1.: Polar cap pressure index tendencies surrounding the SSW on December 25th 1984, as seen in ERA-Interim and as calculated using QG streamfunction ψ in eq. 3.28. Tendencies have been standardised by the variance of the polar cap pressure tendency in reanalysis. The black line shows the position of the thermally-defined tropopause, defined as in fig. 3.2.

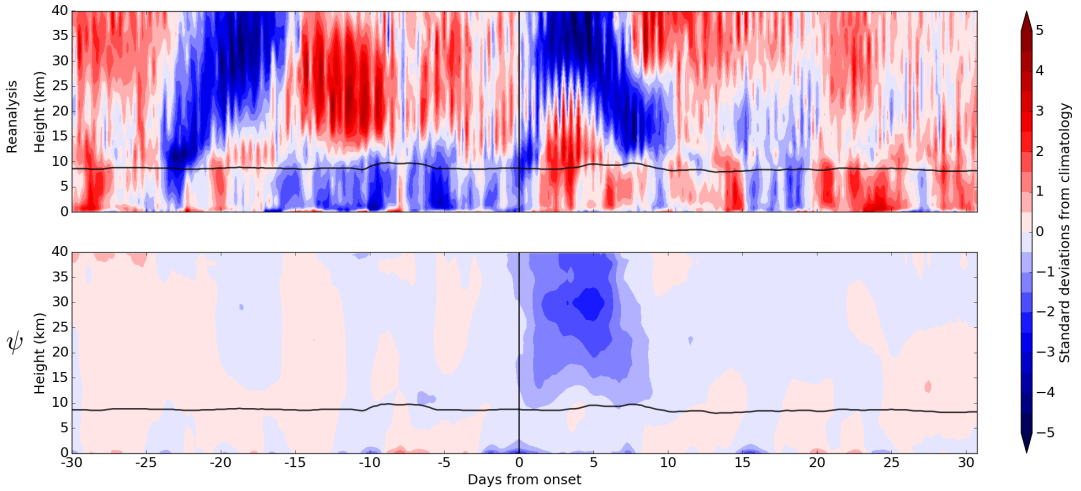

Figure 5.2.: Horizontal mass flux H surrounding the SSW on December 25th 1984, as seen in ERA-Interim and as calculated using QG streamfunction ψ in eq. 3.19. Fluxes have been standardised by the variance of the flux in reanalysis. The black line shows the position of the thermally-defined tropopause, defined as in fig. 3.2.

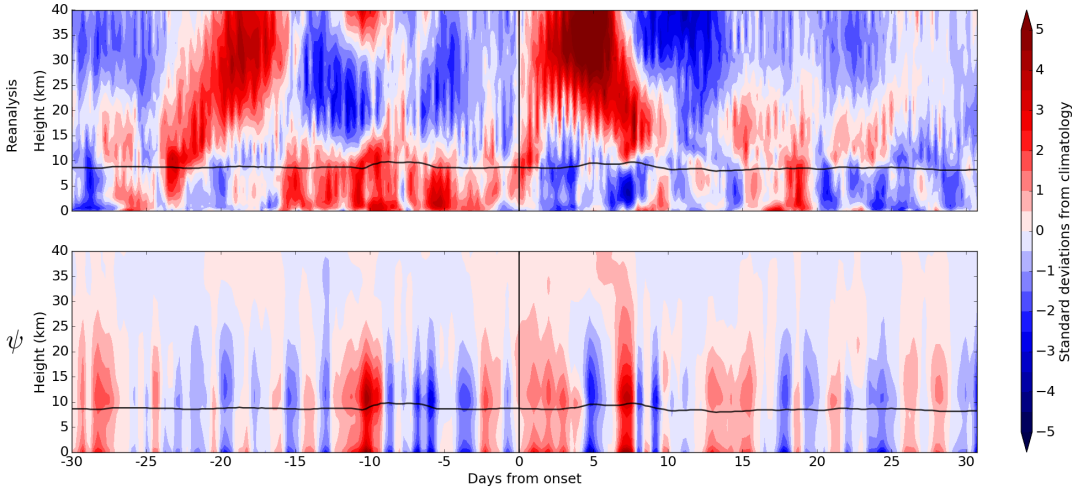

Figure 5.3.: Vertical mass flux V surrounding the SSW on December 25th 1984, as seen in ERA-Interim and as calculated using QG streamfunction ψ in eq. 3.27. Fluxes have been standardised by the variance of the flux in reanalysis. The black line shows the position of the thermally-defined tropopause, defined as in fig. 3.2.

The polar cap pressure index tendencies approximated by QG theory in fig. 5.1 clearly do not correlate with those seen in reanalysis immediately following the onset of the SSW. The large, characteristic positive tendency anomaly in the aftermath of the SSW is not seen in the QG tendency - instead a large negative anomaly is shown. Prior to the onset of the SSW the pressure tendency fields are more similar, with features in the stratosphere and troposphere recreated. However after December 25th the tendencies are not approximated by eq. 3.28 with any real accuracy.

Examining the horizontal and vertical mass fluxes calculated from QG theory immediately shows why this is the case. Following the onset of the SSW reanalysis shows a large, descending negative horizontal mass flux H, corresponding to mass flowing out of the polar region. Simultaneously the vertical mass flux V shows a large positive feature in the stratosphere. As such the movement of mass over the polar region is upwards and outwards, balanced such that the net result is a positive polar pressure anomaly. The proposed QG theory captures the horizontal mass flux in the stratosphere reasonably well, with a large negative flux immediately after the event onset. The vertical flux is not captured correctly at all however, with the QG-approximated V being much too small in the stratosphere immediately after onset, generally too barotropic, and not correlating with the V in reanalysis.

Across the period shown, the H and V in reanalysis appear to be nearly identical but possess opposite signs. The polar pressure tendency which results from their sum therefore relies on the majority of the two fluxes cancelling, leaving a small residual. Accurate approximation of the tendency thus depends on accurate approximation of each term. While the horizontal fluxes in this example are accurately approximated after the SSW onset, the vertical flux is not, and so accurate approximation of the pressure tendency fails.

This was one SSW event however, with many more occurring in reanalysis. Two algorithms' definitions of SSWs across 30 years of reanalysis are now compared in the following section.

5.3. Comparing SSW algorithms

As outlined in section 2.3.2, there are many ways to define SSWs and further ways to categorise them into vortex splits and displacements. To determine the pressure index response to split and displaced vortex events, as well as the associated mass fluxes, two categorisation algorithms are compared. As introduced in chapter 2, these are from CP07 and DM13.

In the algorithm from CP07, an SSW occurs when the zonal mean zonal wind at 10hPa and 60°N falls below 0 m/s between November and March (see p.27 for more details). To distinguish between vortex splits and vortex displacements, first the Laplacian of ξ at 10hPa is used to determine the edge of the polar vortex. The number of closed contours with a value of ξ equal to that at the edge of the vortex within the field are then counted. If two or more such contours exist (of n_C contours enclosing the maximum), and if the ratio of their associated circulations exceeds some threshold R (when subjectively compared to reanalysis $R = 0.5$ and $n_C = 11$ gave the best results) then the SSW is classified as a split. If this criteria is not met then the SSW is classified as a displacement. For further details see Charlton and Polvani (2007).

In the algorithm from M13 the geometry of the vortex is described in terms of the latitude of the centre of the vortex (centroid latitude) and aspect ratio (a measure of how stretched the vortex is). The variable being described is a single contour of PV or geopotential height, representing the vortex edge, chosen to be equivalent to the zonal mean value at 60°N for DJFM at 10hPa or 850K. A displacement SSW event requires the centroid latitude to remain equatorward of 66°N for a week or more. A vortex split SSW requires the aspect ratio of the vortex to remain higher than 2.4 for 7 days or more. See Mitchell et al. (2013) for further details.

These two algorithms classify observed SSWs as splits and displacements differently. The onset dates of these classified events in the ERA-Interim reanalysis between 1979 and 2002 are shown in table D.1 in Appendix D.

5.3.1. Pressure response

Following BD01, composite 'dripping paint' plots associated with DM13- and CP07-defined vortex split and displacement SSWs are shown in fig. 5.4. Note however that while BD01 considers events above some threshold value of the AO index at 10hPa, and plots the descending AO index anomalies, in this figure events are defined by criteria in DM13 and CP07, and the standardised polar pressure anomaly is plotted.

All SSWs defined by the algorithms share key characteristics: a large positive pressure anomaly in the stratosphere immediately following the onset of the SSW, with smaller negative anomalies preceding and following this positive anomaly. There are differences between the algorithms and between the split and displacements in the timing of these anomalies and the tropospheric response to SSWs. Notably the DM13 algorithm finds that vortex displacements are associated with a large stratospheric pressure anomaly which begins almost precisely at the event onset, while vortex splits have a weaker pressure anomaly which begins about five days later. Further, vortex displacements do not have a substantial associated tropospheric pressure anomaly while vortex splits do, approximately one month after SSW onset. This corroborates DM13's conclusion that NAM index anomalies propagate into the troposphere in the aftermath of splits but not in the aftermath of displacements. Conversely, split and displacement SSWs defined by the CP07 algorithm do not display a substantial difference in either their tropospheric pressure response or in the structure of the stratospheric pressure response. This corroborates the conclusion of Maycock and Hitchcock (2015) that the tropospheric NAM index after SSWs does not significantly depend on whether the SSW was a displaced or split vortex.

As in section 3.2.1, the pressure index has been shown to recreate results obtained from annular mode analysis in the aftermath of SSWs. Next the mass fluxes associated with each classification of SSW in reanalysis are examined, and compared to their QG approximations.

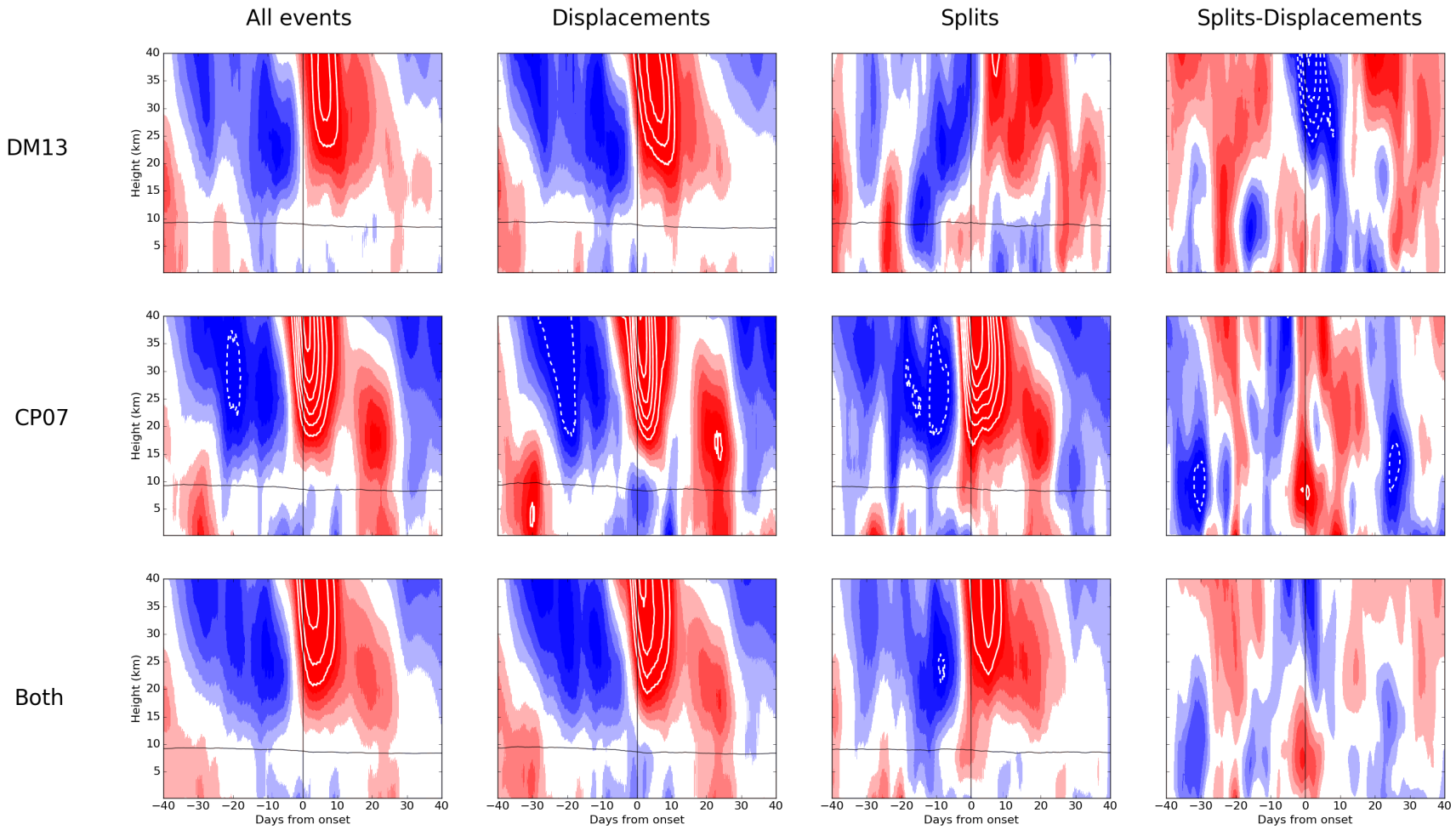

Figure 5.4.: The standardised pressure index around SSWs defined as splits and displacements by DM13 and CP07. Units are standard deviations from the mean, data is from ERA-Interim. The contour interval for the colour shading is 0.25, and 0.5 for the white contours. Values between -0.25 and 0.25 are unshaded. The black line shows the average location of the tropopause in reanalysis, defined as in fig. 3.2, surrounding the dates of SSW events according to DM13 and CP07.

5.3.2. Quasi-geostrophic approximation of SSWs

In this section the approximation of SSWs defined by the CP07 and DM13 algorithm using QG theory is examined. First the mass fluxes associated with each algorithm's classification of vortex splits and displacements seen in reanalysis are examined. Following this the quasi-geostrophic approximation of these fields, and the associated QG approximation of the polar pressure tendency, using streamfunction ψ are compared to reanalysis. Finally the mass fluxes and polar pressure tendencies approximated using the inversion of stratospheric QGPV only are compared to reanalysis, using streamfunction ψ_S, to determine the QG influence of the stratosphere on the troposphere in the aftermath of SSWs.

All of this analysis will refer extensively to figs. 5.5-5.8, shown over the next several pages, which show the fluxes and pressure tendencies associated with each algorithm's definition of vortex split and vortex displacement SSWs.

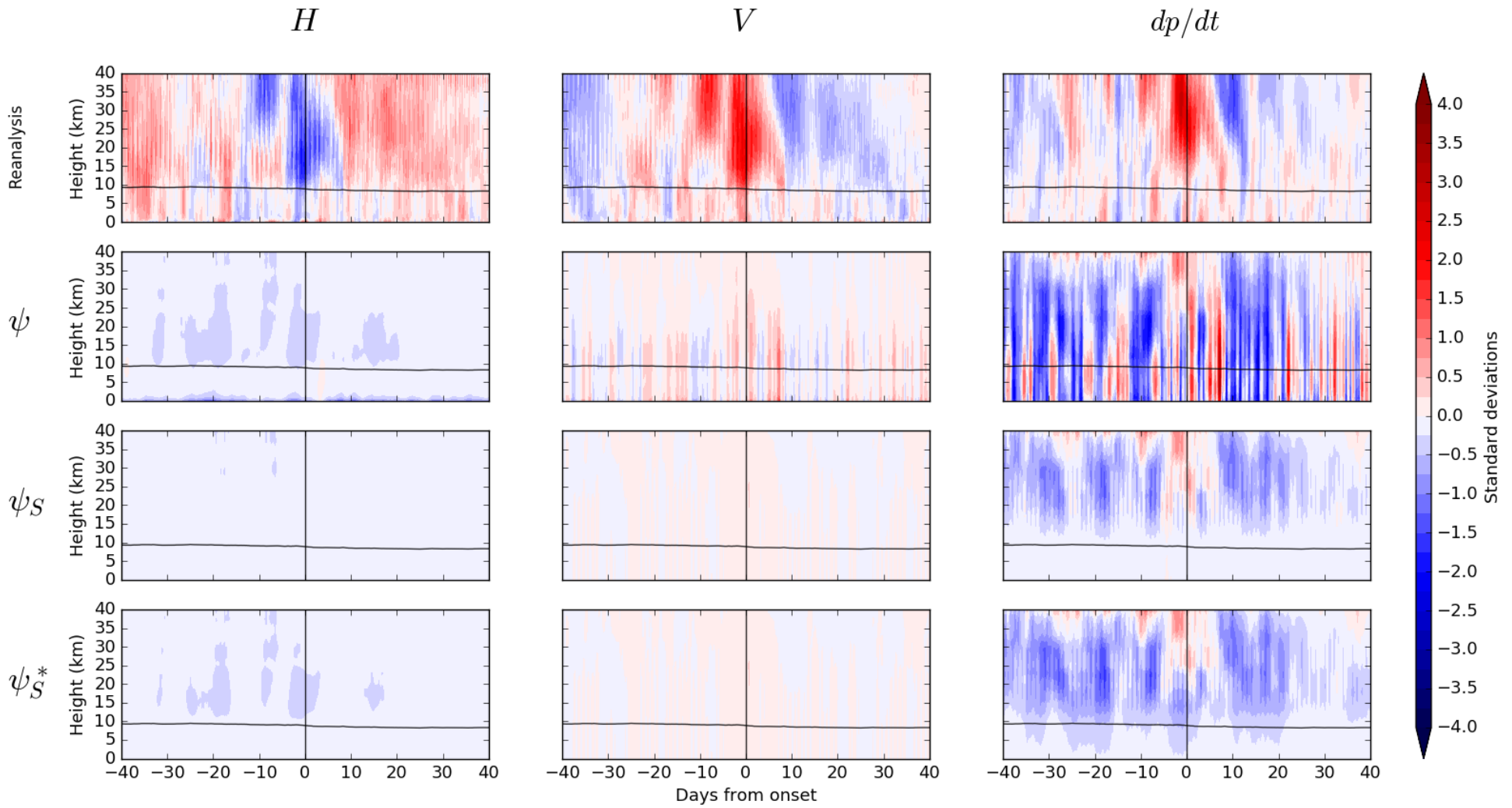

Figure 5.5.: The horizontal mass flux H, vertical mass flux V, and polar cap pressure index tendency dp/dt surrounding vortex displacement SSWs defined by the DM13 algorithm. As seen in reanalysis (ERA-Interim), and as approximated by the streamfunction associated with inversion of QGPV in the whole atmosphere, ψ, the streamfunction associated with stratospheric QGPV only, ψ_S, and the streamfunction associated with stratospheric QGPV only but also accounting for the interference term in eq. 4.2, ψ_S^*. The black line shows the average location of the tropopause in reanalysis, defined as in fig. 3.2.

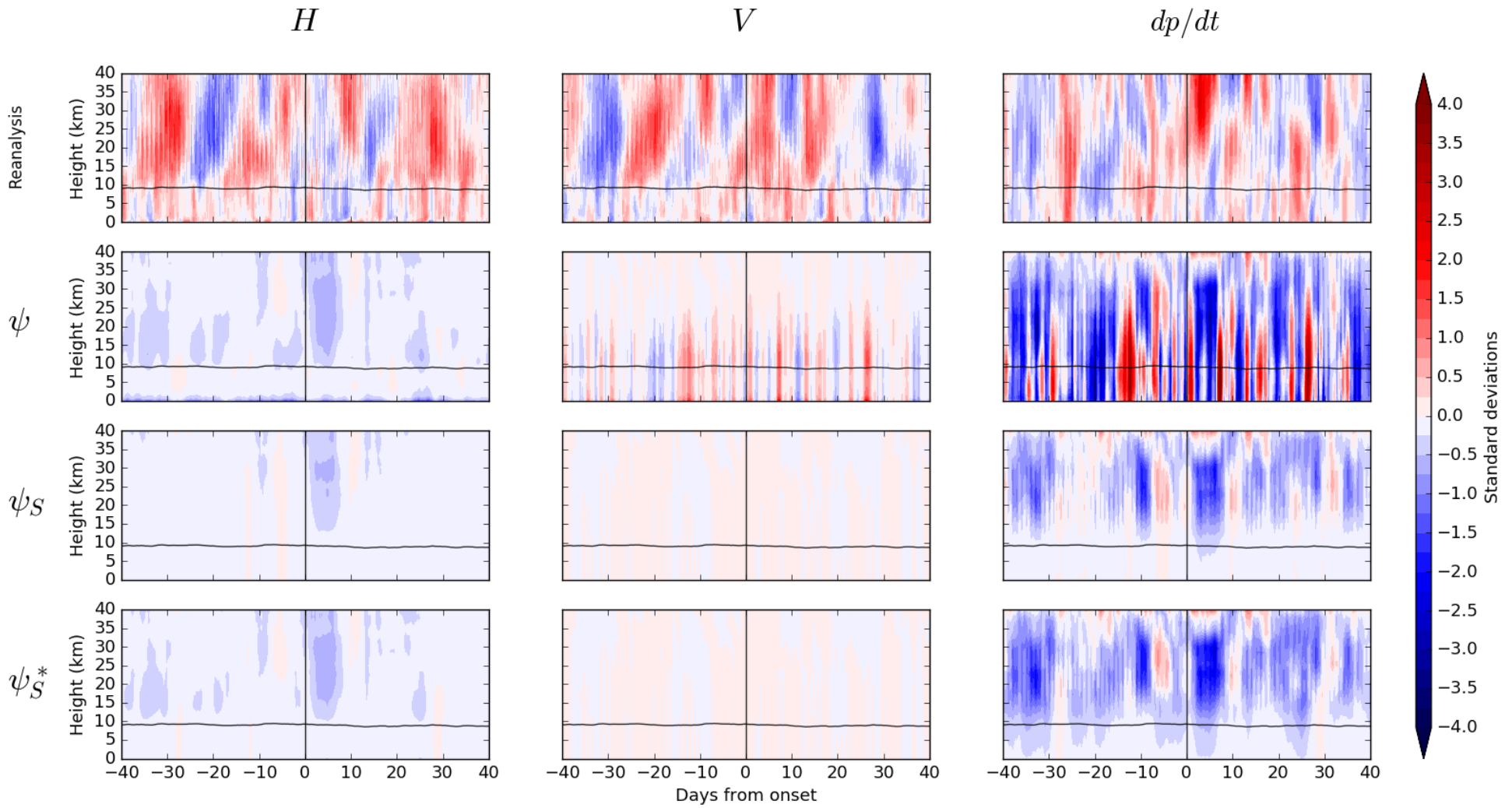

Figure 5.6.: The horizontal mass flux H, vertical mass flux V, and polar cap pressure index tendency dp/dt surrounding vortex split SSWs defined by the DM13 algorithm. As seen in reanalysis (ERA-Interim), and as approximated by the streamfunction associated with inversion of QGPV in the whole atmosphere, ψ, the streamfunction associated with stratospheric QGPV only, ψ_S, and the streamfunction associated with stratospheric QGPV only but also accounting for the interference term in eq. 4.2, ψ_S^*. The black line shows the average location of the tropopause in reanalysis, defined as in fig. 3.2.

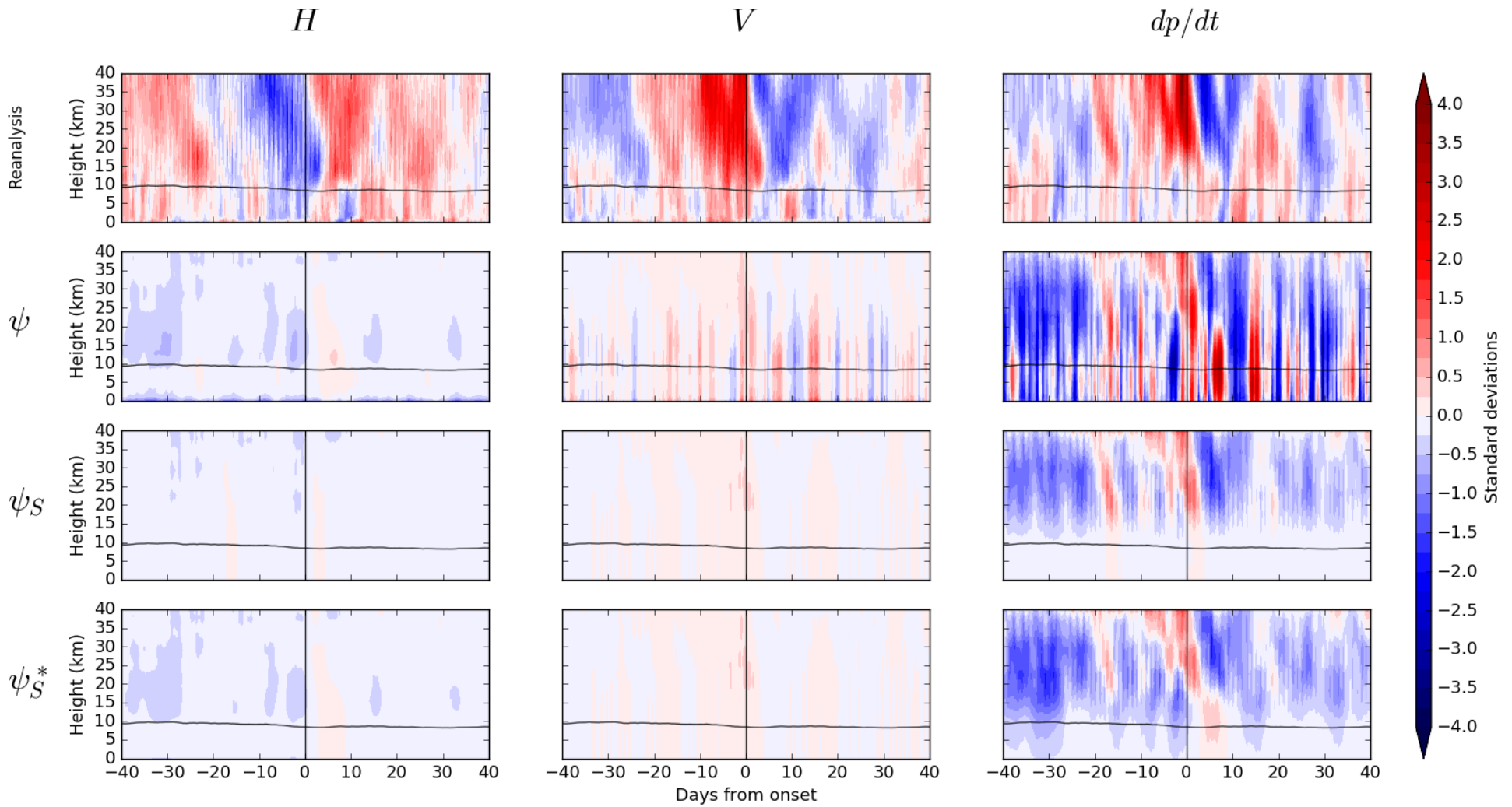

Figure 5.7.: The horizontal mass flux H, vertical mass flux V, and polar cap pressure index tendency dp/dt surrounding vortex displacement SSWs defined by the CP07 algorithm. As seen in reanalysis (ERA-Interim), and as approximated by the streamfunction associated with inversion of QGPV in the whole atmosphere, ψ, the streamfunction associated with stratospheric QGPV only, ψ_S, and the streamfunction associated with stratospheric QGPV only but also accounting for the interference term in eq. 4.2, ψ_S^*. The black line shows the average location of the tropopause in reanalysis, defined as in fig. 3.2.

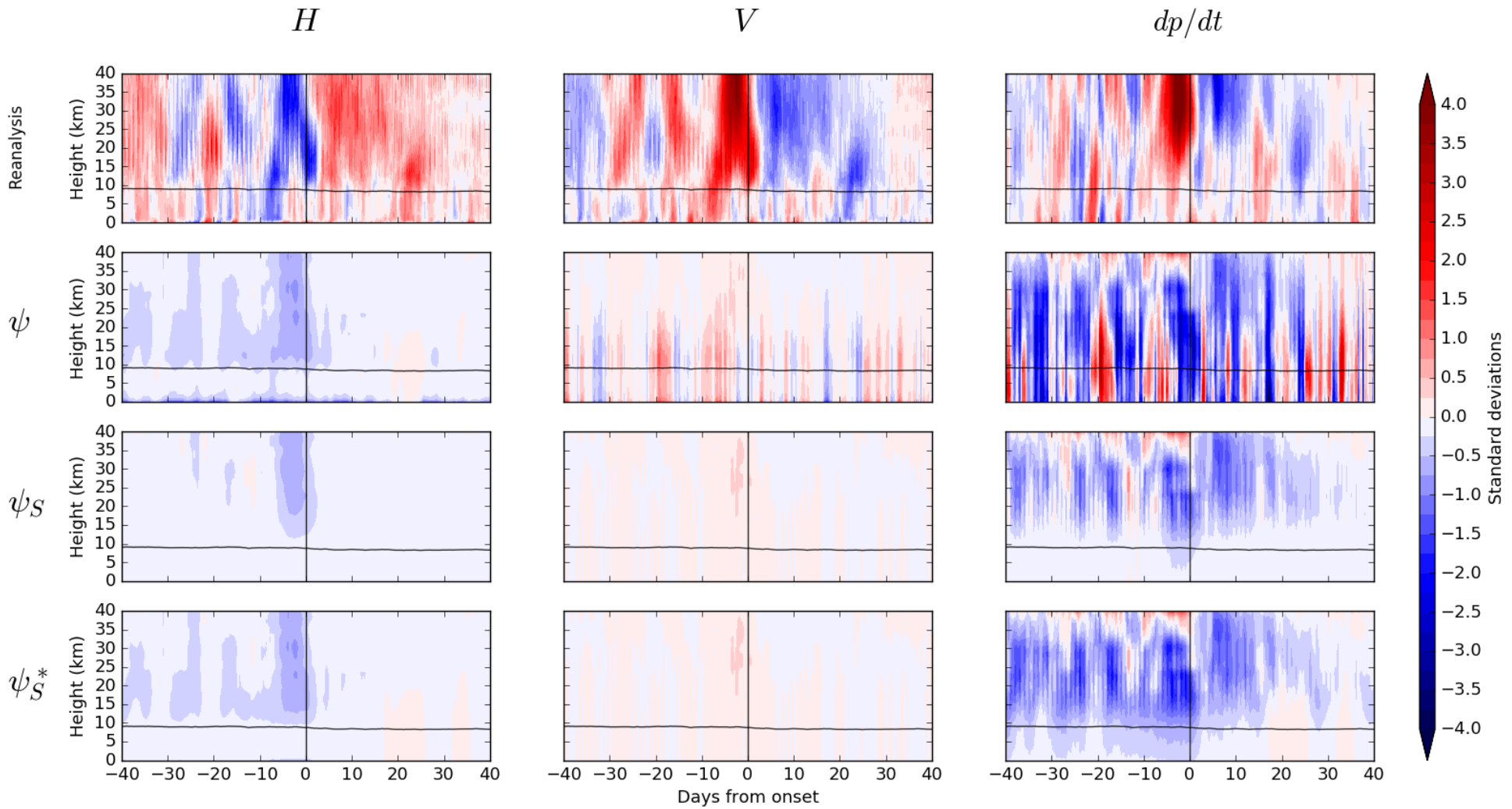

Figure 5.8.: The horizontal mass flux H, vertical mass flux V, and polar cap pressure index tendency dp/dt surrounding vortex split SSWs defined by the CP07 algorithm. As seen in reanalysis (ERA-Interim), and as approximated by the streamfunction associated with inversion of QGPV in the whole atmosphere, ψ, the streamfunction associated with stratospheric QGPV only, ψ_S, and the streamfunction associated with stratospheric QGPV only but also accounting for the interference term in eq. 4.2, ψ_S^*. The black line shows the average location of the tropopause in reanalysis, defined as in fig. 3.2.

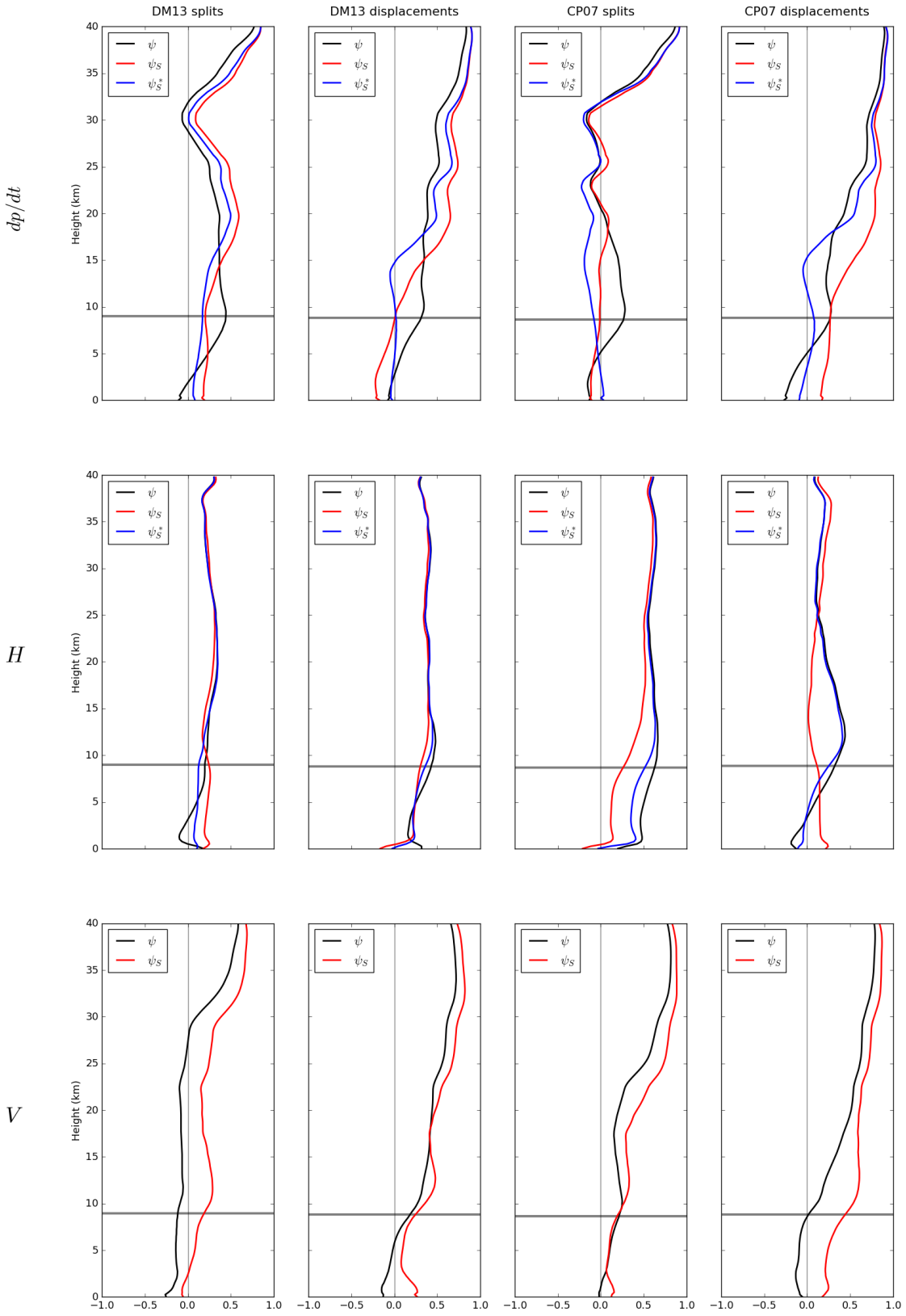

Figure 5.9.: The correlation of composite polar cap pressure index tendency dp/dt, horizontal mass flux H, and vertical mass flux V observed in ERA-Interim and those calculated from quasi-geostrophy for 40 days either side of SSWs defined by the CP07 and DM13 algorithms. The correlation of fields calculated using the streamfunction associated with inversion of QGPV through the whole column, ψ, are shown in black; the correlation of fields calculated using the streamfunction associated with inversion of QGPV in the stratosphere only, ψ_S, are shown in red; and the correlation of fields calculated using stratospheric QGPV but also including non-linear interaction of stratospheric and tropospheric information in eq. 4.2, using streamfunction ψ^*_S, are shown in blue. The horizontal line shows the average position of the thermally-defined tropopause, defined as in fig. 3.2, for the dates surrounding SSWs defined by each algorithm.

Mass fluxes in reanalysis

The composite horizontal and vertical mass fluxes for the 40 days surrounding SSWs are shown in figs. 5.5-5.8. As already shown in the case study of figs. 5.1-5.3, the composite polar pressure tendency is the small residual of the horizontal and vertical mass fluxes with approximately equal magnitudes but opposite signs. This is consistent with the concept of the column of air over the polar cap being forced by the wave-driven pump, with a meridional overturning circulation forcing air masses over the pole to ascend before fluxing southwards and out of the region. Around the onset of SSWs this is seen as large, negative H anomalies and large, positive V anomalies weighted such that they sum to produce a substantial positive pressure tendency, as shown in all figures except fig. 5.6: split vortex SSWs in the DM13 algorithm. In this figure there is no one large magnitude ($> 2\sigma$) flux in the H and V fields, as in figs. 5.5, 5.7, and 5.8, but instead alternating bands of positive and negative anomalies with smaller magnitudes. This suggests that the DM13 algorithm determines the onset of split vortex SSW to have a variable lag to the substantial mass flux associated with the SSW, resulting in events cancelling with one another and overlapping in the plot. Further evidence to support this conclusion is seen in fig. 5.8, showing the vortex split SSWs defined by the CP07 algorithm. The figure does not show a notable difference in H and V between vortex splits and vortex displacements defined by CP07. While the duration of the substantial stratospheric mass flux is shorter (approximately 5 days compared to 15 days) and weaker for vortex splits than for vortex displacements there is still only one mass flux greater than two standard deviations from the mean in the H and V fields. This would suggest that in the CP07 algorithm there is no fundamental difference between the structure of stratospheric mass fluxes which force polar pressure tendencies around vortex splits and vortex displacements.

Based on this analysis of mass fluxes, it appears that the CP07 algorithm defines vortex split SSWs with a more consistent lag to the substantial stratospheric mass flux, which typifies SSWs, than the DM13 algorithm. This would explain the polar pressure anomaly associated with DM13 split vortex events shown in fig. 5.4, distinct from all other definitions of SSWs in its weakened, delayed pressure response.

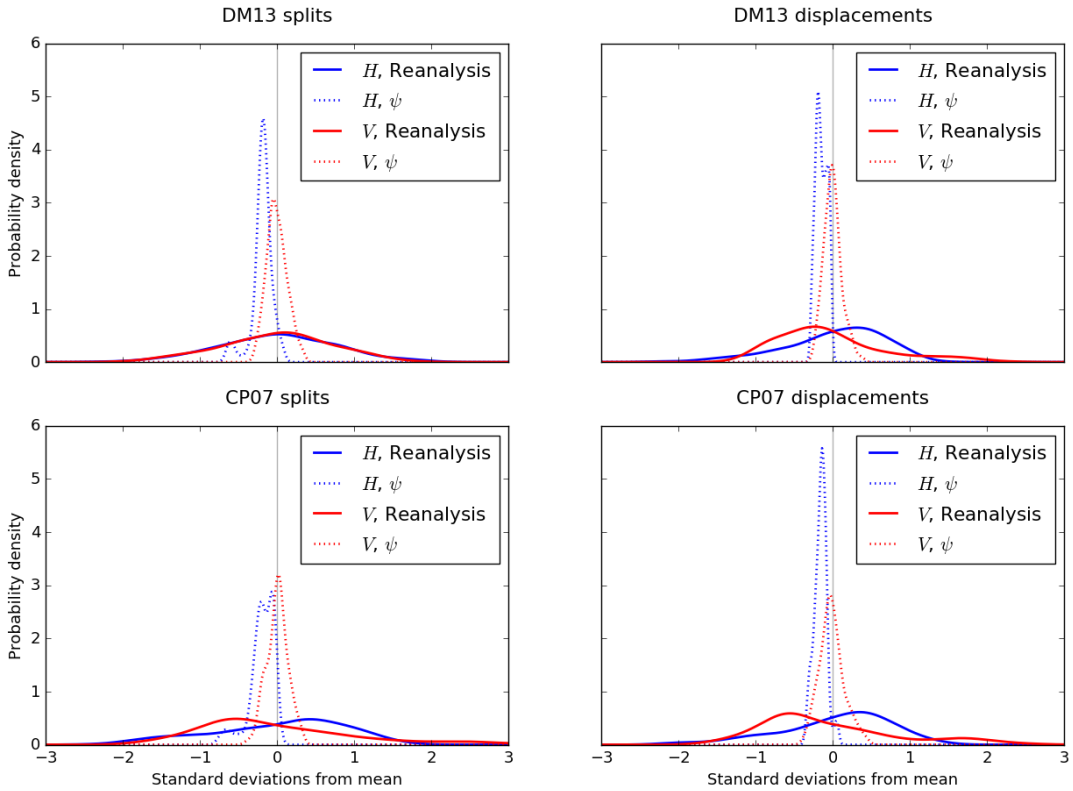

Figure 5.10.: Probability density functions of the standardised H (in blue) and V (in red) at 25km shown in figs. 5.5-5.8, as seen in reanalysis (solid line) and as calculated from the streamfunction ψ associated with inversion of whole atmosphere QGPV (dotted line).

Quasi-geostrophic approximation of sudden stratospheric warmings

The approximations of H and V calculated using QG streamfunction ψ are much too small in magnitude. This is clearly shown in fig. 5.10, where the probability densities functions (PDFs) of the standardised H and V seen in figs. 5.5-5.8 at 25km are plotted. The composite fluxes at 25km calculated from the QG streamfunction ψ have a variance of around 0.02σ across all definitions of SSW, while in reanalysis the same fluxes have a variance of $0.4 - 1\sigma$. Further, for most definitions of SSWs the PDFs for H and V have maxima at around $+0.35\sigma$ and -0.5σ respectively in reanalysis. In the QG-calculated H and V the PDFs have maxima at approximately -0.14σ and -0.01σ respectively. Combined with small variance, the H approximated by QG theory is almost entirely negative around SSWs when it should be largely positive. The vertical flux V does take both positive and negative values, but in a way that is not consistent with most of reanalysis. The exception among the PDFs of H and V is the set associated with splits within the DM13 algorithm, which both peak in reanalysis around zero. This further emphasises the dissimilarity between vortex splits within the DM13 algorithm and all other classifications of SSW considered.

Fig. 5.10 only shows the PDFs of mass fluxes at 25km. Figs. 5.5-5.8 show that QG V is generally too barotropic and too small in magnitude in the stratosphere, but captures the large scale features of the mass flux time series seen in reanalysis with greater accuracy than the QG-approximated H, which is biased towards being negative. This is also seen in fig. 5.9 as a greater correlation between reanalysis V and QG V than between reanalysis H and QG H. This is slightly different for the vortex split SSWs according to the DM13 algorithm, where H has a greater correlation than V. Summing QG-approximated H and V, both being too small in magnitude, still produces pressure index tendencies which are of approximately the correct order of magnitude, and as seen in fig. 5.10 are in fact too large, particularly when the tendency is negative in the stratosphere.

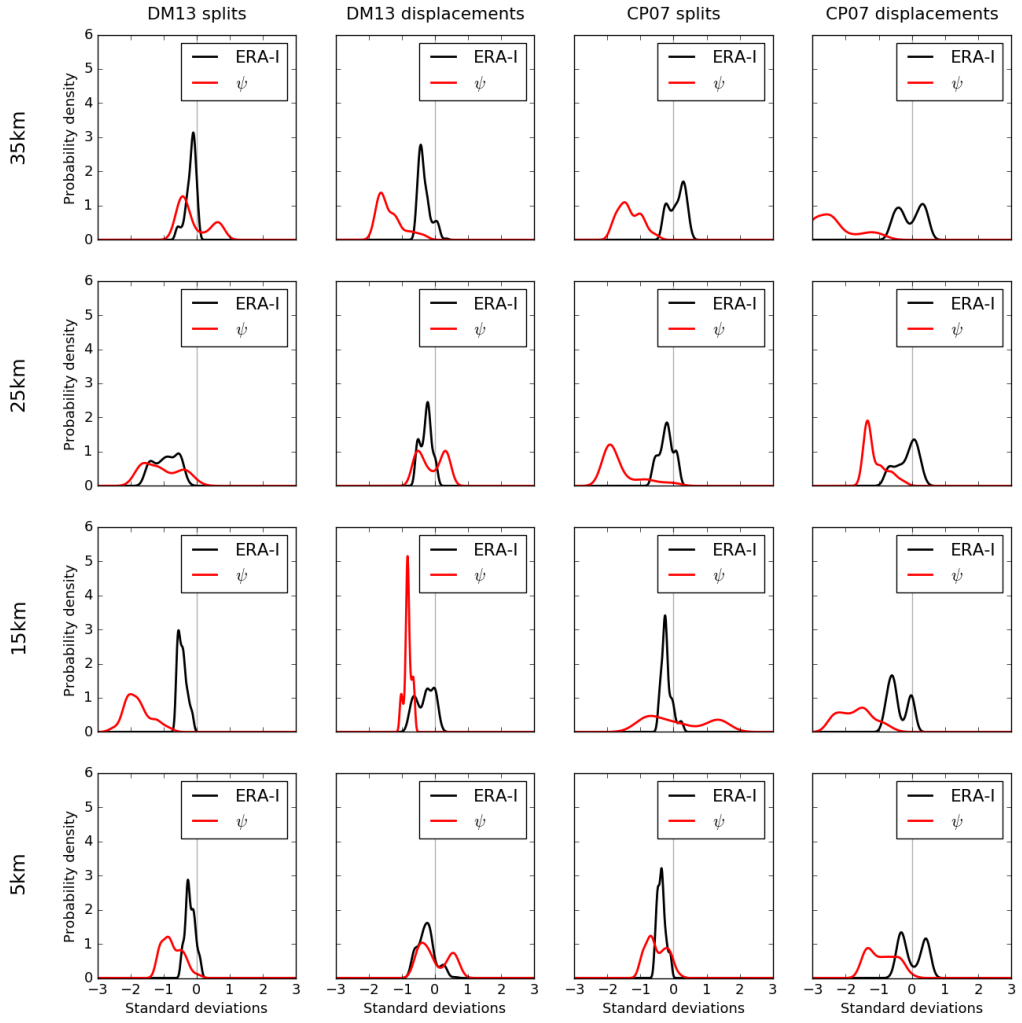

Figure 5.11.: Probability density functions of the standardised polar pressure tendency shown in figs. 5.5-5.8, as seen in ERA-Interim (black line) and as calculated from the streamfunction ψ associated with inversion of whole atmosphere QGPV (red line).

Combining QG-approximated H and V produce QG pressure index tendencies as seen in figs. 5.5-5.8, which vary widely in their accuracy compared to reanalysis, depending on the definition of SSW considered. Generally the pressure tendency is too barotropic

compared to reanalysis, likely due to the barotropic structure of QG-approximated V. The tendencies are, however, closer to the correct magnitude than is the case for the approximation of H or V. This is shown in fig. 5.11, where the bias of QG pressure index tendencies to be negative, forced by H, is also apparent.

Across both DM13 and CP07 definitions of vortex split SSWs, the large stratospheric pressure tendency in the aftermath of SSW onset is not recreated in the QG pressure tendency. Instead a large negative anomaly is calculated from the QG H and V, a consequence of H being approximated as too negative relative to QG V. Comparing vortex splits and displacements within each algorithm, displacement SSWs are approximated with greater accuracy in the stratosphere than vortex splits. This is also seen in fig. 5.9, where correlations of polar pressure tendencies in reanalysis and as calculated by QG theory are greater in the stratosphere for displacement events than for split events. Tropospheric pressure tendencies are not approximated truly accurately by QG theory in any of the definitions of SSWs considered. Tropospheric correlations in fig. 5.9 are consistently small in the troposphere, though increasingly positive with altitude, and the QG PDFs at 5km in fig. 5.11 are biased towards being negative with too large a variance for all definitions of SSWs. However, qualitatively assessing figs. 5.5-5.8 the tropospheric polar pressure tendency in the immediate aftermath of displacement SSWs are approximated by QG theory slightly more accurately than in the aftermath of split SSWs. In particular the tropospheric response following vortex displacements defined by the CP07 shows a strong positive pressure index tendency, similar to that seen in reanalysis but with too great a magnitude.

Stratospheric influence on the troposphere

Pressure tendencies calculated using the QG streamfunction ψ_S, the streamfunction associated with inversion of stratospheric QGPV only, are shown in figs. 5.5-5.8 along with the component horizontal and vertical mass fluxes. The absence of tropospheric information does not substantially alter the approximation of H and V, and so the polar cap pressure index tendency, in the mid-stratosphere, as expected. The fluxes in the lower stratosphere and troposphere are notably different when using stratospheric information only however, with tropospheric pressure tendencies substantially smaller in the aftermath of SSWs. Fluxes H and V calculated using ψ_S are compared to reanalysis in fig. 5.9, showing

that while QG H correlates more weakly with reanalysis when stratospheric information only is used, QG V correlates more strongly. This is the case with all definitions of SSW considered, indicating that tropospheric QGPV decreases the accuracy of approximating V around SSWs using QG theory. The approximation of horizontal flux H does suffer from a lack of tropospheric information, and so too does the approximation of the polar pressure tendency.

As indicated in the previous chapter, however, the inclusion of the interference between ψ_S and ψ_T, the streamfunction associated with inversion of tropospheric QGPV only, substantially contributes to the approximation of H in the lower stratosphere and troposphere. This is seen in fig. 5.9, where the inclusion of this interference term in calculating H, labelled as using streamfunction ψ_S, causes the correlation with reanalysis to increase to nearly the same values as when H is calculated using ψ. This improvement is not shared with calculations of the pressure tendency however, and tendencies calculated using ψ_S^* correlate more weakly with reanalysis than tendencies calculated using ψ_S or ψ. Looking at figs. 5.5-5.8 it is clear that in all but one case the approximation of tropospheric polar pressure tendencies using ψ_S or ψ_S^* in the aftermath of SSWs is not accurate. The exception is the QG approximation of pressure tendencies following vortex displacements according to the CP07 algorithm, shown in fig. 5.7. After the onset of these SSWs the large positive pressure tendencies seen in the mid-stratosphere descend to the lower stratosphere and then the troposphere. The tropospheric impact is seen when calculating fluxes using ψ_S but intensified when using ψ_S^*.

As such, the hypothesis of this thesis that stratospheric PV substantially forces, through far-field effects, the tropospheric pressure index around SSWs via horizontal and vertical mass fluxes is not corroborated by these results. While the use of a QG streamfunction in a mass flux framework has been shown to approximate pressure tendencies with moderate accuracy, comparable to when using a reanalysis streamfunction, the limitations of the QGPV inverter used prohibit definitive statements about the hypothesis in the lower troposphere. So while QG mass fluxes have not been shown to communicate a direct, significant influence of the stratosphere on the troposphere, this remains a possibility. Further, it remains possible that stratospheric variability forces the troposphere in some way which is amplified and modified by tropospheric processes, but this is beyond the scope of this thesis.

5.4. Summary

This chapter approximated the average mass transport and associated polar cap pressure tendencies surrounding the extreme stratospheric events known as sudden stratospheric warmings (SSWs), using two different definitions of SSWs. This approximation was done using equations derived in chapter 3, and attempted to answer the question 'can the tropospheric response to SSWs be calculated using stratospheric information only?' The main results from this chapter are:

- Small, but in context significant, polar pressure tendencies around SSWs result from the slight imbalance of large horizontal and vertical mass fluxes out of and above the polar region;

- When considering mass transport, the algorithm used in DM13 does not distinguish between vortex split and vortex displacement SSWs in as meaningful a way as the algorithm used in CP07;

- Equations 3.19 and 3.27 approximate average mass fluxes around SSWs which are too small but sum to give approximately correct polar pressure tendencies in the stratosphere, but less so in the troposphere. This is more the case for vortex displacement SSWs than for vortex split SSWs, in both definitions used;

- The tropospheric response to SSWs is not approximated accurately using stratospheric information only, and only partly accurately approximated in the aftermath of vortex displacements defined by the algorithm used in CP07.

Based on these results, it cannot be concluded that tropospheric variability in the aftermath of SSWs is significantly forced by stratospheric information. This may be due to flaws in the QGPV inverter used, as discussed in section 4.3, or because tropospheric processes are essential in approximating the aftermath of SSWs in the troposphere, either through some internal variability, or amplification of a signal from the stratosphere.

6. Conclusions

"Scotty, beam us up."

- *(Kirk, JT)*

This thesis has examined the influence of the stratosphere on the troposphere in the aftermath of extreme events such as December 25th 1984. In this chapter the main findings will be reviewed, the limitations of the thesis discussed, and further work based on its conclusions suggested.

6.1. Thesis summary

In chapter 2 the events known as called sudden stratospheric warmings (SSWs) were introduced, which have been shown to influence the troposphere via downward propagation of anomalies in the Arctic Oscillation (AO) index, a simplified measure of variability at different heights in the northern hemisphere. These anomalies descend from the stratosphere into the troposphere in the aftermath of SSWs and persist for up to two months. Some studies suggest that two different types of SSW (split vortex and displaced vortex) influence the troposphere differently, but this is not certain.

In chapter 3 a new method of examining the tropospheric impact of SSWs was introduced. The traditionally-considered AO index anomaly was shown to be equivalent to a constructed polar pressure index. This index considers pressure fields on z-surfaces rather than geopotential on p-surfaces, and averages pressure anomalies over an area roughly corresponding to the polar vortex. This pressure index is forced by horizontal and vertical mass fluxes into and above the polar region in a way that is described by the continuity equation. Seeking a first-order expression for these mass fluxes, it was shown that geostro-

phy is not sufficient to generate non-zero horizontal mass flux into the polar region. Using quasi-geostrophic (QG) theory, however, approximations for the horizontal and vertical mass fluxes were derived, given a streamfunction associated with inversion of some QG potential vorticity (QGPV) distribution. It was hypothesised that information contained within stratospheric QGPV, communicated by an associated streamfunction, induced mass fluxes in the troposphere in the aftermath of SSWs, causing observed changes in the polar pressure index.

The mass flux framework of this plunger hypothesis was tested in chapter 4. Mass fluxes were calculated using derived QG equations and an established reanalysis streamfunction and found to compare poorly to observations of mass fluxes. The sum of these mass fluxes, the approximated polar pressure tendency, did compare favourably throughout the atmospheric column to observations however. It was then concluded that the QG mass flux equations were valid, though with intrinsic flaws, and thus that approximations of mass fluxes and pressure tendencies using QG streamfunctions will not be exact even with a perfectly inverted QGPV distribution. The inversion process used in this thesis was then evaluated and found to perform well in the stratosphere, but less well in the troposphere. The fluxes associated with inversion of QGPV in the northern hemisphere were then calculated, and while the eddy horizontal fluxes appeared to compare favourably with reanalysis, the zonal mean flux only correlated moderately with reanalysis in the stratosphere but poorly in the troposphere. The vertical flux performed similarly. As the QGPV equation is linear in the streamfunction used, the superposition principle allows for QGPV in the stratosphere and troposphere to be considered in isolation. This allowed for the influence of stratospheric information on QG mass fluxes to be determined by inverting stratospheric QGPV only, and using the calculated streamfunction in the calculation of mass fluxes. This was also done in chapter 4, where it was shown that when inverting stratospheric QGPV only the performance of the QG approximation of mass fluxes in the troposphere is significantly worse. However, the derived QG expression for horizontal mass flux into the polar region is non-linear in the streamfunction. As such the interaction of the streamfunction associated with inversion of stratospheric QGPV only and the streamfunction associated with tropospheric QGPV only must be accounted for. This term is found to be substantial in the troposphere, and if included in the calculation of mass fluxes, the associated approximated changes in the polar pressure index correlate marginally better with reanalysis. Further, the correlation of approximated changes in

the pressure index and reanalysis were shown to increase as the magnitude of the index tendency in reanalysis increased.

In chapter 5 the QG approximations of mass fluxes were compared to reanalysis surrounding SSWs, using two different algorithms to both define SSWs and classify them as splits or displacements. Using the polar cap pressure index defined in chapter 3, the algorithm used in DM13 was found to not distinguish between vortex splits and vortex displacements in a physically meaningful way, while the algorithm used in CP07 performed better. SSWs were shown, across both algorithm definitions, to result from a small imbalance of large negative horizontal and large positive vertical mass flux, corresponding to mass flowing up and out of the polar region. Vortex displacements were more accurately approximated using QG theory than vortex splits, largely due to a failure of QG theory to accurately calculate the vertical mass flux around the onset of vortex splits. When approximating the mass fluxes surrounding SSWs using stratospheric information only, stratospheric fluxes were largely accurately approximated, but the tropospheric fluxes were not.

As such the observed response of the tropospheric pressure index to SSWs was not recreated using QG theory and stratospheric information alone. It cannot be concluded then that the hypothesis of stratospheric PV substantially forcing tropospheric mass fluxes, and so the tropospheric pressure index, via far-field effects is correct. While the mass flux framework was shown to be capable of approximating polar pressure tendencies with good accuracy using a reanalysis streamfunction, both QG streamfunctions used did not do so in the troposphere. The inability to recreate ageostrophic velocities from a QG streamfunction is a possible cause for this. This indicates that the hypothesis may still be correct, but that the inverter used in this study did not allow for sufficient accuracy in the troposphere to make definitive statements. In the stratosphere, use of QG streamfunctions and the mass flux framework worked well, and statements about the importance of the novel interaction of tropospheric and stratospheric information can be made with some confidence. Ultimately no statements can be made with such confidence about the tropospheric response to SSWs. Tropospheric processes may also be important in amplifying or modulating any stratospheric influence in the aftermath of SSWs.

6.1.1. Limitations

The conclusions of this thesis are largely based on the output of a QGPV inverter. Two limitations of this output are the data used and the performance of the inverter. Firstly, for speed of computation on the hardware available the reanalysis data used in calculating QGPV was on a $3° \times 3°$ grid, and as such particularly at the low latitude limit of the area considered the coarseness of this data will result in errors when approximating derivatives as finite differences. Further, the highest temporal resolution of reanalysis available was 6-hourly data. This will have resulted in similar errors in the approximation of time-derivatives such as polar pressure tendencies, and not accounting for short timescale processes. Secondly, the output of the inverter has significant errors, as discussed at length in section 4.3. This is likely partly due to the resolution of the data as mentioned above, and the ill-conditioning of the zonal mean field. However as the inverter was written for this thesis, rather than being a more complex, established tool, it is likely that some errors are systematic to the design of the inverter. For example, in the sensitivity of the convergence criteria, being a trade-off between computation time and accuracy, and particularly the handling of orography.

Further to these two points however, there are problems with the construction of pressure index tendencies from horizontal and vertical mass fluxes. The ill-conditioning of the zonal mean horizontal mass flux has already been noted in chapter 4, with the eddy mass fluxes comparing to reanalysis substantially better than the zonal mean. Similarly, as found in chapter 5, observed changes in the polar pressure index are a small residual of two large mass fluxes. Any accurate approximation of changes to this index depend on accurate approximation of both of these fluxes, and as found in chapter 5 the QG result eq. 3.27 in particular fails in this regard, jeopardising the approximation of pressure tendencies. Further to this, as shown in section 3.3, the pressure index tendency predicted by an established reanalysis streamfunction does not correlate perfectly with observed pressure tendencies. This is likely due to the coarseness of the data, but demonstrates that there is a systematic error inherent to the mass flux framework. This error could likely be reduced by considering finer resolution data, but is ultimately intrinsic to the hypothesis. A likely cause for this error is the inability of the QG streamfunction to capture ageostrophic velocities, which could be substantial in the troposphere.

Lastly, this thesis was concerned with the QG influence of stratospheric variability on tropospheric fields. While quasi-geostrophy is a valid approximation for the dynamics of the stratosphere, this is not the case closer to the surface, with the horizontal length scales of tropospheric features being substantially shorter than those of stratospheric features, and so the flow being further from geostrophic balance. This breaks one of the key assumptions of quasi-geostrophy, that the flow is in near-geostrophic balance. As such the use of QG theory, in the construction of QGPV and in obtaining fields from the associated streamfunction, becomes less justifiable closer to the surface. So while the conclusion of this thesis is that stratospheric information, communicated quasi-geostrophically, is not sufficient to significantly force the tropospheric pressure field, it is unclear whether this represents a lack of relevant information (from the troposphere) or a failure of the assumptions of quasi-geostrophy.

6.2. Suggestions for further work

While the QG mass flux framework used in this thesis has problems associated with it, it would be interesting to see if the same conclusions are reached using data with a higher spatial resolution, and further if the same conclusions are reached with an inverter which has been proven to work accurately in other studies. Specifically an inverter proven to work accurately over areas of large topography would improve the confidence of findings in the lower troposphere. To improve the confidence of the results comparing SSW algorithms in chapter 5 it would also be interesting to consider SSW events beyond 2001, something not done in this thesis due to a lack of time.

Appendices

A. Calculating Empirical Orthogonal Functions

Empirical Orthogonal Functions (EOFs) are calculated from some space-time data $\boldsymbol{X}$ where element X_{ij} represents the value of a variable at the point $i = 1, 2, ..., n$ in the time dimension, and the point $j = 1, 2, ...m$ in the spatial dimension.

The objective of EOF analysis is to "reduce the dimensionality of a data set containing a large number of interrelated variables, while retaining as much as possible of the variation present in the data set." (Jolliffe, 1986). This is achieved by transforming to a new set of variables, the principal components, which are uncorrelated, and which are ordered so that the first few retain most of the variation present in all of the original variables.

One way to do this is to construct the sample covariance matrix $\boldsymbol{S}$ of $\boldsymbol{X}$:

$$\boldsymbol{S} = \frac{1}{n-1}\boldsymbol{X}^T\boldsymbol{X},$$

where it is assumed that $\boldsymbol{X}$ contains anomalies from the time mean, such that the columns of $\boldsymbol{X}$ have zero mean. Each entry in the $m \times m$ matrix describes the temporal covariance between two spatial points. To find the spatial patterns which account for the maximum variance in $\boldsymbol{X}$ it is necessary to calculate the eigenvectors $\boldsymbol{\epsilon}^a$ of $\boldsymbol{S}$, where a is the index of the given eigenvector and eigenvalue,

$$\boldsymbol{S}\boldsymbol{\epsilon}^a = \lambda_a\boldsymbol{\epsilon}^a,$$

where λ_a is the eigenvalue associated with $\boldsymbol{\epsilon}^a$. Because $\boldsymbol{S}$ is real and symmetric, the $\boldsymbol{\epsilon}^a$ are orthogonal (provided the λ are non-degenerate), i.e.

$$(\boldsymbol{\epsilon}^a)^T \boldsymbol{\epsilon}^b = \sqrt{\lambda_a \lambda_b}\delta_{a,b}$$

where $\delta_{a,b}$ is 1 if $a = b$ and otherwise 0 (the Kronecker delta function).

Because the physical dimension of the eigenvalues is the square of the physical dimension of the original variable, the eigenvectors $\boldsymbol{\epsilon}^a$ have the same dimension as the original variable. These eigenvectors are called the *empirical orthogonal functions*, EOFs. The magnitude of the eigenvalue associated with an EOF indicates what fraction of the total variance of $\boldsymbol{X}$ (i.e. the sum of the diagonal values of $\mathbf{S}$, the summative variance) is accounted for by that EOF. This is often expressed as a percentage, i.e. $(\lambda_a / \Sigma_k \lambda_k) \times 100\%$.

The EOFs can be used to reconstruct the data matrix $\boldsymbol{X}$ as follows:

$$X_{ij} = \sum_{a=1}^{\mathrm{rank}(\boldsymbol{X})} p_i^a \epsilon_j^a,$$

where the coefficients $\boldsymbol{p}^a = \boldsymbol{X}^T \boldsymbol{\epsilon}^a$ are referred to as the *principal component time series* of the EOF. If the λ_a are ranked in decreasing order of magnitude, the data can be sequentially reconstructed using the EOFs which account for the majority of the variance first, and then greater accuracy reached with the addition of higher order EOFs.

B. Inverting Quasi-Geostrophic Potential Vorticity

The streamfunction ψ associated with a given QGPV distribution q can be found by inverting the equation $q = \mathcal{L}\psi$, where $\mathcal{L}$ is a linear operator consisting of finite difference approximations to derivatives of eqn. 2.6. In this thesis the iterative technique of successive over-relaxation (Young, 1950) was used to invert this equation. An arbitrary initial streamfunction ψ_0 is used to find a corresponding QGPV distribution q_0. The error between this output and the QGPV field which we wish to invert, $q_0 - q$, is then quantified and used to create a new test streamfunction ψ_1. Using this technique the $(k+1)$th iteration of the streamfunction at location i is given by

$$\psi_i^{(k+1)} = (1-\omega)\psi_i^{(k)} + \frac{\omega}{\mathcal{L}_{ii}}\left(q_i - \sum_{j<i}\mathcal{L}_{ij}\psi_j^{(k+1)} - \sum_{j>i}\mathcal{L}_{ij}\psi_j^{(k)}\right)$$

where ω is a constant relaxation factor $\omega \geq 1$ and $\mathcal{L}_{ij}$ is the (i,j)th element $\mathcal{L}$.

This process is then iterated n times until either a set maximum number of iterations is reached, or the error $q_n - q$ is smaller than a set tolerance. The successful convergence of the streamfunction is interpreted as the difference between the most recent test streamfunction ψ_n and the true streamfunction associated with QGPV q, ψ, being satisfactorily small.

Quasi-geostrophic potential vorticity was calculated from ERA-Interim velocity and temperature data at 6-hourly resolution, on a 3°× 3°grid on pressure surfaces from 1000hPa to 1hPa, using a finite difference form of eqn. 2.6:

$$q(k,j,i) = f(i) + \frac{\psi(k,i,j+1) + \psi(k,i,j-1) - 2\psi(k,j,i)}{2 \times dx(i)} + \frac{\psi(k,i+1,j) + \psi(k,i-1,j) - 2\psi(k,j,i)}{2 \times dy} - \frac{Rf(i)}{\rho_0(k)} \left(\frac{\frac{T(k+1,i,j)}{S^2(k+1)p(k+1)} - \frac{T(k-1,i,j)}{S^2(k-1)p(k-1)}}{p(k+1) - p(k-1)} \right),$$

where k, i, j represent locations in height, latitude, and longitude respectively, dx and dy represent the distance between gridpoints in longitude and latitude, and S^2 is a stability term. This was done on p surfaces and then interpolated on z surfaces as the temperature and velocity data are not available on z surfaces. The QGPV q was then filtered into anomaly and climatology fields using a low-pass filter (see Appendix C), and the anomaly field inverted.

The horizontal and lateral boundary conditions of the inversion are crucially important (Haynes and Shepherd, 1989). The lateral boundaries are the north pole (as the data is considered on a latitude-longitude grid) and the low latitude limit of the data (30°N). Meridional gradients of datapoints at the pole can be approximated by using the meridional gradient from one datapoint further south, and approximating the zonal gradient as being equivalent to this. The low latitude limit of the data is low enough - and far enough away from the range of the output that we are concerned with - that the boundary condition of no meridional flow across the boundary (i.e. $\partial\psi/\partial\lambda = 0$) is appropriate. In practise this corresponds to holding ψ constant on this boundary and, by considering anomalies, it is appropriate to hold $\psi = 0$. The two horizontal boundaries - at 1000hPa and 1hPa - can be specified through prescribing temperature anomalies and thus the vertical gradient of the streamfunction on these surfaces.

The inverter was custom-written for this thesis in FORTRAN90, with a driving script in python. Geopotential height fields were inverted to a precision of 1m, taking around 1500 iterations to converge to this accuracy using a relaxation parameter of $\omega = 1.8$.

C. Filtering data

Temporal data in this thesis were filtered into climatology and anomalies using a Butterworth filter (Butterworth, 1930). This filter was used based on its flat frequency response in the pass band, and conversations with post-doctoral researchers in my research group. To demonstrate the use of the filter, a simple example is shown below.

Figure C.1 shows the six-month timeseries of pressure at 25km over the polar cap from October 1982 to April 1983, interpolated using geopotential data on pressure levels from ERA-Interim. This data is filtered with a sampling frequency of 4 (as the data is sampled every six hours) and a frequency cut-off of 1/90, being equivalent to filtering signals with a frequency of greater than 90 days. The filtered data, i.e. the pressure anomaly, is shown in fig. C.2, and the climatology obtained by subtracting this anomaly from the original timeseries is shown alongside the original data in fig. C.1.

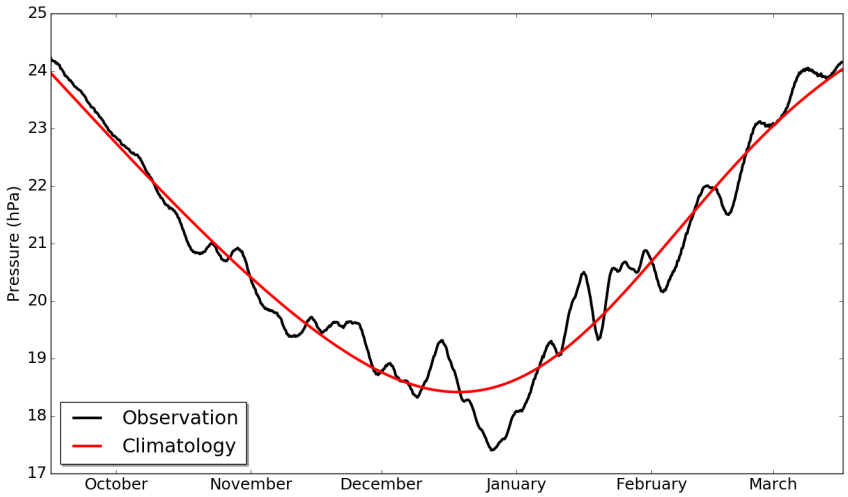

Figure C.1.: Polar cap pressure at 25km from 1982 to 1983 on stated months, data from ERA-Interim. The observed pressure and the filtered climatology are shown.

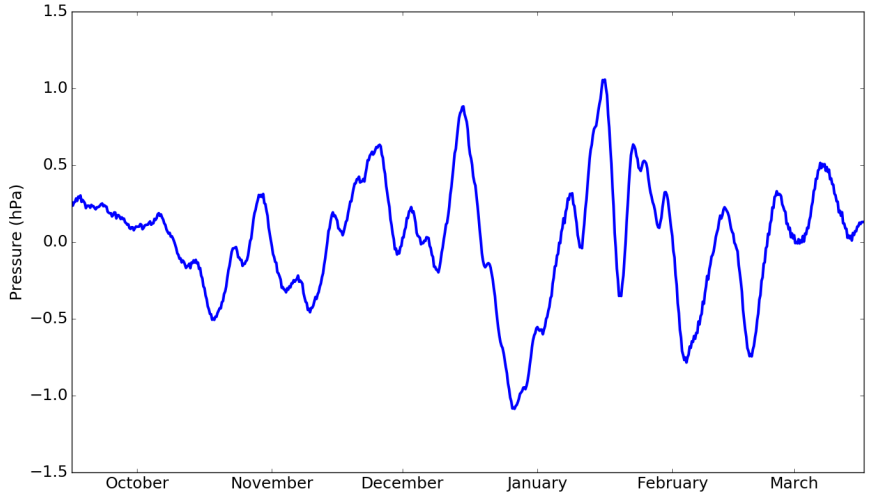

Figure C.2.: Polar cap pressure anomaly at 25km, calculated from the application of a Butterworth filter to data shown in fig. C.1.

D. Sudden Stratospheric Warming events

DM13 Onset	DM13 Classification	CP07 Onset	CP07 Classification
18/2/1979	S	22/2/1979	S
15/2/1980	S	29/2/1980	D
16/3/1980	D	29/2/1980	D
-	-	4/12/1981	D
21/1/1982	S	-	-
22/2/1983	D	-	-
26/2/1984	D	24/2/1984	D
25/12/1984	S	1/1/1985	S
3/1/1986	S	-	-
13/3/1986	D	-	-
18/1/1987	D	23/1/1987	D
-	-	7/12/1987	S
10/3/1988	D	14/3/1988	S
17/2/1989	D	21/2/1989	S
6/2/1990	D	-	-
12/1/1992	D	-	-
20/3/1992	D	-	-
10/1/1995	S	-	-
13/1/1998	S	-	-
19/2/1998	D	-	-
-	-	15/12/1998	D
27/2/1999	D	26/2/1999	S
-	-	20/3/2000	D
3/2/2001	D	11/2/2001	D
-	-	30/12/2001	D

Table D.1.: Classification of sudden stratospheric warmings (SSWs) using the DM13 and CP07 algorithms; events are classed as either splits (S), displacements (D). Events are shown to be comparable if onset dates are within a month of one another. If an algorithm does not predict an event where the other algorithm does, this is represented by a dash. Events predicted by DM13 to be a 'Mixed' SSW are disregarded. Adapted from DM13.

Bibliography

Ambaum, M. and Hoskins, B. (2002). The NAO troposphere-stratosphere connection. *J. Clim.*, pages 1969–1978.

Ambaum, M., Hoskins, B., and Stephenson, D. (2001). Arctic oscillation or North Atlantic oscillation? *J. Clim.*, 14(16):3495–3507.

Andrews, D., Holton, J., and Leovy, C. (1987). *Middle Atmosphere Dynamics*. Academic Press, San Diego, Calif.

Assmann, R. (1907). Über die existenz eines wärmeren Luftstromes in der Höhe von 10 bis 15 km. *Sitzber K Preuss Aka*, 24:495–504.

Baldwin, M., Birner, T., and Ayarzagüena, B. (2018). Polar Amplification of Stratospheric Variability. *Manuscript submitted for publication*.

Baldwin, M., Cheng, X., and Dunkerton, T. (1994). Observed correlations between winter mean tropospheric and stratospheric circulation anomalies. *Geophys. Res. Lett.*, 21:1141–1144.

Baldwin, M. and Dunkerton, T. (1999). Propagation of the Arctic Oscillation from the stratosphere to the troposphere. *J. Geophys. Res.*, 104:30937–30946.

Baldwin, M. and Dunkerton, T. (2001). Stratospheric harbingers of anomalous weather regimes. *Science*, 294(5542):581–4.

Baldwin, M., Gray, L., and Dunkerton, T. (2001). The quasi-biennial oscillation. *Rev. Geophys.*, 39(2).

Baldwin, M. and Thompson, D. W. (2009). A critical comparison of stratosphere – troposphere coupling indices. *Q. J. R. Meteorol. Soc.*, 1672(September):1661–1672.

Bethan, S., Vaughan, G., and Reid, S. J. (1996). A comparison of ozone and thermal tropopause heights and the impact of tropopause definition on quantifying the ozone content of the troposphere. *Q. J. R. Meteorol. Soc.*, 122(532):929–944.

Bishop, C. and Thorpe, A. (1994). Potential vorticity and the electrostatics analogy: Quasi-geostrophic theory. *Q.J.R. Meterol. Soc.*, 120:713–731.

Black, R. X. (2002). Stratospheric Forcing of Surface Climate in the Arctic Oscillation. *J. Clim.*, 15(3):268–277.

Black, R. X. and McDaniel, B. A. (2007). The Dynamics of Northern Hemisphere Stratospheric Final Warming Events. *J. Atmos. Sci.*, 64.

Boville, B. (1984). The influence of the polar night jet on the tropospheric circulation in a GCM. *J. Atmos. Sci.*, 41:1132–1142.

Butchart, N., Charlton-Perez, A., Cionni, I., Hardiman, S., Haynes, P., Krüger, K., Kushner, P. J., Newman, P., Osprey, S. M., Perlwitz, J., Sigmond, M., Wang, L., Akiyoshi, H., Austin, J., Bekki, S., Baumgaertner, A., Braesicke, P., Brhl, C., Chipperfield, M., Dameris, M., Dhomse, S., Eyring, V., Garcia, R., Garny, H., Jöckel, P., Lamarque, J. F., Marchand, M., Michou, M., Morgenstern, O., Nakamura, T., Pawson, S., Plummer, D., Pyle, J., Rozanov, E., Scinocca, J., Shepherd, T., Shibata, K., Smale, D., Teyssèdre, H., Tian, W., Waugh, D. W., and Yamashita, Y. (2011). Multimodel climate and variability of the stratosphere. *J. Geophys. Res. Atmos.*, 116(5):1–21.

Butler, A. H., Seidel, D. J., Hardiman, S., Butchart, N., Birner, T., and Match, A. (2015). Defining sudden stratospheric warmings. *Bull. Am. Meteorol. Soc.*, 96(11):1913–1928.

Butterworth, S. (1930). On the theory of filter amplifiers.

Charlton, A. and Polvani, L. M. (2007). A New Look at Stratospheric Sudden Warmings. Part I : Climatology and Modelling Benchmarks. *J. Clim.*, 20:449–470.

Charney, J. (1948). On the Scale of Atmospheric Motions. *Geof. Publ.*, 17(2):3–17.

Charney, J. and Drazin, P. G. (1961). Propagation of Planetary-Scale Disturbances from the Lower into the Upper Atmosphere. *J. Geophys. Res.*, 66(1):83–109.

Chen, P. and Robinson, W. (1992). Propagation of Planetary Waves between the Stratosphere and Troposphere. *J. Atmos. Sci.*, 49(24):2533–2545.

Christiansen, B. (1999). Stratospheric Vacillations in a General Circulation Model. *J. Atmos. Sci.*, 56:1858–1872.

Christiansen, B. (2001). Downward propagation of zonal mean zonal wind anomalies from the stratosphere to the troposphere: Model and reanalysis. *J. Geophys. Res.*, 106(D21):27307.

Cornu, A. (1881). Sur l'absorption atmosphérique des radiations ultra-violettes. *J. Phys. Théorique Appliquée*, 10(1):5–17.

Deser, C. (2000). On the teleconnectivity of the 'Arctic Oscillation'. *Geophys. Res. Lett.*, 27(6):779–782.

Egger, J. and Hoinka, K.-P. (2005). Downward Control from the Lower Stratosphere? *J. Atmos. Sci.*, 62(10):3808–3817.

Gerber, E. P., Baldwin, M., Akiyoshi, H., Austin, J., Bekki, S., Braesicke, P., Butchart, N., Chipperfield, M., Dameris, M., Dhomse, S., Frith, S. M., Garcia, R., Garny, H., Gettelman, A., Hardiman, S., Karpechko, A., Marchand, M., Morgenstern, O., Nielsen, J. E., Pawson, S., Peter, T., Plummer, D., Pyle, J., Rozanov, E., Scinocca, J., Shepherd, T., and Smale, D. (2010). Stratosphere-troposphere coupling and annular mode variability in chemistry-climate models. *J. Geophys. Res.*, 115.

Gray, L., Beer, J., Geller, M., Haigh, J. D., Lockwood, M., Matthes, K., Cubasch, U., Fleitmann, D., Harrison, G., Hood, L., Luterbacher, J., Meehl, G. a., Shindell, D., van Geel, B., and White, W. (2010). Solar influence on climate. *Rev. Geophys.*, 48(2009):RG4001.

Griffiths, D. (1998). *Introduction to Electrodynamics*. Addison Wesley, 3rd edition.

Hannachi, A., Mitchell, D., Gray, L., and Charlton-Perez, A. (2011). On the Use of Geometric Moments to Examine the Continuum of Sudden Stratospheric Warmings. *J. Atmos. Sci.*, 68(3):657–674.

Hartley, D. E., Villarin, J. T., Black, R. X., and Davis, C. (1998). A new perspective on the dynamical link between the stratosphere and troposphere. *Nature*, 8311(1996):1996–1999.

Hartmann, D. L., Wallace, J., Limpasuvan, V., Thompson, D. W., and Holton, J. (2000). Can ozone depletion and global warming interact to produce rapid climate change? *Proc. Natl. Acad. Sci. U. S. A.*, 97(4):1412–1417.

Haynes, P. (2005). Stratospheric dynamics. *Annu. Rev. Fluid Mech.*, 37(1):263–293.

Haynes, P., McIntyre, M., Shepherd, T., Marks, C. J., and Shine, K. P. (1991). On the "Downward Control" of Extratropical Diabatic Circulations by Eddy-Induced Mean Zonal Forces. *J. Atmos. Sci.*, 48(4):651–678.

Haynes, P. and Shepherd, T. (1989). The importance of surface pressure changes in the response of the atmosphere to zonally-symmetric thermal and mechanical forcing. *Q. J. R. Meteorol. Soc.*, 115:1181–1208.

Hines, C. (1960). Internal Atmospheric Gravity Waves at Ionospheric Heights. *Can. J. Phys.*, 38:1441–1481.

Hitchcock, P. and Simpson, I. R. (2014). The Downward Influence of Stratospheric Sudden Warmings*. *J. Atmos. Sci.*, 71(10):3856–3876.

Hoerling, M. P., Schaack, T. K., and Lenzen, A. J. (1991). Global Objective Tropopause Analysis. *Mon. Weather Rev.*, 119(8):1816–1831.

Holton, J., Haynes, P., McIntyre, M., Douglass, A. R., and Rood, B. (1995). Stratosphere-Troposphere Exchange. *Rev. Geophys.*, 33(4):403–439.

Holton, J. and Mass, C. (1976). Stratospheric vacillation cycles. *J. Atmos. Sci.*

Jolliffe, I. (1986). *Principal Component Analysis*. Springer-Verlag, New York, 2nd edition.

Juckes, M. and McIntyre, M. (1987). A high-resolution one-layer model of breaking planetary waves in the stratosphere. *Nature*, 328:590–596.

Kidston, J., Scaife, A., Hardiman, S., Mitchell, D., Butchart, N., Baldwin, M., and Gray, L. (2015). Stratospheric influence on tropospheric jet streams, storm tracks and surface weather. *Nat. Geosci.*

Kilifarska, N. A. (2012). Climate sensitivity to the lower stratospheric ozone variations. *J. Atmos. Solar-Terrestrial Phys.*, 90-91(1):9–14.

Kodera, K., Yamazaki, K., Chiba, M., and Shibata, K. (1990). Downward propagation of upper stratospheric mean zonal wind perturbation to the troposphere. *Geophys. Res. Lett.*, 17(9):1263–1266.

Labitzke, K. (1977). Interannual Variability of the Winter Stratosphere in the Northern Hemisphere. *Mon. Weather Rev.*, 105(6):762–770.

Labitzke, K. and Naujokat, B. (2000). The lower arctic stratosphere in winter since 1952. Technical report, SPARC Newsletter No. 15.

Lewis, R. P. W. (1991). *Meteorological Glossary*. HMSO, 6th edition.

Limpasuvan, V. and Hartmann, D. L. (1999). Eddies and the annular modes of climate variability 1. *Geophys. Res. Lett.*, 26(20):3133–3136.

Limpasuvan, V. and Hartmann, D. L. (2000). Wave-Maintained Annular Modes of Climate Variability. *J. Clim.*, 13(24):4414–4429.

Lorenz, E. N. (1956). Empirical Orthogonal Functions and Statistical Weather Prediction.

Matsuno, T. (1971). A dynamical model of the stratospheric sudden warming. *J. Atmos. Sci.*, 28:1479–1494.

Matthewman, N. J., Esler, J. G., Charlton-Perez, A., and Polvani, L. M. (2009). A new look at stratospheric sudden warmings. Part III: Polar vortex evolution and vertical structure. *J. Clim.*, 22(6):1566–1585.

Maycock, A. C. and Hitchcock, P. (2015). Do split and displacement sudden stratospheric warmings have different annular mode signatures? *Geophys. Res. Lett.*, 42(24):10943–10951.

Maycock, A. C., Shine, K. P., and Joshi, M. M. (2011). The temperature response to stratospheric water vapour changes. *Q. J. R. Meteorol. Soc.*, 137(657):1070–1082.

McCormick, M., Thomason, L., and Trepte, C. (1995). Atmospheric effects of the Mt Pinatubo eruption. *Nature*, 373:399–404.

McIntyre, M. (2003). Balanced Flow. In Holton, J., Pyle, J., and Curry, J., editors, *Encycl. Atmos. Sci.*, page 12. Academic/Elsevier, London, 2 edition.

McIntyre, M. (2015). Potential Vorticity. In Holton, J., Pyle, J., and Curry, J., editors, *Encycl. Atmos. Sci.*, volume 2, pages 375–383. Academic/Elsevier, London, 2 edition.

McIntyre, M. and Palmer, T. (1983). Breaking planetary waves in the stratosphere. *Nature*, 305(13):593–600.

Mitchell, D., Charlton-Perez, A., and Gray, L. (2010). Characterizing the Variability and Extremes of the Stratospheric Polar Vortices Using 2D Moment Analysis. *J. Atmos. Sci.*, 68(6):1194–1213.

Mitchell, D., Gray, L., Anstey, J., Baldwin, M., and Charlton-Perez, A. (2013). The Influence of Stratospheric Vortex Displacements and Splits on Surface Climate. *J. Clim.*, 26:2668–2682.

Mitchell, D., Gray, L., and Charlton-Perez, A. (2011). The structure and evolution of the stratospheric vortex in response to natural forcings. *J. Geophys. Res. Atmos.*, 116(15):1–11.

Mote, P. W., Rosenlof, K. H., McIntyre, M., Carr, E. S., Gille, J. C., Holton, J., Kinnersley, J. S., Pumphrey, H. C., Russell, J. M., and Waters, J. W. (1996). An atmospheric tape recorder: The imprint of tropical tropopause temperatures on stratospheric water vapor. *J. Geophys. Res.*, 101(D2):3989.

Murray, F. W. (1960). Dynamic stability in the stratosphere. *J. Geophys. Res.*, 55(10):3273–3305.

Newman, P. and Nash, E. (2005). The unusual Southern Hemisphere stratosphere winter of 2002. *J. Atmos. Sci.*, 62:614–628.

Pearson, K. (1901). On lines and planes of closest fit to systems of points in space. *London, Edinburgh, Dublin Philos. Mag. J. Sci.*, 2(1):559–572.

Perlwitz, J. and Harnik, N. (2003). Observational Evidence of a Stratospheric Influence on the Troposphere by Planetary Wave Reflection. *J. Clim.*, 16(18):3011–3026.

Perlwitz, J. and Harnik, N. (2004). Downward Coupling between the Stratosphere and Troposphere: The Relative Roles of Wave and Zonal Mean Processes. *J. Clim.*, 17(24):4902–4909.

Plumb, R. and Semeniuk, K. (2003). Downward migration of extratropical zonal wind anomalies. *J. Geophys. Res.*, pages 1–8.

Quiroz, R. (1975). The Stratospheric Evolution of Sudden Warmings in 1969-74 Determined from Measured Infrared Fields. *J. Atmos. Sci.*, 32.

Randel, W. and Boville, B. (1987). Observations of a Major Stratospheric Warming during December 1984. *J. Atmos. Sci.*, 44(15):2179–2.

Richman, M. (1986). Rotation of Principal Components. *J. Climatol.*, 6:293–335.

Riley, K., Hobson, M., and Bence, S. (2006). *Mathematical Methods for Physics and Engineering*. Cambridge University Press, Cambridge, 3rd edition.

Robinson, W. (1988). Analysis of LIMS data by Potential Vorticity Inversion. *J. Atmos. Sci.*, 45(16).

Rossby, C.-G. (1939). Relation between variations in the intensity of the zonal circulation of the atmosphere and the displacements of the semi-permanent centers of action.

Rossby, C.-G. (1940). Planetary flow patterns in the atmosphere.

Scaife, A. and James, I. (2000). Response of the stratosphere to interannual variability of tropospheric planetary waves. *Q. J. R. Meteorol. Soc.*, 126:215–291.

Scherhag, R. (1952). Die explosionsartige Stratosphärenerwarmung des Spät-winters 1951/52. *Ber. Deut. Wetterdieuste*, 6:51–63.

Schlatter, T. W. (2009). Atmospheric Composition and Vertical Structure. *Natl. Ocean. Atmos. Adm.*, 6:1–54.

Schoeberl, M. and Strobel, D. (1978). The zonally averaged circulation of the middle atmosphere. *J. Atmos. Sci.*, 35:577–591.

Schubert, W., Ruprecht, E., Hertenstein, R., Ferreira, R. N., Taft, R., Rozoff, C., Ciesielski, P., and Kuo, H. C. (2004). English translations of twenty-one of Ertel's papers on geophysical fluid dynamics. *Meteorol. Zeitschrift*, 13(6):527–576.

Seviour, W. J. M., Mitchell, D., and Gray, L. (2013). A practical method to identify displaced and split stratospheric polar vortex events. *Geophys. Res. Lett.*, 40(19):5268–5273.

Sigmond, M., Scinocca, J., and Kushner, P. J. (2008). Impact of the stratosphere on tropospheric climate change. *Geophys. Res. Lett.*, 35(12):1–6.

Song, Y. and Robinson, W. (2004). Dynamical Mechanisms for Stratospheric Influences on the Troposphere. *J. Atmos. Sci.*, 61(14):1711–1725.

Spengler, T. and Egger, J. (2012). Potential Vorticity Attribution and Causality. *J. Atmos. Sci.*, 69.

Stephenson, D., Wanner, H., Brönnimann, S., and Luterbacher, J. (2001). The History of Scientific Research on the North Atlantic Oscillation. In Hurrell, J. W., Kushnir, Y., Ottersen, G., and Visbeck, M., editors, *North Atl. Oscil. Clim. Significance Environ. Impact*, pages 37–50. American Geophysical Union, Washington, DC.

Teisserenc de Bort, M. (1902). Variations de la temperature de l'air libre dans la zone comprise 8 km et 13 km d'altitude. *C R Hebd Seances Acad Sci*, 24:987–989.

Thompson, D. W., Baldwin, M., and Wallace, J. (2002). Stratospheric connection to Northern Hemisphere wintertime weather: Implications for prediction. *J. Clim.*, 15:1421–1428.

Thompson, D. W. and Wallace, J. (1998). The Arctic Oscillation signature in the wintertime geopotential height and temperature fields. *Geophys. Res. Lett.*, 25(9):1297–1300.

Thompson, D. W. and Wallace, J. (2001). Regional climate impacts of the Northern Hemisphere annular mode. *Science*, 293(5527):85–9.

Thompson, D. W., Wallace, J., and Hegerl, G. C. (2000). Annular Modes in the Extratropical Circulation. Part II: Trends. *J. Clim.*, 13(5):1018–1036.

Thuburn, J. and Craig, G. (2000). Stratospheric Influence on Tropopause Height : The Radiative Constraint. *J. Atmos. Sci.*, 57:17–28.

Tomassini, L., Gerber, E. P., Baldwin, M., Bunzel, F., and Giorgetta, M. (2012). The role of stratosphere-troposphere coupling in the occurrence of extreme winter cold spells over northern Europe. *J. Adv. Model. Earth Syst.*, 4(10):1–14.

Vallis, G. (2006). *Atmospheric and Oceanic Fluid Dynamics: Fundamentals and Large-Scale Circulation*. Cambridge University Press, Cambridge, 1st edition.

Wallace, J. (2000). North Atlantic Oscillation / annular mode: two paradigms - one phenomenon. *Quart. J. Roy. Meteor. Soc.*, 126:791–805.

Wallace, J. and Hobbs, P. (2006). *Atmospheric Science: An Introductory Survey*. Academic Press, San Diego, Calif, 2nd edition.

Waugh, D. W. (1997). Elliptical diagnostics of stratospheric polar vortices. *Q. J. R. Meteorol. Soc.*, 123(542):1725–1748.

Waugh, D. W. and Polvani, L. M. (2010). The Stratosphere: Dynamics, Transport, and Chemistry - Stratospheric Polar Vortices. *Geophys. Monogr. Ser.*, 190:43–58.

Waugh, D. W. and Randel, W. (1999). Climatology of Arctic and Antarctic Polar Vortices Using Elliptical Diagnostics. *J. Atmos. Sci.*, 56(11):1594–1613.

Whipple, F. (1935). The propagation of sound waves to great distances. *Quart. J. Roy. Meteor. Soc.*, 61:285–308.

Woollings, T., Charlton-Perez, A., Ineson, S., Marshall, A. G., and Masato, G. (2010). Associations between stratospheric variability and tropospheric blocking. *J. Geophys. Res. Atmos.*, 115(6):1–17.

Yoden, S. (1987). Bifurcation Properties of a Stratospheric Vacillation Model. *J. Atmos. Sci.*, 44(13).

Young, D. (1950). *Iterative methods for solving partial differential equations of elliptic type*. PhD thesis, Harvard University.

Zeng, G. and Pyle, J. (2003). Changes in tropospheric ozone between 2000 and 2100 modeled in a chemistry-climate model. *Geophys. Res. Lett.*, 30(7):1–4.